Electronic Theses and Dissertations   Theses, Dissertations, and Major Papers

2012

A methodology to determine the functional workspace of a 6R robot using forward kinematics and geometrical methods

Arun Gowtham Gudla
University of Windsor

Follow this and additional works at: https://scholar.uwindsor.ca/etd

A methodology to determine the functional workspace of a 6R robot using forward
kinematics and geometrical methods

by

Arun Gowtham Gudla

A Thesis
Submitted to the Faculty of Graduate Studies
through Industrial and Manufacturing Systems Engineering
in Partial Fulfillment of the Requirements for
the Degree of Master of Applied Science at the
University of Windsor

Windsor, Ontario, Canada

2012

A methodology to determine the functional workspace of a 6R robot using forward kinematics and geometrical methods

by

Arun Gowtham Gudla

APPROVED BY:

_____
{Dr. Zbigniew Pasek}
Department of Industrial and Manufacturing Systems Engineering

_____
{Dr. Bruce Minaker}
Department of Mechanical, Automotive and Materials Engineering

_____
{Dr. Jill Urbanic}, Advisor
Department of Industrial and Manufacturing Systems Engineering

_____
{Dr. Mitra Mirhassani}, Chair of Defense
Department of Electrical and Computer Engineering

{September 17, 2012}

DECLARATION OF CO-AUTHORSHIP/PREVIOUS PUBLICATION

I. Co-Authorship Declaration

I hereby declare that this thesis incorporates material that is result of joint research, as follows:

This thesis incorporates the outcome of a joint research undertaken in collaboration with Dr.Jill Urbanic, Assistant Professor, University of Windsor, Windsor, ON, Canada. The collaboration is covered in Section 3.1 and 4.4 of the thesis.

I am aware of the University of Windsor Senate Policy on Authorship and I certify that I have properly acknowledged the contribution of other researchers to my thesis, and have obtained written permission from each of the co-author(s) to include the above material(s) in my thesis.

I certify that, with the above qualification, this thesis, and the research to which it refers, is the product of my own work.

II. Declaration of Previous Publication

This thesis includes 1 original papers that have been previously published/submitted for publication in peer reviewed journals, as follows:

Thesis Chapter	Publication title/full citation	Publication status*
Section 3.1	Urbanic, J., Gudla, A.,. "Functional Work space Estimation of a Robot Using Forward Kinematics, D-H Parameters and Shape Analyses." *The ASME 2012 11th Biennial Conference on Engineering Systems Design and Analysis (ESDA2012).* Nantes: ASME	Published

	ESDA 2012, 2012.	
Section 4.4	Urbanic, J., Gudla, A.,. "Functional Work space Estimation of a Robot Using Forward Kinematics, D-H Parameters and Shape Analyses." *The ASME 2012 11th Biennial Conference on Engineering Systems Design and Analysis (ESDA2012).* Nantes: ASME ESDA 2012, 2012.	Published

I certify that I have obtained a written permission from the copyright owner(s) to include the above published material(s) in my thesis. I certify that the above material describes work completed during my registration as graduate student at the University of Windsor.

I declare that, to the best of my knowledge, my thesis does not infringe upon anyone's copyright nor violate any proprietary rights and that any ideas, techniques, quotations, or any other material from the work of other people included in my thesis, published or otherwise, are fully acknowledged in accordance with the standard referencing practices. Furthermore, to the extent that I have included copyrighted material that surpasses the bounds of fair dealing within the meaning of the Canada Copyright Act, I certify that I have obtained a written permission from the copyright owner(s) to include such material(s) in my thesis.

I declare that this is a true copy of my thesis, including any final revisions, as approved by my thesis committee and the Graduate Studies office, and that this thesis has not been submitted for a higher degree to any other University or Institution.

ABSTRACT

The work envelope of a robot does not capture the effect of tool orientation. Applications will require the tool to be at a certain orientation to perform the tasks necessary. It is therefore important to introduce a parameter that can capture the effect of orientation for multiple robots and configurations. This is called the functional work space, which is a subset of the work envelope would capture the effect of orientation. This research discusses the development of establishing an assessment tool that can predict the functional work space of a robot for a certain tool-orientation pair thus aiding in proper tool, tool path, fixture, related configuration selection and placement.

Several solutions are studied and an analytical and a geometric solution is presented after a detailed study of joint dependencies, joint movements, limits, link lengths and displacements through visual, empirical and analytical approaches. The functional workspace curve for a manipulator with similar kinematic structure can be created using the geometrical solution discussed in this research. It is difficult to derive a general paradigm since different parameters such as, joint limits, angles and twist angles seem to have a different effect on the shape of the workspace. The geometrical solution employed is simple, easy to deduce and can be simulated with a commercial software package. Design decisions pertaining to configuration and reconfiguration of manipulators will benefit by employing the solution as a design/analysis tool. A case study involving an X-ray diffraction technique goniometer is presented to highlight the merits of this work.

DEDICATION

A long dedication is due for the long journey I am on.

"He didn't tell me how to live; he lived, and let me watch him do it."

-Clarence Budington Kelland

   To my father, who has taught me life and more.

"When the Good Lord was creating mothers, He was into His sixth day of "overtime" when the angel appeared and said. "You're doing a lot of fiddling around on this one."

And God said, "Have you read the specs on this order?" She has to be completely washable, but not plastic. Have 180 moveable parts...all replaceable. Run on black coffee and leftovers. Have a lap that disappears when she stands up. A kiss that can cure anything from a broken leg to a disappointed love affair. And six pairs of hands." "

-Erma Bombeck, *When God created Mothers*

   To my mother, for being the Superwoman, that she is.

"Brothers don't necessarily have to say anything to each other- they can sit in a room and be together and just be completely comfortable with each other."

- Leonardo Dicaprio

   To my brother and my confidante who does not talk much, but says a lot.

"A teacher affects eternity; he can never tell where his influence stops."

-Henry Brooks Adams

   To all my teachers, past, present and future for moulding me.

"A friend is one that knows you as you are, understands where you have been, accepts

what you have become, and still, gently allows you to grow."

-William Shakespeare

   To a friend and other ones, who have stood by me and supported me.

ACKNOWLEDGEMENTS

TABLE OF CONTENTS

LIST OF TABLES

LIST OF FIGURES

CHAPTER 1

INTRODUCTION

In today's manufacturing scenario, product life cycles are decreasing and customers are demanding cheaper and high quality products in a timely manner. To satisfy a variety of customer needs, companies need to introduce the option of customizability to their portfolio by making their operations more flexible. Flexibility in manufacturing today plays a vital role and can decide the future of an organization. Adaptation to the ever changing market will ensure profits and growth while lack of innovation and variety will lead to stagnation. Flexibility of a manufacturing system can be defined as the ability to produce a variety of products with minimum or no changes to the layout, manufacturing cells and the machines that are part of that system. There is a constant need to better the existing flexible systems to meet the production demands. Furthermore, the automation in the system needs to be aimed at reducing cycle times, lead times and handling while increasing production and maintaining quality. It is therefore, important to automate in a resourceful and reliable manner.

To achieve the above said characteristics, effective and robust systems are required. An effective system should be a well-designed system that is well tested leading to minimum or no errors during operation wherein most parameters are already set. This particularly applies to machine and robot cells. For example, in a robotic work cell there are various parameters such as link length, payload, range, accuracy, workspace etc. that have to be defined for it to be able to work in synchronized manner with others on the required tasks.

The assessment of the reach of the robot and the feasibility of its kinematic structure for the tasks to be performed is of prime importance amongst decisions pertaining to sensor selection and location, the control systems, power supplies, manipulators and the software used to run the robot. It is important to know whether the robot end-effector can reach a particular point in its workspace at a desired orientation to allow modification or change in the placement or configuration (in case of reconfigurable robots) before setting up the robot on the shop floor. Currently, this reach problem is solved by visual inspection, simulation packages, by manually operating a teach pendant and by visually analysing the workspace of the robot. The work space of a kinematic structure can be defined as the set of all points that it can reach in space. Workspaces are of different complicated shapes. Some workspaces are flat, some spherical and some cylindrical depending on the coordinate geometry of a kinematic structure. It is important to know the workspace of a kinematic structure, to be able to assess its flexibility and workability (Panda, et al., 2009). Defining the workspace is very evidently important for more than one reason; pertaining to, but not limited to design, optimization, safety and layout of a kinematic structure. The work envelope, however, does not provide a solution for a desired configuration, as the effect of orientation is not captured. Consider the ABB 6R robot in Fig.1-1. On the left is the complete work envelope of the robot. On the right is the figure of all the reachable points of joint-5 at 90° to the work piece(normal to the base). It can be seen that at this particular orientation the robot arm cannot reach all the points in the work envelope.

Point inside the work envelope but out of the functional workspace at 90° orientation to the work piece

a) Three joint 3D work envelope

b) 2D Functional workspace as a subset of the work envelope
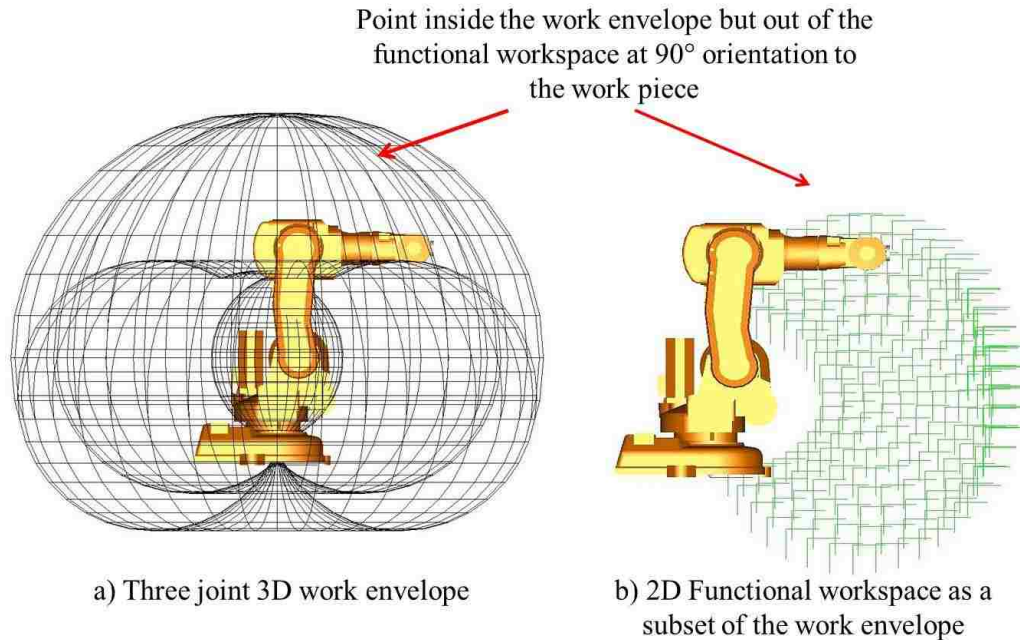
Figure 1-1 Functional work space of a ABB 6R robot as a subset of the three joint work envelope

The depiction of the work envelope does not capture the effect of orientation of joint-5. The fixed orientation of the tool is important in many machining and deposition applications. Consider another scenario, shown in Fig.1-2, where, for a robot, tool and travel path configuration, joint-5 or θ_5 has reached it limits.
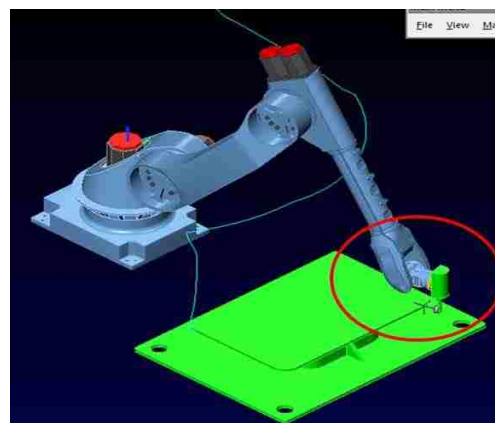
Tool orientation Parallel to the work piece

Figure 1-2 Failed robot simulation due to Joint-5 at its limit. Reference: Urbanic, J., Gudla, A., 2012

This fault can be corrected by rotating the tool by 90° around the Y axis, while keeping all the other parameters fixed. The manipulator can now access the complete work piece and the simulation is successful (Fig. 1-3).

Changed tool orientation- 90° normal to the base
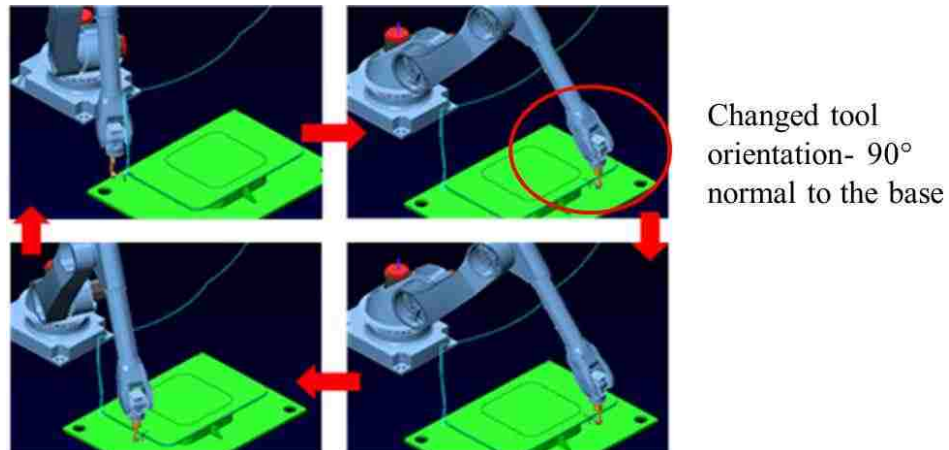
Figure 1-3 Successful robot simulation after changing joint 5 orientation

1.1 Problem Definition

There is a need for an assessment methodology to visualise the effect of orientation that can better define the flexibility and limitation of a kinematic structure leading to subsequent downstream optimization; introduced in this work as the functional work space. The functional work space introduced in this research is the subset of the work envelope of a robot defined as the valid functional space for a configuration to allow a kinematic structure (robot, machine tool, and so forth) to follow a desired orientation to the part or base, or both. Defining a valid solution space for a particular orientation will enable down-stream optimization for path planning, robot structure. The objective of this research is to develop an assessment methodology leading to a design tool that will help process planners, select configuration/reconfiguration solution alternatives during the design phase.

The research aims to:

- Study the relation between the tool(s), object/work piece(s) and the production space, which involves many coordinate frames. Using forward kinematics, the correlation between two or more different coordinate frames can be assessed, which can show the correct object/work piece placement and the tool placement.

- Obtain the relation between different entities within a system by evaluating the position and orientation of each entity relative to any selected frame.

- Study in detail the frame transformations and forward kinematics to understand the joint dependencies and movements.

- Perform shape analyses of the functional work space of an ABB IRB 140 robot arm through visual, empirical, analytical and geometrical methods.

- Reduce the kinematic structure into the essential links and joints to obtain the functional work space of the robot.

- Develop an algorithm to project the functional work space in two dimensions for serial 6R robots.

- Automate a geometric and an analytical solution that can be further developed as a design/analysis tool and can be extended into the 3D domain.

This research is aimed to be a foundational study in deriving a methodology to find the functional work space of a robotic arm for multiple orientations of the tool. This work includes the serial manipulators case and does not involve study of parallel manipulators. The research solution is arrived at in reference to a six axis rotational ABB IRB 140 industrial robot. This solution will apply to any robot that can be reduced to a four bar linkage in the two dimensional space. Each robot configuration has to be treated as a special case and a variety of configurations need to be studied to derive a general and all

inclusive solution for the functional work space problem. The approach taken in the research is to study the forward kinematics and geometry of the robot and project the functional work space in a two dimensional environment. Factors such as joint speeds, linear velocities of the links and joints, inverse kinematics and singularities have not been studied. It must be noted that, before considering these factors, the problem of the functional work space itself needs to be well understood; which should be done by considering the most important and basic parameters that effect the functional work space.

A Fanuc LR MATE 200iC robot was used to understand and emulate the problem. The LR MATE also helped visually infer possible solutions by programming it to perform various tasks. Teach Pendant programming was done to make the robot reach different points of a rapid prototyped work piece with complex geometry at certain orientations to understand the complexity involved in the task. Workspace5™ was used to derive an empirical solution. CATIAV5™ was used to arrive at a geometric solution. MATLAB™ was used to program the solution algorithm and simulate the equations.

The following chapter presents the review of literature and discusses the research gap in this area. Chapter 3 deals with kinematic analysis and frame transformations needed to relate the end effector with the base frame and forward kinematics of ABB IRB 140 robot. Chapter 4 discusses the visual, empirical and analytical approaches establishing the need for decomposition of the robotic structure and how that helps to achieve the two dimensional depiction of functional work space. This is followed by a case study of an X-Ray diffraction Goniometer in Chapter 5. The summary and conclusions are presented in Chapter 6 followed by future work in Chapter 7.

CHAPTER 2

LITERATURE REVIEW

Considerable research has been done on the nature and optimization of workspace, with respect to different robotic manipulators (Zacharias, F., et al.), (Gupta, K.C. 1984), (Szep, C., et al., 2009), (Carbone, G., et al., 2010), (Gupta, K.C., et al., 1982), (Cebula, A.J., et al., 2006), (Ceccarelli, 1995), (Cao, Y., et al., 2009), (Abdel-Malek, Harn-Jou Yeh, 1997), (Lee, et al., 2011), (Bi, Z.M., Lang, S.Y.T., 2007), (Cao, Y., et al., 2011), (Vijaykumar, R., et al., 1986), (Borcea, Streinu, 2011), (Badescu, Mavroidis, 2003). Cao, et al., (2009) provided an integrated approach in presenting and analyzing the workspace of robot manipulator based on Monte Carlo method and modeling capabilities of popular commercially-available 3D software. A 5R robot was used as an example to demonstrate the generality and feasibility of the method. The approximate boundary points in the main working plane are obtained by dividing the planar robot's workspace into a series of rows and searching for the needed points in each row. A tool for optimizing the workspace of a 3R robot manipulator has been discussed by Panda, (2009). The optimization problem is formulated considering the workspace volume as the objective function, while constraints are imposed to control the total area. Four different optimization techniques, SQP, fminmax, goal attainment and constrained non -linear minimization were used to solve a numerical example with the same conditions imposed to demonstrate the efficiency of optimization processes.

Gupta (1984) in his paper, "On the Nature of Robot Workspace" defined the workspace W_i (P) with respect to i^{th} axis, as the totality of points that can be reached by

the gripper point or tool tip P. The total workspace is divided into primary (or dexterous) and secondary workspaces. In the primary workspace, all tool orientations around the tool tip point P are possible. A robot configuration with six degrees of freedom consists of a three-degrees-of-freedom positioning of a wrist point H, followed by a three-roll wrist (or equivalent configuration with three revolutes cointersecting at a wrist point) has been considered. A method to calculate the primary workspace in such cases is mentioned in the paper. First, the workspace W_1 (H) of the wrist point H is determined. Next a sphere of radius HP is moved with its center on the boundary of the workspace W_1 (H). The inner and outer envelopes are the boundaries of primary and total workspaces, respectively. The paper further discusses the use of geometric inversion method for the prediction of the number of solution sets, the existence of solution transition boundaries within the workspace (dexterous or total), and the influence of joint variable limits on the workspace and the multiplicity of solution sets. Much of the current research classifies the work space into a primary and secondary workspace. There is, however, no feasible work region or a functional work space derivation for a set of robotic configurations that will help define the valid space for an end effector orientation.

A new method to calculate the boundary workspace was developed by Djuric, A.M., ElMaraghy, W.H., (2008) called the Filtering Boundary Points (FBP). This method enabled the calculation of the workspace boundary surface so that the user can ensure that all the points along the trajectory of a robot arm lie inside the robot's workspace before the set points of the robot joints are generated. A generic robotic model that could be easily reconfigured to identify a specific kinematic model for a specific robot was

developed for this purpose. This research did not take into account the functional work space based on orientation of the tool.

Djuric, A.M., Urbanic, J., (2009) first defined the work window as the functional subset of the work window. A basic algorithm to calculate the work window for a configuration was presented in this paper. The shape of the work window of a few selected configuration pairs was also shown.

An important problem in robotic cell design is the optimal placement of the robot structure. Feddema, (1996) discussed an algorithm to determine the correct placement of a robotic manipulator in an industrial scenario. Optimal placement of a robot or a machine is a very common problem in the manufacturing scenario, which if solved can result in substantial cost and time savings.
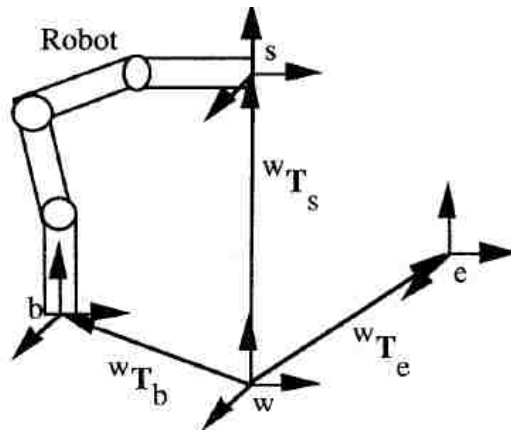
Figure 2-1 Optimal Robot Placement on shop floor. Reference: Feddema (1996)

$^{W}T_{b}$ is to be moved to a position which can minimize the time required to move between $^{W}T_{s}$, and $^{W}T_{e}$. The optimization algorithm presented uses kinematics and the maximum acceleration of each joint. The research considers FANUC robots as case studies; each vendor uses a different method for trajectory generation and also the settling

times are different. The research shows several discrepancies between the estimated and the actual experimental times due to the above mentioned reason.

The specification of the position and orientation of a base of a robotic manipulator in a predefined work environment is necessary in placement of a robotic manipulator, (Abdel-Malek, Yu, 2004). Using dexterity as a measure, a method for determining the exact boundary of the workspace was described. An algorithm was presented and implemented in computer code to solve the case study of a three DOF manipulator with three revolute joints.
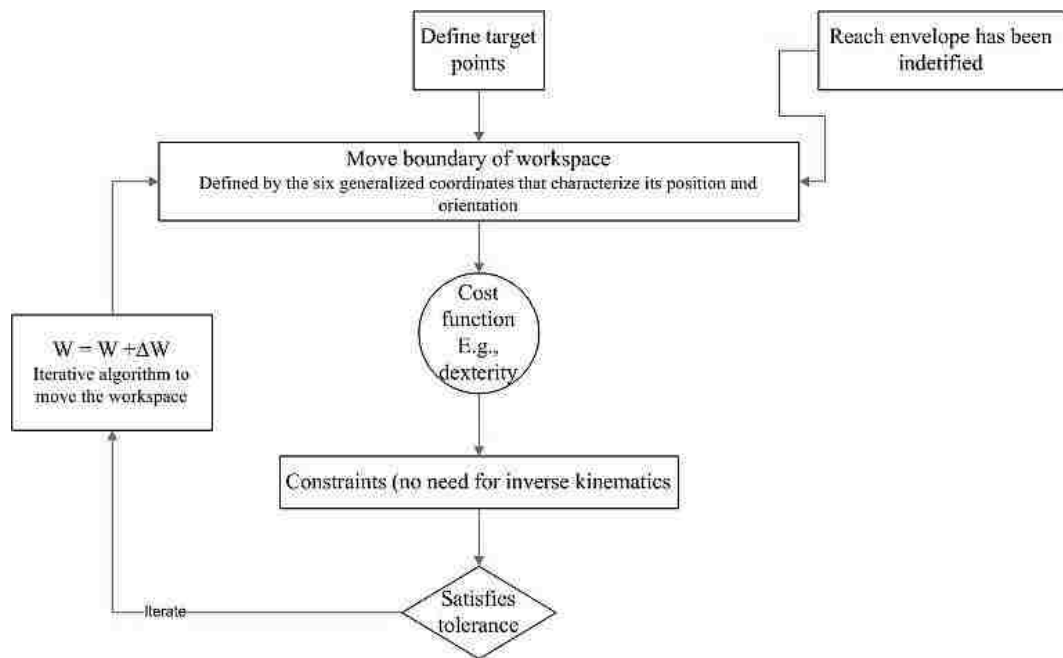
Figure 2-2 Algorithm for achieving placement using dexterity as a measure. Reference: Abdel-Malek, Yu 2004

A solution to determine the optimal path and workspace has also been researched. Ghoshray (1997) aimed at developing an algorithm that determines a collision-free path for a robot or a set of robots. Using Quadtree, a geometrical hierarchical decomposition method, a region was divided into four quadrants. A quadrant was said to be full if the

area defined by the quadrant is filled with a 2D object, empty if area is devoid of the object and mixed if the object is partially inside the region and partially outside. Li, (2006) used random probability to generate the boundary curves of a spatial robot in a two dimensional plane. The kinematic relationship of the joint spaces to the workspace was studied. The differential geometry between 2D and 3D figures, analytical in nature, was studied and the 3D space is addressed by enveloping the boundary curves and displaying it graphically.

Cao, (2011) used the Monte Carlo method and the Beta distribution to determine the valid two dimensional workspace of a three axis planar and spatial robot manipulator. A point cloud of non-uniform densities in the Monte Carlo method is generated using 6000 random numbers with uniform distribution for revolute joints. To improve the accuracy of the workspace boundary, the density distribution of Monte Carlo points has to be known and then the reason for such problems analyzed.
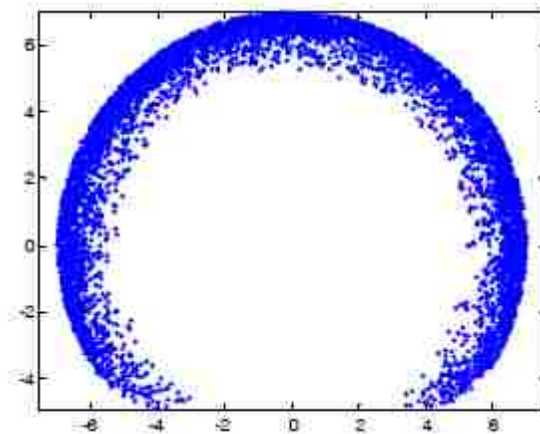
Figure 2-3 Monte Carlo distribution of points in planar workspace. Reference: Cao (2011)

The density of the points of one block in the workspace was analyzed using the following equation:

$$\rho D = \text{Z(Height of histogram)} \frac{\text{Z(Height of histogram)}}{\text{Gross number of point cloud}} \text{ X } 100\% \qquad (2.1)$$

Where, Z (height of histogram) means the point number in the histogram block. Furthermore, using the beta distribution method, a smoother workspace curve with less error was obtained. The curve shown in the figure below was obtained by searching the boundary points and connecting them to construct a closed polygon. Although the figure is not completely representative of the exact workspace and contains some error, the results are certainly better than when uniform distribution is used.
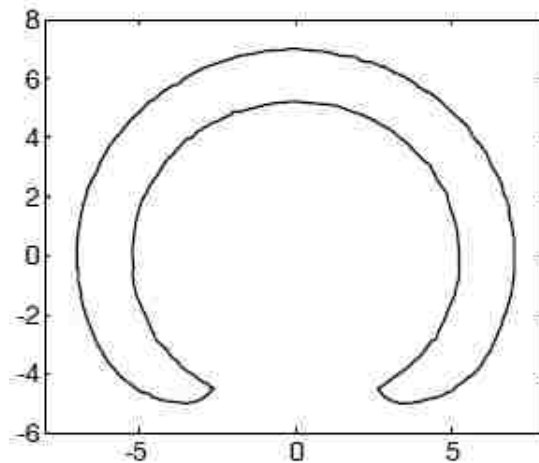
Figure 2-4 Boundary curve of workspace obtained with Beta distribution. Reference: Cao(2011)

With an increasing adaptation of flexible manufacturing systems and the need to reduce setup and launch times, it is important to know beforehand the possible limitations of a robotic manipulator, eliminating the need for trial and error and repeated adjustments in either the virtual or physical domains. The depiction of the workspace is thus very important. It is also; however, very important to figure out a methodology to show the functional work space of a robot that includes the orientation. This is important in several applications such as Non-Destructive testing (NDT), welding, deposition techniques, etc.

12

An analysis considering the geometric and kinematic characteristics combined to solve the functional work space problem has not been done yet. A methodology needs to be developed to define the functional work space for a configuration, and any potential reconfigurations. A literature matrix table has been shown in Appendix A showcasing the research gap in this area.

CHAPTER 3

DESIGN METHODS

3.1 Geometrical assessment of functional workspace problem[1]

The functional workspace of a manipulator is essentially a subset of the work envelope that takes into consideration the orientation of the end-effector. Examining this subset will provide the user/ designer with enough data to evaluate the valid functional space of the tool at a particular or multiple orientations. Many analytical methods are in place to determine the closed work envelope boundary of the robotic manipulator. However, the analytical and mathematical solutions are often complicated by the use of non-linear equations and matrix inversions. Another viable approach, in this case, would be to assess the geometry of the kinematic structure.

A 3D functional workspace of a 6R manipulator is obtained by revolving joint-1 along the Z axis. The 3D functional workspace boundary is essentially an envelope of the planar or 2D curves. The functional workspace is generated by the union of the curves that can be traced by the points of a sequence of arcs or line segments that are caused by the revolution. Therefore, any manipulator that has revolute and prismatic joints can always be geometrically reduced and described by circular arcs and lines while obeying the constraints of the manipulator. The projection of the kinematic structure in 2D

---

[1] Section 3.1 incorporates the outcome of a joint research undertaken in collaboration with
Jill Urbanic, University of Windsor, Windsor, ON, Canada.

geometrically does not dissolve the legitimacy of the manipulator. Care has to be taken, however, to maintain the uniformity of selecting the axes. This is demonstrated below with the kinematic structure of a six-axis revolute serial manipulator – ABB IRB 140.
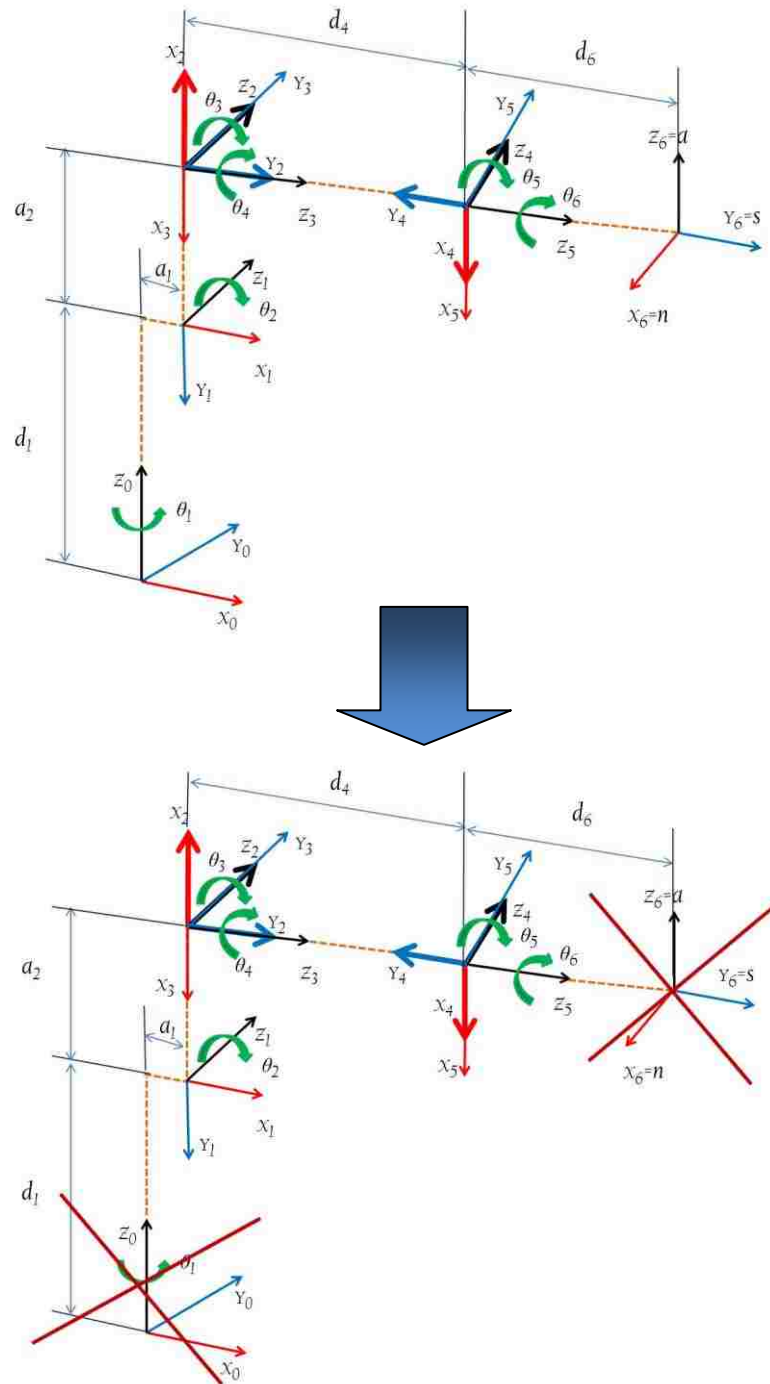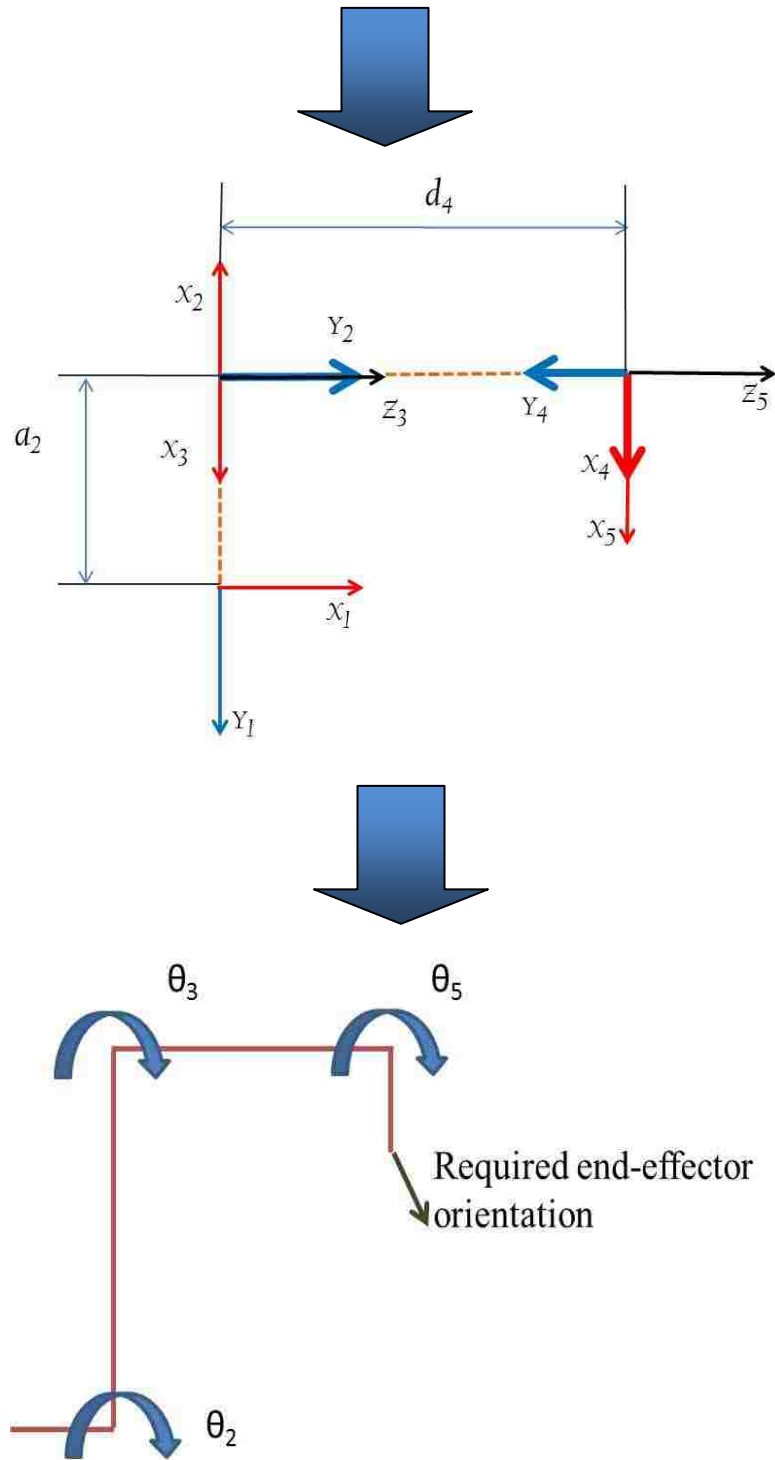
Figure 3-1 Geometric Assessment of the ABB IRB140

When the structure is observed from the side view, it can be reduced into essential links and joints. The problem is broken down into concentrate on only the necessary elements and solution is derived from the first principles. The solution can be engineered further by including the effect of varying joint angles, 4 and 6. The objective here is to find out a solution space, but not to optimise an existing reach issue. Several optimisation techniques such as Monte Carlo method and Beta distribution (Alciatore 1994), (Y. L. Cao 2011), (Ghoshray 1997) have been used to reduce a 3D dimensional problem into 2D. These methods however, require a huge set of data and are not always accurate. Although this research does not intricately deal with path generation and optimal path models, it is possible to reduce a 3D path in the geometrical approach into a set of points in 2D and the functional space assessed. A detailed explanation of the geometrical method is given in Section 4.4.

3.2 ABB IRB 140

The approach in this research is to first explain the frame transformations that are needed to understand the kinematic analysis. The forward kinematic equations are then applied to the ABB IRB-140 robot which is studied in this research. Further, the effect of end-effector positioning is discussed followed by a visual approach taken to adapt θ_5 to be at the required orientation. A working of the empirical approach with the aid of a previously derived formula (Djuric, Urbanic-2009) is then discussed with an adapted manual point generation algorithm. The problem solved using an analytical approach in MATLAB. Several geometric approaches that were tried to find the functional work space are discussed in Appendix C. A projection of two dimensional work space, solved with a geometrical approach, proposed as a solution is then explained with a MATLAB

visual simulation. The change in the functional work space with the change in the orientation of θ_5 is also discussed.

ABB is a leading robot manufacturer that has more than 200,000 robots installed worldwide (Ref: Manufacturer website- www.abb.com; Sep2012). The robot model IRB 140 used in this research is a compact, powerful industrial robot that can handle a variety of applications such as arc welding, spraying, material handling, cutting/deburring, die casting etc. It is a 6 rotational axis robot with a payload of 5kg and multiple mounting options. The axis 5 reach of the IRB 140 is long at 810mm.

Figure 3-2 ABB IRB 140. Reference: ABB IRB 140 Datasheet

Also, the IRB 140 represents the configuration of most widely used six-axis industrial robots. The IRB 140 has good flexibility (with respect to joint limits) and a large work envelope which is useful in solving the functional work space problem. The table below shows the joint limits of the IRB 140.

Table 3-1 Joint limits of the ABB IRB 140

Joint	Type	Limits (°)
1	Rotational	+180 to -180
2	Rotational	+110 to -90
3	Rotational	+50 to -230
4	Rotational	+200 to -200
5	Rotational	+120 to -120
6	Rotational	+400 to -400

The Denavit-Hartenberg or the D-H parameters are commonly used in the robotics domain. Using the D-H parameters the rotation and the position vectors of the end-effector can be found. Each joint in a serial kinematic chain is assigned a coordinate frame. Using the D-H notations, four parameters are needed to describe how a frame i is connected to a previous frame $i-1$. This is used as a foundation to develop the forward kinematic representation. The D-H parameters of the IRB 140 are given in the Table 3-2. The manufacturer stipulated work envelope of the ABB IRB 140 is detailed in Fig.3-4.

Table 3-2 D-H Parameters of the ABB IRB 140 at home position

Joint	θ (°)	D [mm]	A [mm]	α (°)
1	0	352	70	-90
2	-90	0	360	0
3	180	0	0	90
4	0	380	0	-90
5	0	0	0	90
6	-90	65	0	90

The forward kinematic equations for IRB 140 are solved in Section 3.3.5.
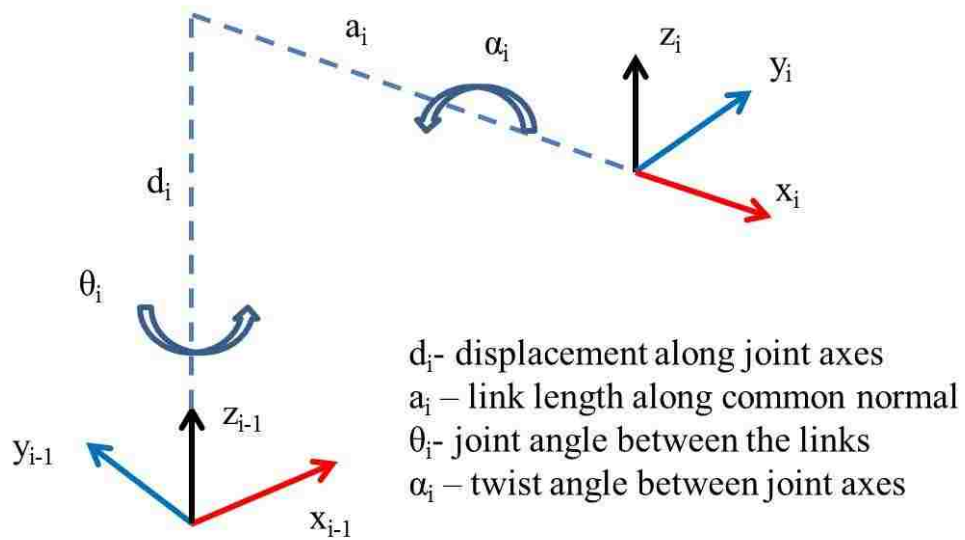
Figure 3-3 Notations used in D-H Parameters
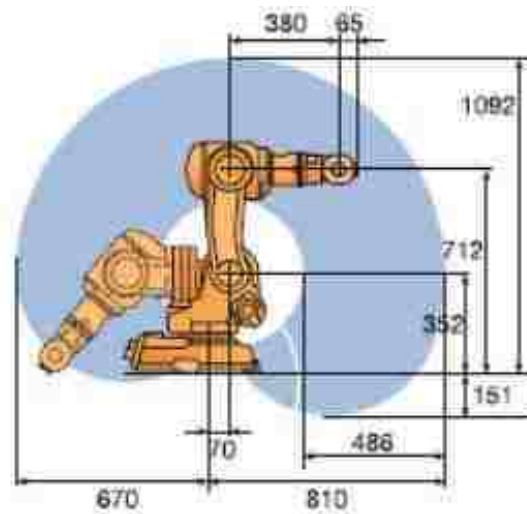
Figure 3-4 Working range(work envelope) of the ABB IRB 140

3.3 Frame Transformations

Before proceeding with kinematic analysis, it is important to understand the frame transformations. Once the homogenous transformation matrix is obtained the forward kinematic equations can be applied to the robot to obtain the coordinates of the end-effector with respect to the base frame. The point 'P' in the Fig.3-5 is described with respect to two co-ordinate frames x, y, z and x*, y*, z*. Note that, the frame x*, y*, z* is nothing but a simple rotation of the frame x, y, z. Though, this rotation does not affect the vector, its co-ordinates and components are changed. These new descriptions which involve different frames are of interest and are used to define different frames and rigid bodies with a base frame as well as each other. Considering the case of the rigid bodies (Fig.3-6), 'Q' is the frame at a point on the rigid body. 'O' is a fixed frame with respect to which the frame 'Q' needs to be defined. The position of frame 'Q' can be found by drawing a vector, OP between the origins of the two frames. The orientation of the frame 'Q' is given by the vectors $\{^{O}\hat{x}_Q, ^{O}\hat{y}_Q, ^{O}\hat{z}_Q\}$. These vectors can be used to describe the orientation of 'Q' in any frame. In this case, the vectors are used to describe frame 'Q' with respect to frame 'O'. These vectors define the rotation of frame 'Q' with respect to frame 'O'. The notation $^{O}\hat{x}_Q$ should be read as "xQ in frame O" meaning that this is the coordinate of xQ in frame 'O'.
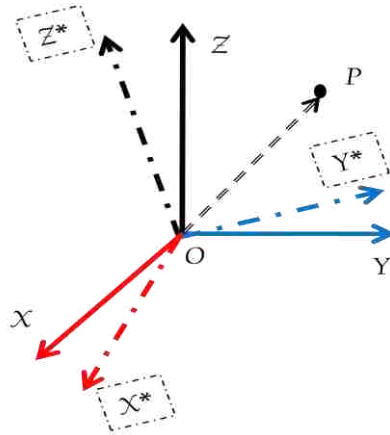
Figure 3-5 Rotation of frame `O` to obtain a new frame x*, y*, z*
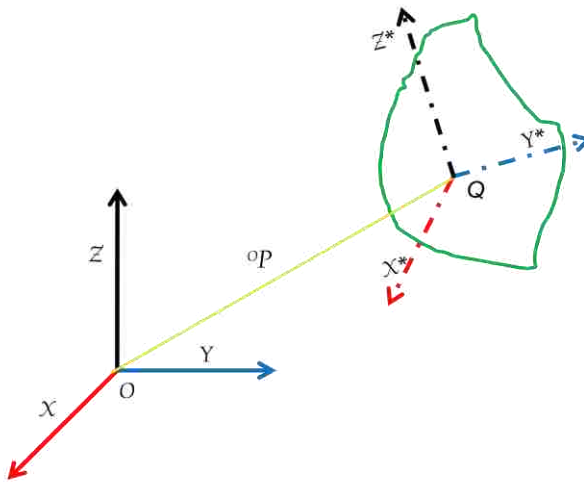
Figure 3-6 Description of frame Q with respect to frame O

The rotation matrix needs to be obtained to describe the rotations of the frame 'Q' with respect to frame 'O'. To arrive at the rotation matrix, consider only the rotation of frame 'Q' neglecting the distance between the frames, ^{O}P.
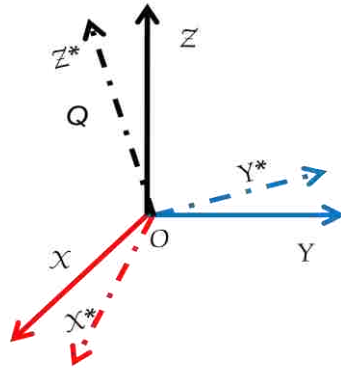
Figure 3-7 Rotation of frame Q

The rotation of frame Q is given by a rotational matrix:

$$^{O}R_{Q} = \begin{bmatrix} r_{11} & r_{12} & r_{13} \\ r_{21} & r_{22} & r_{23} \\ r_{31} & r_{32} & r_{33} \end{bmatrix}$$ (3.1)

With the help of this rotation matrix we can transform the description of x* in Q to $^{O}\hat{x}_{Q}$ as follows:

$$^{O}\hat{x}_{Q} = {}^{O}\hat{R}_{Q} \cdot {}^{Q}\hat{x}_{Q}$$ (3.2)

$\hat{x}_{Q}$ in frame Q is given by matrix: $\begin{bmatrix} 1 \\ 0 \\ 0 \end{bmatrix}$ since the x-vector in its own frame has a unit value along the x-axis. Hence,

$$^{O}\hat{x}_{Q} = {}^{O}\hat{R}_{Q} \begin{bmatrix} 1 \\ 0 \\ 0 \end{bmatrix}$$ (3.3)

Similarly,

$$^{O}\hat{y}_Q =^{O} \hat{R}_Q \begin{bmatrix} 0 \\ 1 \\ 0 \end{bmatrix} \tag{3.4}$$

and,

$$^{O}\hat{z}_Q =^{O} \hat{R}_Q \begin{bmatrix} 0 \\ 0 \\ 1 \end{bmatrix} \tag{3.5}$$

The rotation matrix is therefore, defined as,

$$^{O}R_Q = \begin{bmatrix} ^{O}\hat{X}_Q & ^{O}\hat{Y}_Q & ^{O}\hat{Z}_Q \end{bmatrix} \tag{3.6}$$

The rotation matrix in Eq. (3.6) is nothing but the component(s) of x_Q, y_Q and z_Q in frame

O.

$$^{O}\hat{X}_Q = \begin{bmatrix} \hat{x}_Q.\hat{x}_O \\ \hat{x}_Q.\hat{y}_O \\ \hat{x}_Q.\hat{z}_O \end{bmatrix} \tag{3.7}$$

Therefore, the rotation matrix $^{O}R_Q$ can be written as,

$$^{O}R_Q = \begin{bmatrix} \hat{x}_Q..\hat{x}_O & \hat{y}_Q..\hat{x}_O & \hat{z}_Q..\hat{x}_O \\ \hat{x}_Q.\hat{y}_O & \hat{y}_Q.\hat{y}_O & \hat{z}_Q.\hat{y}_O \\ \hat{x}_Q.\hat{z}_O & \hat{y}_Q.\hat{z}_O & \hat{z}_Q.\hat{z}_O \end{bmatrix} \tag{3.8}$$

From the matrix above it is evident that, $^{O}R_Q = ^{Q}R_O{}^{T}$. An important property can be

derived from the above statement, which is,

$$^{O}R_Q{}^{-1} = ^{Q}R_O = ^{O}R_Q{}^{T} \tag{3.9}$$

As stated above, $^{O}R_Q = ^{Q}R_O{}^{T}$

The columns of the rotational matrix represent the components of x*, y* and z* in frame

O while and the rows are simply, $^{O}\hat{X}_{Q}{}^{T}$, $^{O}\hat{Y}_{Q}{}^{T}$ and $^{O}\hat{Z}_{Q}{}^{T}$.

$$^{O}R_{Q} = \begin{bmatrix} 0 & 0 & 0 \\ 0 & 0 & 1 \\ 0 & -1 & 0 \end{bmatrix} \begin{matrix} \leftarrow & ^{Q}\hat{X}_{O}{}^{T} \\ \leftarrow & ^{Q}\hat{Y}_{O}{}^{T} \\ \leftarrow & ^{Q}\hat{Z}_{O}{}^{T} \end{matrix}$$

$$\uparrow \quad \uparrow \quad \uparrow$$

$$^{O}\hat{X}_{i} \quad ^{O}\hat{Y}_{Q} \quad ^{O}\hat{Z}_{Q}$$

After having defined the rotational matrix, the location of the rigid body Q with orientation and position needs to be defined. Frame {Q} can now completely be defined as: $^{O}\hat{X}_{Q}$, $^{O}\hat{Y}_{Q}$ and $^{O}\hat{Z}_{Q}$

$$\{Q\} = \left\{ ^{O}R_{Q} \quad ^{O}P \right\} \tag{3.10}$$

3.3.1 Mapping

Consider the initial case where a point P in space was described (Fig-3.3) with respect to two frames, O and Q. The vector P was expressed in relation to both the frames and also one frame was expressed with respect to the other frame and also vice-versa. This is called mapping. The description of vector P is changed from frame to frame although the vector remains the same. The description of vector P can be given with regard to frame O as

$$^{O}P = \begin{bmatrix} \hat{X}_{O}.P \\ \hat{Y}_{O}.P \\ \hat{Z}_{O}.P \end{bmatrix} = \begin{bmatrix} \hat{X}_{O}{}^{T} \\ \hat{Y}_{O}{}^{T} \\ \hat{Z}_{O}{}^{T} \end{bmatrix}.P \tag{3.11}$$

This equation can be used to describe the vector P not only in frame O but any other frame. If P is given in frame Q, ^{Q}P would be given as,

$$^{Q}P = \begin{bmatrix} \hat{X}_Q.P \\ \hat{Y}_Q.P \\ \hat{Z}_Q.P \end{bmatrix} = \begin{bmatrix} \hat{X}_Q{}^T \\ \hat{Y}_Q{}^T \\ \hat{Z}_Q{}^T \end{bmatrix}.P \tag{3.12}$$

3.3.2 Translations

In the figure below, the orientation of the {O} and {Q} are same but the position of the two frames is different. A vector is drawn to point P and is located at a distance QP from the origin of frame Q. The distance of point P from the origin of {O} is OP. The distance between the origins of {O} and {Q} is PQORG. The same point P is described here with respect to two frames O and $\overrightarrow{Q}$. $\overrightarrow{QP}$=> OP (Two different vectors).

When performing translations, the description of a vector is changed by changing the vectors involved in the description.
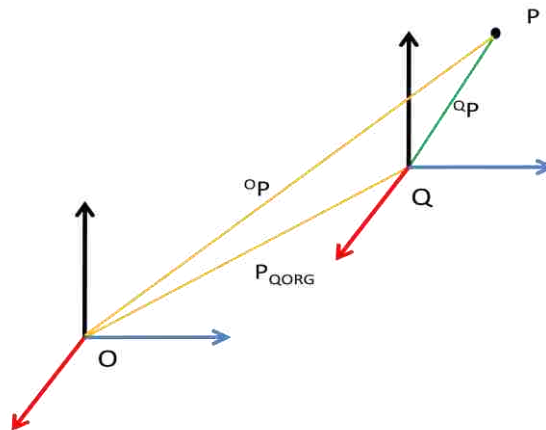
Figure 3-8 Distance of point P with respect to frame O and Q

Here,

$$^{O}P = {}^{Q}P + P_{QORG} \tag{3.13}$$

26

3.3.3 General transformation when rotation and translation are involved

In this case there is an arbitrary frame Q which is not only translated but also rotated about the frame O. The above equation would then be modified to,

$$^O P =^O R_Q{}^Q P + P_{QORG} \tag{3.14}$$
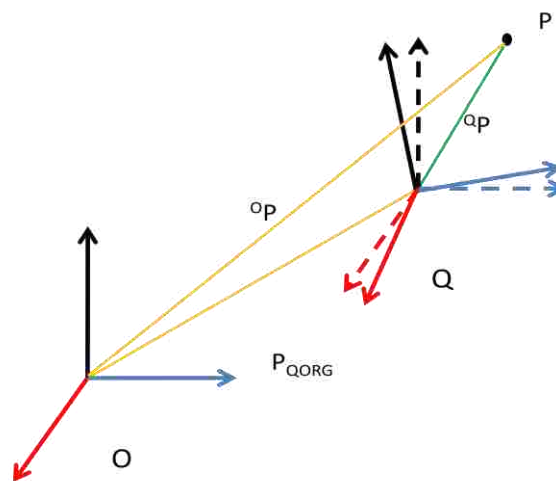
Figure 3-9 Translation and orientation of Q with respect to frame O

This is the general transform.

3.3.4 Homogenous transformation

Using the general transform we can compute and propagate between links. But the description is not easy to carry forward in case of multiple links. Hence, we need a homogenous transform. A homogenous form is not possible to achieve with 3-D space.

To overcome this problem a dimension needs to be added i.e. 4-D. The above equation can then be modified as,

$$\begin{bmatrix} ^O P \\ 1 \end{bmatrix} = \begin{bmatrix} ^O R_Q & P_{QORG} \\ 0 \ \ 0 \ \ 0 & 1 \end{bmatrix} \begin{bmatrix} ^Q P \\ 1 \end{bmatrix} \tag{3.15}$$

The homogenous property is captured in the above equation using the rotation and the translation matrix. The above equation is rewritten as,

$$^O P_{(4X1)} = ^O T_{Q(4X4)} \, ^Q P_{(4X1)} \tag{3.16}$$

Where, $^O T_Q$ is called the homogenous transformation.

3.3.5 Forward Kinematics

Each link frame is completely described with its pose matrix with reference to the preceding link, and sequence of pose matrices are used to compute the pose matrix of the end-effector frame with respect to the base frame $^0 A$.

The D-H Parameters are used to explain the relationship between two links, $^{i-1}A_i$, where 'i' is the number of joints. The homogenous transformation matrix is given as:

$$^{i-1}A_i = \begin{bmatrix} cos\theta_i & -cos\alpha_i \, sin\theta_i & sin\alpha_i sin\theta_i & a_i cos\theta_i \\ sin\theta_i & cos\alpha_i cos\theta_i & -sin\alpha_i cos\theta_i & a_i sin\theta_i \\ 0 & sin\alpha_i & cos\alpha_i & d_i \\ 0 & 0 & 0 & 1 \end{bmatrix} \tag{3.17}$$

The D-H parameters for ABB family of robots with the 6R configuration are given below in Table 3-3.

Table 3-3 D-H Parameters of ABB IRB 140 robot

Z	d_i	θ_i	a_i	α_i
1	352	$\theta_1°$	70	-90°
2	0	$\theta_2°$	360	0°
3	0	$\theta_3°$	0	90°
4	380	$\theta_4°$	0	-90°
5	0	$\theta_5°$	60	90°
6	65	$\theta_6°$	0	90°

The coordinates of the end effector frame, ^0A_n is obtained by consecutively applying the homogenous transformations:

$$^0A_n = {^0A_1}.{^1A_2}.{^2A_3}.....{^{i-1}A_i}.....{^{n-1}A_n} \tag{3.18}$$

Where, ^0A_n is the end-effector frame with respect to the base frame, $^{i-1}A_i$ is the frame transform of the ith joint with respect to i-1, and n is the number of links.

$$^0A_1 = \begin{bmatrix} \cos\theta_1 & -\cos\alpha_1\sin\theta_1 & \sin\alpha_1\sin\theta_1 & a_1\cos\theta_1 \\ \sin\theta_1 & \cos\alpha_1\cos\theta_1 & -\sin\alpha_1\cos\theta_1 & a_1\sin\theta_1 \\ 0 & \sin\alpha_1 & \cos\alpha_1 & d_1 \\ 0 & 0 & 0 & 1 \end{bmatrix} = \begin{bmatrix} \cos\theta_1 & 0 & -\sin\theta_1 & a_1\cos\theta_1 \\ \sin\theta_1 & 0 & \cos\theta_1 & a_1\sin\theta_1 \\ 0 & -1 & 0 & d_1 \\ 0 & 0 & 0 & 1 \end{bmatrix}$$

$$\tag{3.19}$$

$$^1A_2 = \begin{bmatrix} \cos\theta_2 & -\cos\alpha_2\sin\theta_2 & \sin\alpha_2\sin\theta_2 & a_2\cos\theta_2 \\ \sin\theta_2 & \cos\alpha_1\cos\theta_1 & -\sin\alpha_2\cos\theta_2 & a_2\sin\theta_2 \\ 0 & \sin\alpha_2 & \cos\alpha_2 & d_2 \\ 0 & 0 & 0 & 1 \end{bmatrix} = \begin{bmatrix} \cos\theta_2 & 0 & -\sin\theta_2 & a_2\cos\theta_2 \\ \sin\theta_2 & 0 & \cos\theta_2 & a_2\sin\theta_2 \\ 0 & 0 & 1 & 0 \\ 0 & 0 & 0 & 1 \end{bmatrix}$$

$$\tag{3.20}$$

$$
^2A_3 = \begin{bmatrix} \cos\theta_3 & -\cos\alpha_3\sin\theta_3 & \sin\alpha_3\sin\theta_3 & a_3\cos\theta_3 \\ \sin\theta_3 & \cos\alpha_3\cos\theta_3 & -\sin\alpha_3\cos\theta_3 & a_3\sin\theta_3 \\ 0 & \sin\alpha_3 & \cos\alpha_3 & d_3 \\ 0 & 0 & 0 & 1 \end{bmatrix} = \begin{bmatrix} \cos\theta_3 & 0 & -\sin\theta_3 & a_3\cos\theta_3 \\ \sin\theta_3 & 0 & -\cos\theta_3 & a_3\sin\theta_3 \\ 0 & 1 & 0 & 0 \\ 0 & 0 & 0 & 1 \end{bmatrix}
$$

$$(3.21)$$

$$
^3A_4 = \begin{bmatrix} \cos\theta_4 & -\cos\alpha_4\sin\theta_4 & \sin\alpha_4\sin\theta_4 & a_4\cos\theta_4 \\ \sin\theta_4 & \cos\alpha_4\cos\theta_4 & -\sin\alpha_4\cos\theta_4 & a_4\sin\theta_4 \\ 0 & \sin\alpha_4 & \cos\alpha_4 & d_4 \\ 0 & 0 & 0 & 1 \end{bmatrix} = \begin{bmatrix} \cos\theta_4 & 0 & -\sin\theta_4 & 0 \\ \sin\theta_4 & 0 & \cos\theta_4 & 0 \\ 0 & -1 & 0 & d_4 \\ 0 & 0 & 0 & 1 \end{bmatrix}
$$

$$(3.22)$$

$$
^4A_5 = \begin{bmatrix} \cos\theta_5 & -\cos\alpha_5\sin\theta_5 & \sin\alpha_5\sin\theta_5 & a_5\cos\theta_5 \\ \sin\theta_5 & \cos\alpha_5\cos\theta_5 & -\sin\alpha_5\cos\theta_5 & a_5\sin\theta_5 \\ 0 & \sin\alpha_5 & \cos\alpha_5 & d_5 \\ 0 & 0 & 0 & 1 \end{bmatrix} = \begin{bmatrix} \cos\theta_5 & 0 & \sin\theta_5 & 0 \\ \sin\theta_5 & 0 & -\cos\theta_5 & 0 \\ 0 & 1 & 0 & 0 \\ 0 & 0 & 0 & 1 \end{bmatrix}
$$

$$(3.23)$$

$$
^5A_6 = \begin{bmatrix} \cos\theta_6 & -\cos\alpha_6\sin\theta_6 & \sin\alpha_6\sin\theta_6 & a_6\cos\theta_6 \\ \sin\theta_6 & \cos\alpha_6\cos\theta_6 & -\sin\alpha_6\cos\theta_6 & a_6\sin\theta_6 \\ 0 & \sin\alpha_6 & \cos\alpha_6 & d_6 \\ 0 & 0 & 0 & 1 \end{bmatrix} = \begin{bmatrix} \cos\theta_6 & 0 & \sin\theta_6 & 0 \\ \sin\theta_6 & 0 & -\cos\theta_6 & 0 \\ 0 & 1 & 0 & d_6 \\ 0 & 0 & 0 & 1 \end{bmatrix}
$$

$$(3.24)$$

The pose matrix of the end-effector with relation to its base frame is thus obtained as given in the equation below:

$$
^0A_6 = \begin{bmatrix} n_x & s_x & a_x & p_x \\ n_y & s_y & a_y & p_y \\ n_z & s_y & a_z & p_z \\ 0 & 0 & 0 & 1 \end{bmatrix}
\tag{3.25}
$$

The upper 3x3 matrix represents the rotational matrix while the 3x1 matrix represents the position of the end-effector. To help visualize the frame transforms, the end–effector matrix is shown below with the D-H Parameters given in Table 3-4.

Table 3-4 D-H Parameters at a particular position for the ABB IRB 140 ROBOT

I	d_i	θ_i	a_i	α_i
1	352	0°	70	-90°
2	0	40°	360	0°
3	0	180°	0	90°
4	380	50°	0	-90°
5	0	0°	60	90°
6	65	-90°	0	90°

$$
^0A_6 = \begin{bmatrix} -0.5909 & -0.6357 & 0.4966 & 35.0813 \\ -0.6446 & 0.0020 & -0.7645 & 46.6506 \\ 0.4850 & -0.7719 & -0.4109 & -196.1634 \\ 0 & 0 & 0 & 1 \end{bmatrix}
\tag{3.26}
$$

The position and orientation of the end effector with respect to its base is well translated through the homogenous transformations. The forward kinematic equations are used to describe, analytically, all the joint positions and orientations of the manipulator in order to obtain a feasible solution within the limits of the manipulator.

CHAPTER 4

METHODS FOR DETERMINATION OF THE FUNCTIONAL WORKSPACE

4.1 Manual approach to project three dimensional functional workspace

To create a valid solution space, it is important to understand the joint movements, joint dependencies, and orientation of the end effector. Furthermore, it is necessary to visually represent the functional work space so that a more analytical and mathematical methodology can be established.

Workspace5 simulation software was used to explore the functional workspace manually. Multiple orientations were investigated for this purpose and the results from the tool orientation considered being at 90° facing down and normal to the work piece has been shown. To keep the tool at this orientation it was observed that θ_5 has to be adjusted/ adapted to be normal to the work piece every time there was a rotation in θ_2 or θ_3. A flow chart explaining the initial algorithm used to create a functional work space is given below. The notations used in the flowchart (Fig.4-1) are as follows:

ϕ = Desired orientation angle.

Δ = Increment/decrement of 10°

θ_{max} = Maximum rotational limit of the joint

θ_{min} = Minimum rotational limit of the joint
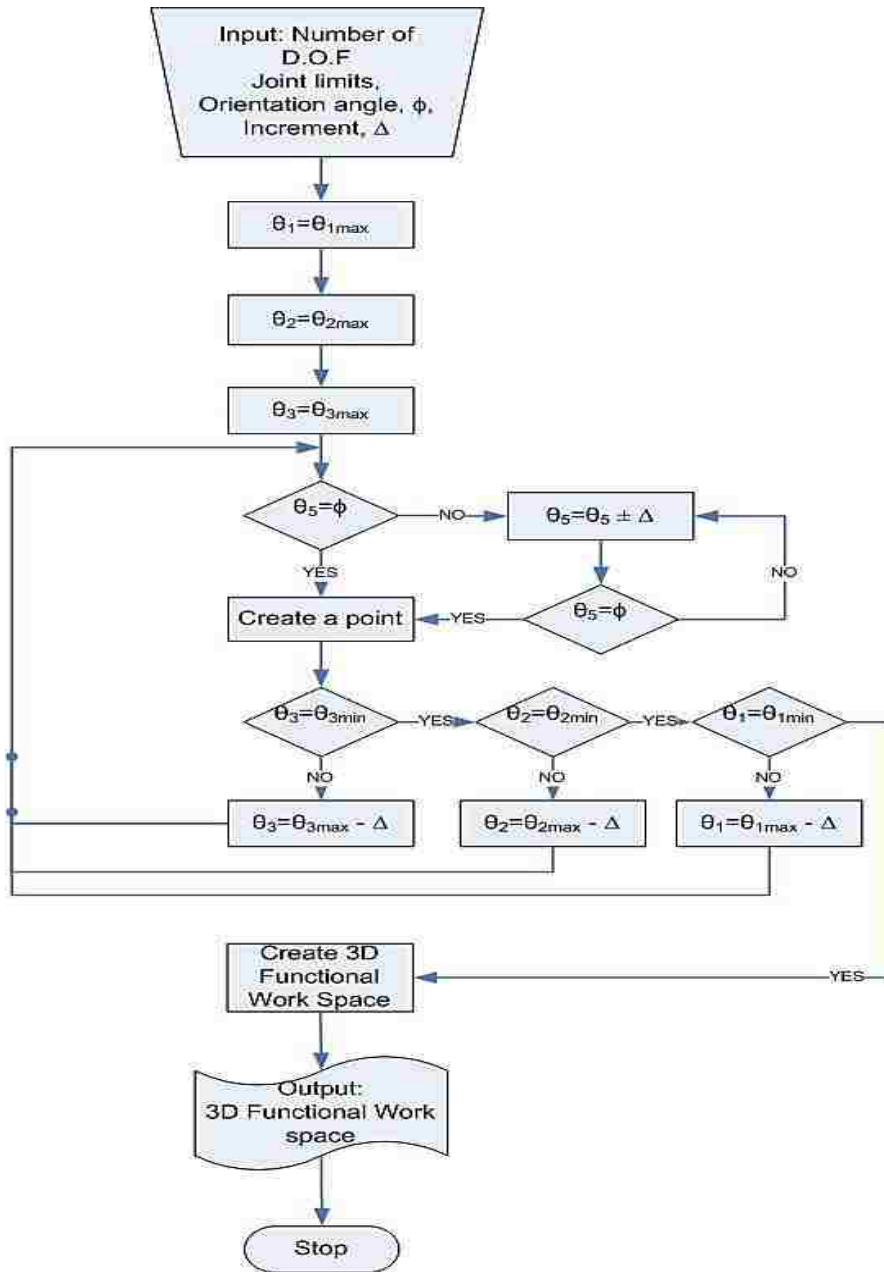
Figure 4-1 Three dimensional functional workspace algorithm

The increment Δ is considered to be $10°$. This is considered to be an optimum value because a value lesser than $10°$ will populate the point cloud without any contribution to value or shape of the workspace set. A value higher than $10°$ will result in a scattered

illustration of the functional workspace which will result in an inaccurate shape. The orientation angle, ϕ is the required orientation set by the user, considered to be 90° vertically downwards in this case.

To visually construct the functional workspace, θ_1, θ_2 and θ_3 are moved to their maximum limits, i.e. +180, +90 and +50 respectively. θ_5 is then visually adjusted to be exactly 90° vertically downwards. A Geometric Point (GP) is recorded at this position. The value of θ_3 is then reduced by a decrement of 10° and θ_5 is adjusted again to achieve desired orientation, ϕ. The process is repeated till θ_3 reaches it minimum limit. Now, the joint angle, θ_2 is decremented by Δ till its minimum limit and θ_3 is moved from its maximum limit to minimum limit while θ_5 is adjusted to be at ϕ. For an IRB140, approximately 300-400 GPs are created between the maximum and minimum limits of θ_2. This process is repeated for all values of θ_1, θ_2 and θ_3. The joint angles θ_4 and θ_6 are kept constant in this process as they do not contribute to achieve a desired orientation of the tool.

Each point thus created can be also be evaluated using the forward kinematic equations. The kinematic equations can reveal the position of the robot in space which can further help with understanding the physical boundaries of the functional workspace, distance of a point from the boundary of the functional workspace etc. Fig.4-2 shows a step-by-step process of how each point is created in a commercial simulation software package.

Step-1: Move theta 2 and theta 3 to maximum

Step-2: Visually adjust theta 5 to required orientation

Step-3: Move theta 3 through decrement while adjusting theta 5

Step-4: Create functional work space for all possible values of theta 2 and theta 3
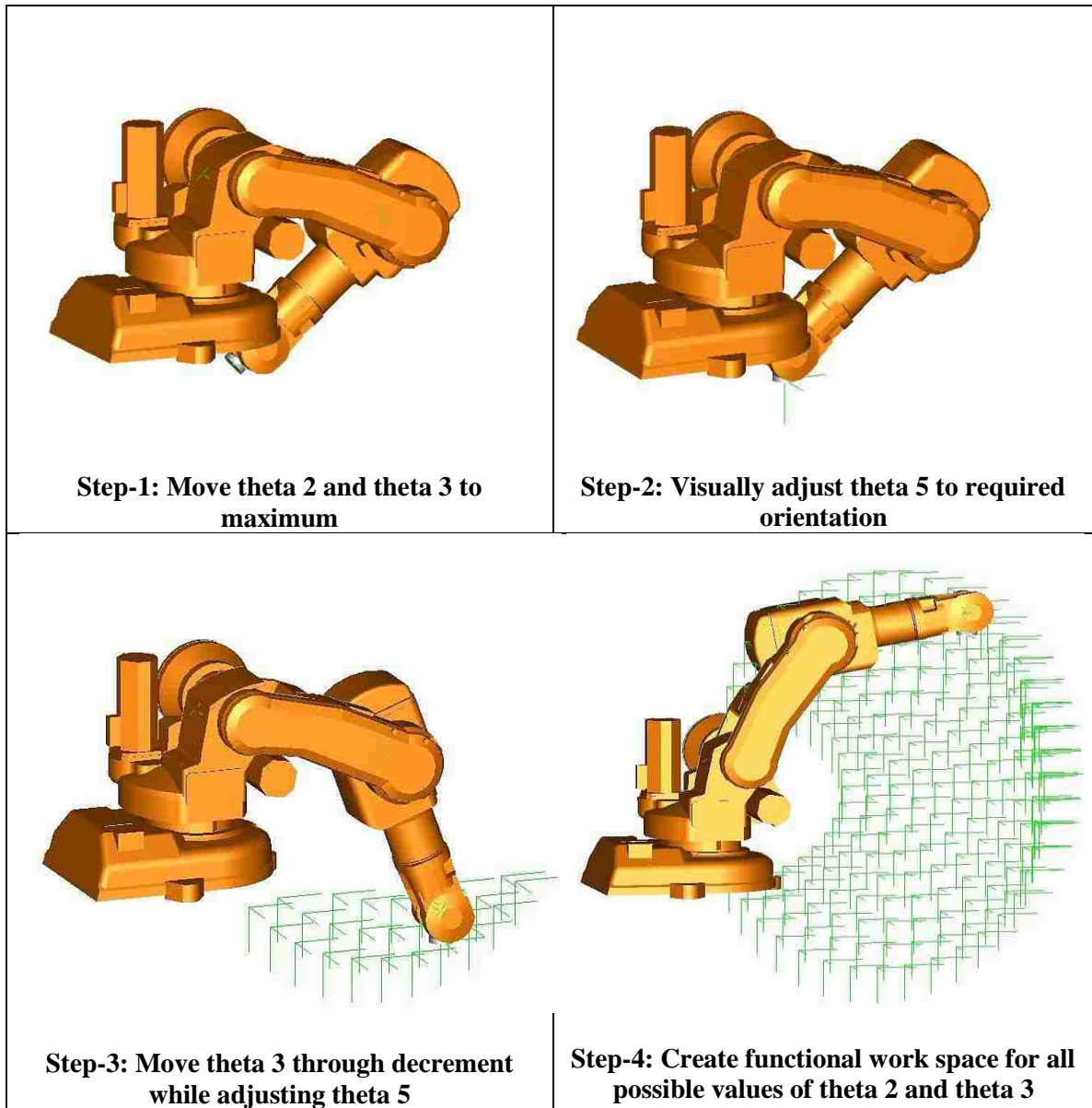
Figure 4-2 Steps invloved for visually sketching the functional workspace at 90° (normal to the base) orientation

The visual representation helps in understanding the possible geometry of the functional workspace. It provides an appreciation of the size and space of the functional workspace with an understanding of how the joint limits of the robot affect the functional workspace. Several parameters are used to describe the geometry of the robot. Some of

these are; the distance 'a' between two joints i and i+1, the angle 'θ' between the vectors i and i+1. All these geometric parameters are bound by constraints.

For example, the angle θ must be such that $|\cos\theta_i| \geq \cos\theta_d$ where θ_d is the orientation of the joint. This shows that the functional workspace can possibly be restricted to lie in a specific region of space and this region will define all the position/orientation(s) that can be reached. For example, the link length 'a' of joint-2 should always lie between its limits $0 \leq a \leq 360$ and $\cos\theta_i$ (90 in this case) should always lie between $|\cos 90| \geq \cos 110$ to obtain the functional work space.

The investigation of the visual plotting of the functional work space can be separated into two parts. The one geometrical, the other mechanical (related to joints). The robotic functional work space can then be investigated without the causes of motion and can be represented with analytical formulae which will define the position of each point on the body. This separation from geometry with joint motion and links will enable the problem to be broken down into much simpler and basic form where the mechanics and geometry can be solved separately.
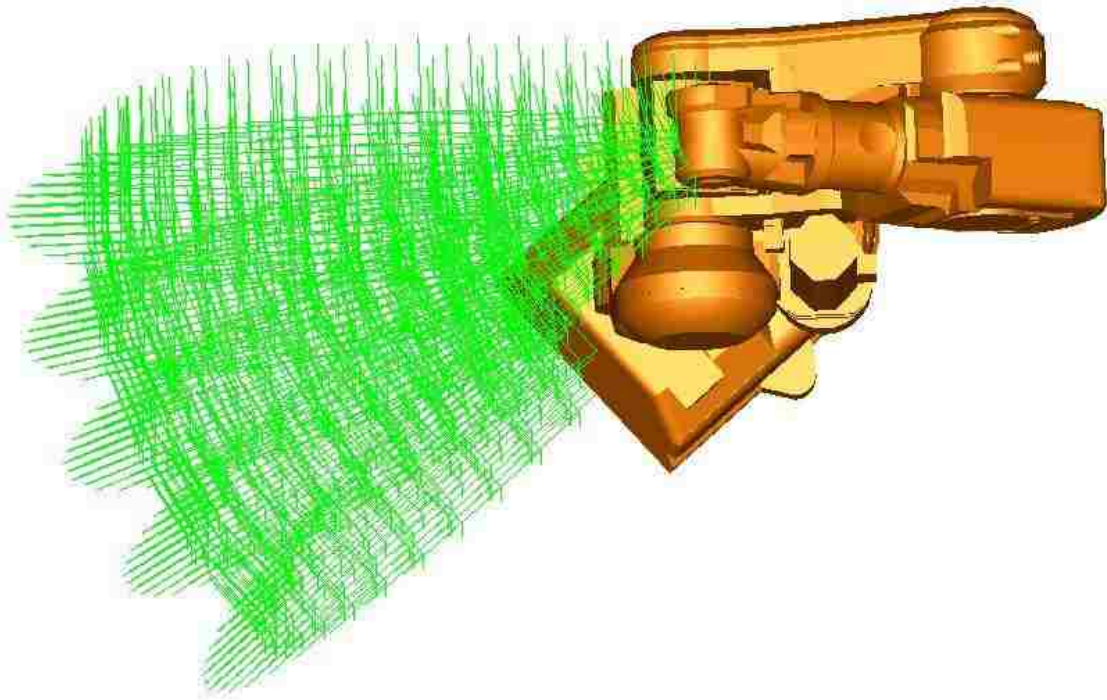
Figure 4-3 3D functional workspace with iteration in θ_1

Creating a complete 3D map of the functional work space is tedious and complex. The number of points needed to sketch is many and is time consuming. The visual method is not foolproof and it is often difficult to judge if θ_5 is at the required orientation. There is often a risk of missing a point in the cloud and the high density of points at certain areas makes it difficult to understand a new point plot. A figure showing a partial sketch of the functional workspace in 3D is shown in Fig.4-3. The visual depiction does help in creating a methodology and developing an empirical approach that will help validate an analytical and a geometrical solution.

4.2 Empirical interpretation to project two dimensional functional workspace

Creating a three dimensional workspace is complex and can be confusing when considering multiple orientations. The inclusion of different constraints for θ_4 and θ_6 increases the complexity even for the 2D (Refer Table-4-2). It can be seen from Fig. 4-3, that the slices of functional work space region that are created for every increment of θ_1 are similar to each other. The shift in the plot depends on the movement of joint-1 across the 3D space in this case. Hence, it is viable to create a two dimensional functional workspace plot in the X-Y plane and further extend the 2D shape into 3D. This will not only reduce the complexity but will help in standardizing a methodology that can be used to create the functional workspace for a family of robots.

The cloud of points is considerably reduced and simplified leading to a better understanding of the position and orientation of the robot in space through forward kinematics. Additionally, the projection of the functional workspace in 2D will not undermine the kinematics or the parameters of the robot that are needed to be studied in creating a functional workspace. In fact, the 2D geometry will help understand which parameters are important to create an accurate representation of the functional workspace and which joints and links are to be studied to obtain an accurate shape.

Special cases that result in disjoint and irregular shaped 3D workspaces are discussed in subsequent chapters. An empirical approach algorithm for manual point generation was presented by Djuric, Urbanic; 2009 which has been adapted to suit this research. Also, a functional workspace formula to find out a resulting θ_5 angle for a set of θ_2 and θ_3 values was also presented.

Joint limits, increment Δ,

Orientation angle ϕ

Twist angles α_1, α_2

$K = \cos \alpha_2$

$\theta_1 = \theta_{1\max}$

$\theta_2 = \theta_{2\max}$

$\theta_3 = \theta_{3\max}$

$\theta_5 = K\phi - (\theta_2 + K\theta_3)$

$\theta_5 < \theta_{5\min}$ — *Yes* → $\theta_3 = \theta_{3\max} - \Delta$

No

Create a point

$\theta_5 = \theta_{5\max}$ *or* $\theta_5 = \theta_{5\min}$ — *Yes*

No

$\theta_3 = \theta_{3\min}$ — *Yes* → $\theta_2 = \theta_{2\min}$ — *Yes* → *Do you want 2 − 3 Workwindow?* — *Yes* → OUTPUT: 2 - 3 Workwindow

No → $\theta_3 = \theta_{3\max} - \Delta$

No → $\theta_2 = \theta_{2\max} - \Delta$

No → $\theta_1 = \theta_{1\min}$ — *Yes* → OUTPUT: 1 - 2 - 3 Workwindow

No → $\theta_1 = \theta_{1\max} - \Delta$
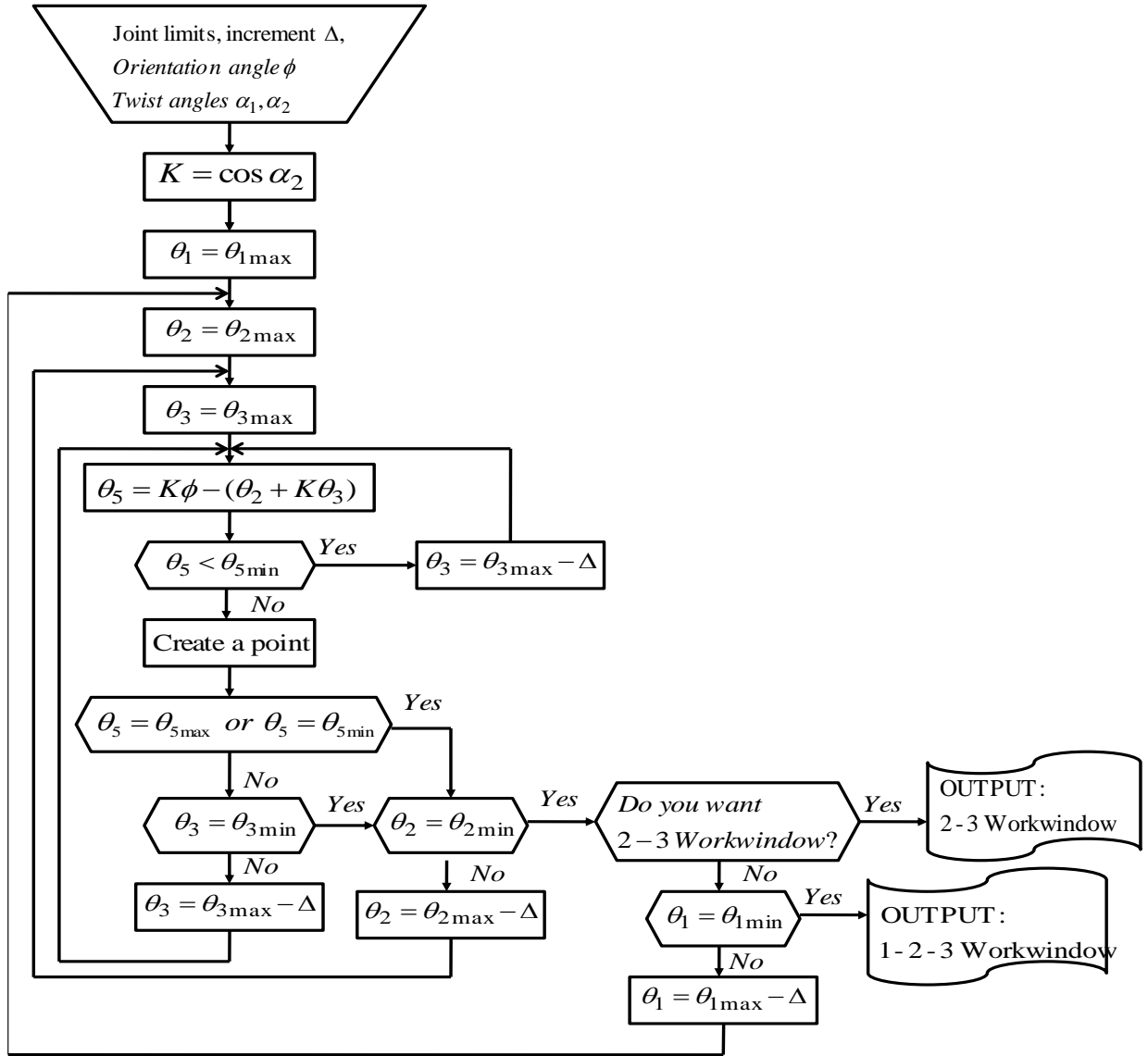
Figure 4-4 : Manual point generation algorithm. Reference: Djuric, Urbanic (2009)

The algorithm considers two different types of output depending on whether θ_1 is considered to be varying or fixed. A formula to calculate a resultant θ_5 value for a value of θ_2 and θ_3 is derived. The visual algorithm wherein θ_5 is adjusted to be at a particular orientation, compliments the formula. The terms in the formula are as explained below:

$$\theta_5 = k\phi - (\theta_2 + k\theta_3) \tag{4.1}$$

39

Where,

K= $\cos\alpha_2$

α = Twist angle

ϕ = Desired orientation angle.

   The above algorithm has been further simplified and adapted for this research. This modified algorithm is given in Fig. 4-6. θ_1, θ_4 and θ_6 are kept constant and these joint angles do not affect the functional workspace. These angles do not contribute to the construction of functional workspace. θ_m in the algorithm (Fig.4-6), is the rotation angle for a particular increment. A comparison of the functional workspace created by this algorithm and a two joint (θ_2 and θ_3) work envelope is given in Fig. 4-5.
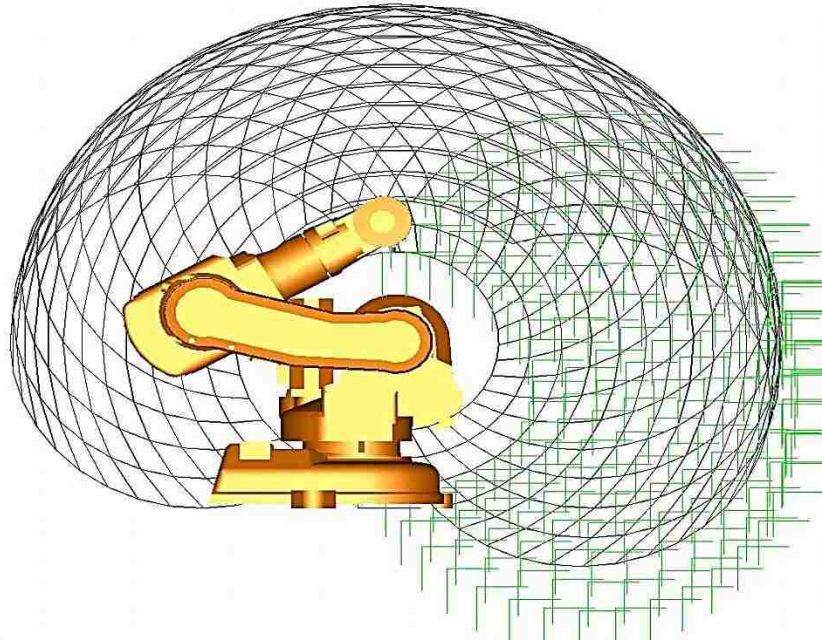
Figure 4-5 : Comparison of functional workspace for 90° orientation with two joint work envelope

   In Fig.4-5 the black net represents the work envelope while the green points represent the functional workspace. The functional workspace exceeds the work envelope in the

lower right region since the whole kinematic structure is assessed for the functional workspace while only two joints – 2 and 3 are considered while creating work envelope.
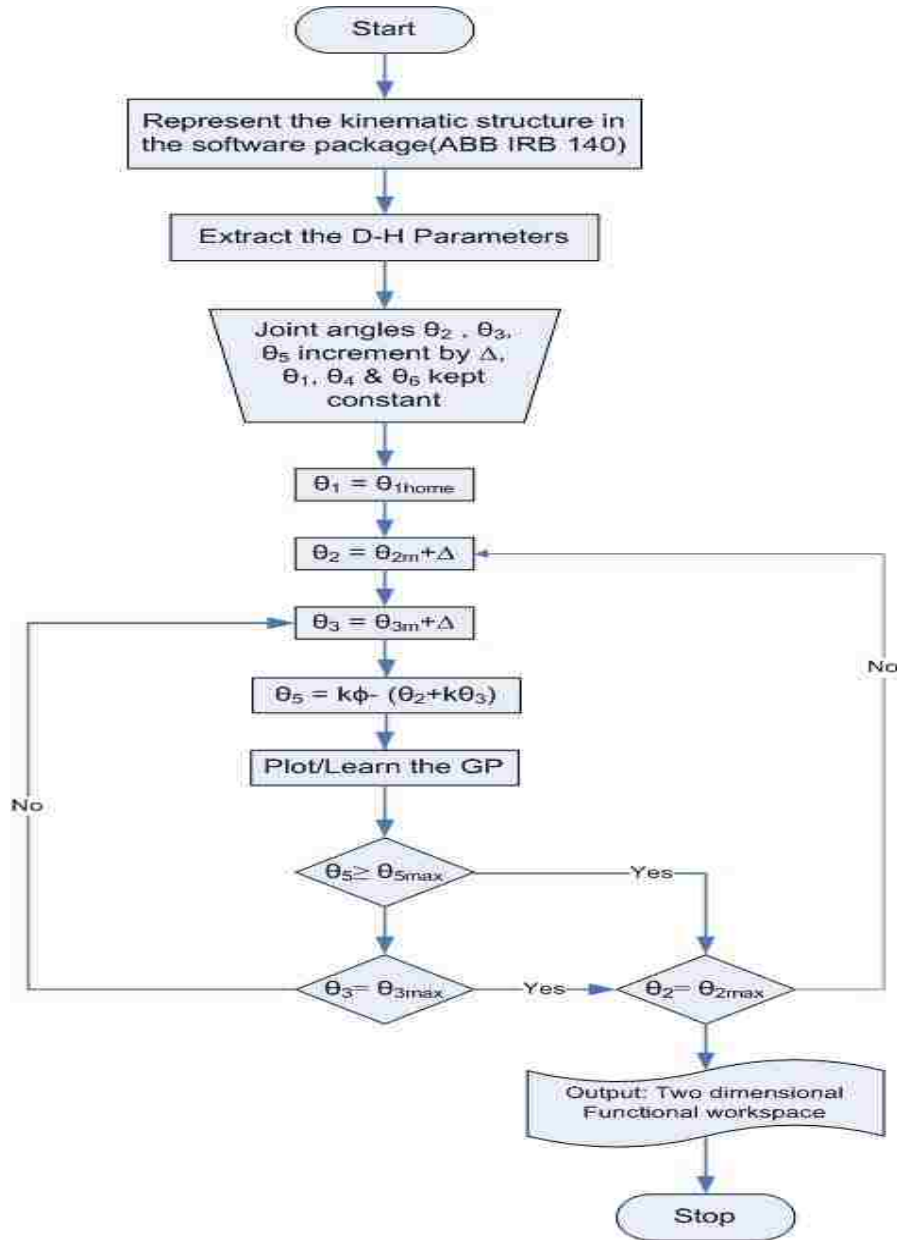
Figure 4-6 : Modified point generation algorithm

This empirical investigation provides a complete idea of the geometry and makes it easier to extract a particular point and assess the orientation and position of the robot using forward kinematics. Furthermore, the empirical investigation reaffirms the findings

of the manual method and helps achieve a methodology and a formula to solve the functional workspace problem. The empirical formula is well suited to capture the complexity and contextual data. It is verified that θ_2, θ_3 and θ_5 are responsible in projecting the functional workspace while θ_1, θ_4 and θ_6 can be kept constant. Based on the parameters that affect the functional workspace the geometrical and mechanical aspects of the problem can now be well demarcated.

The algorithm is applied to another robot, Nachi SC80LF. The D-H parameters of the 80LF are given below.

Table 4-1 D-H Parameters Nachi SC80LF

i	d_i (mm)	$\theta_i°$	ai (mm)	$\alpha_i°$
1	1070	180°	-340	-90°
2	0	180°	910	0°
3	0	90°	200	90°
4	1860	0°	0	-90°
5	0	0°	0	90°
6	215	-90°	0	90°

The same exact algorithm is found to be inapplicable to the Nachi SC80LF. θ_2, θ_3 and θ_5 need to be pushed to minimum and then incremented by Δ to sketch the functional workspace. The formula to know the θ_5 angle is also to be changed to suit the Nachi. The formula is adapted as below:

$$\theta_5 = k\phi - (\theta_2 - k\theta_3) \tag{4.2}$$

Where,

$K = -cos\alpha_2$

α = Twist angle

ϕ = Desired orientation angle.

The difference is in the constant, K, which is now equal to - $\cos\alpha_2$. Also, $(\theta_2 + k\theta_3)$ in the formula is changed to $(\theta_2 - k\theta_3)$. The shape of the functional workspace thus generated is given in Fig. 4-7.

The empirical investigation although helps with create a methodology for the IRB 140, the same exact methodology is inapplicable to a robot with similar configuration. The realisation of important parameters through the empirical method also requires that more information be provided with respect the necessary parameters, to enable solving for different configurations and also orientations. To adapt and enable inclusion of a new configuration requires going back to the visual approach again to modify the empirical solution.

A more inclusive and generalised approach that can include a family of robots, i.e. said to be similar through their kinematic structure will enable a better solution. Although it will require little modification, it will be less complex and will take shorter time to develop. Additionally, the solution needs to be simpler and rudimentary to be applied and understood while retaining the limitation inferred by the structural kinematics of the robot. The next section deals with adopting a more analytical approach that considers the Equation 4.1.
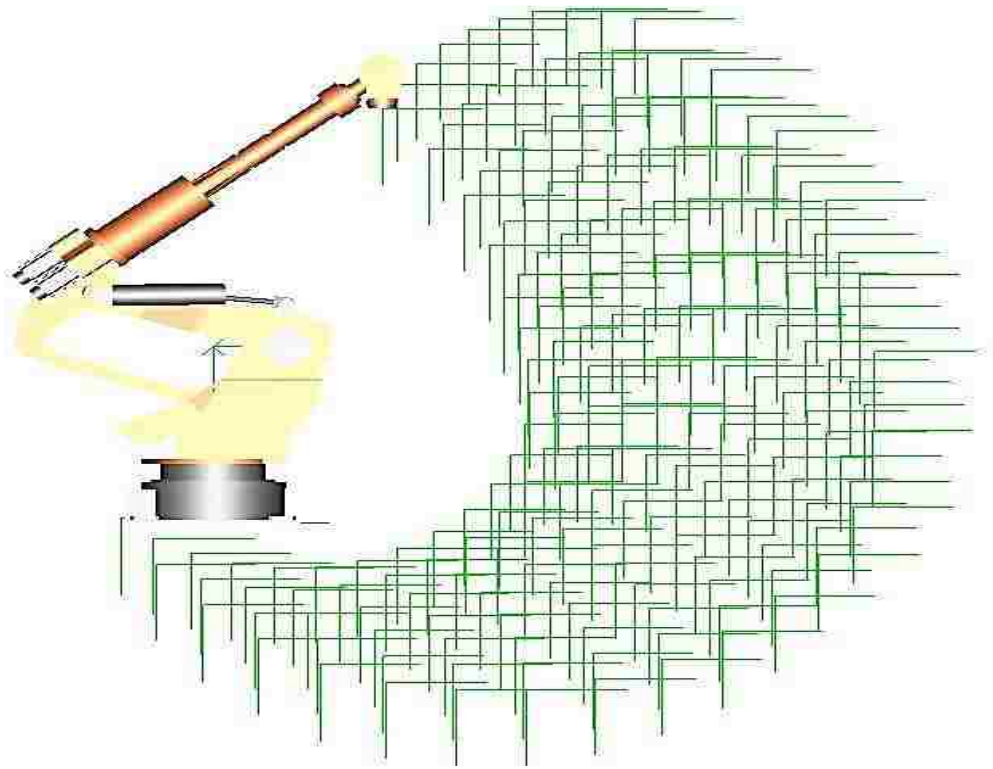
Figure 4-7 Functional workspace of 90° orientation for Nachi SC80LF

4.3 Analytical approach to project two dimensional functional workspace

The analytical approach is adopted to reduce the system to the elements necessary to plot the functional work space curve and study the type of interactions that exist between these elements. Each variable, such as joint angles are modified one at a time and the results are inferred. The analytical approach allows for the isolation of each joint angle. MATLAB, a math based programming environment is used to visualize and simulate the analytical approach. The results obtained are compared to the empirical and geometrical approaches.

The empirical investigation needs much information to be able to arrive at a solution and also needs visualisation of what the user is doing at every step. The aim of the analytical approach is to arrive at a visual shape of the functional workspace just from the D-H parameters and the joint limits, which lends itself to automation for various robot configurations, reconfigurations and other related scenario analyses.

Programming a solution also eliminates the need for having to calculate the forward kinematic equations for each point and orientation. Using the D-H parameters and the forward kinematic equations (Eq. 3.18- Eq.3.25) the position vectors of the X and Z coordinate for the end-effector of the IRB 140 is extracted for every point between the limits and sketched on a 2D graph. The code in MATLAB with D-H parameters and joint limits of IRB 140 is given in Appendix B. A flowchart describing the logic is presented in Fig. 4-8.
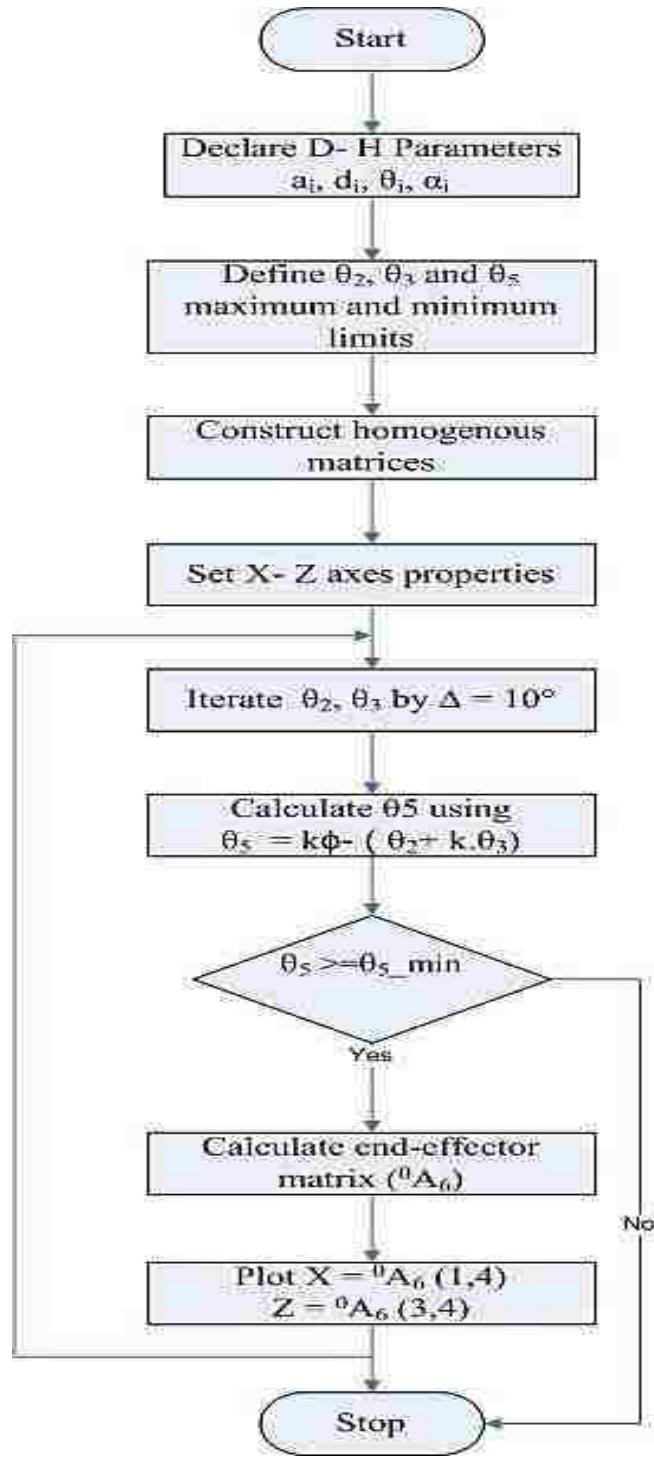
Figure 4-8 Logic used to program analytical approach for functional workspace in MATLAB

The D-H parameters for the IRB 140 are first declared, followed by the minimum and maximum limits for the joints 2, 3 and 5. The homogenous matrices are then computed for all the points within the maximum and minimum limits of the joints. The condition for orientation of θ_5 is then applied to all the feasible points using the formula in Eq. 4.1. For all the possible values between the limits of θ_2 and θ_3 at every increment of $\Delta = 10°$, θ_5 is calculated between its own limits. From all such points, the position vectors for X and Z are extracted and plotted on an X-Y plane. The algorithm in Fig. 4-6 is replicated in the program. The result of the program is given below:
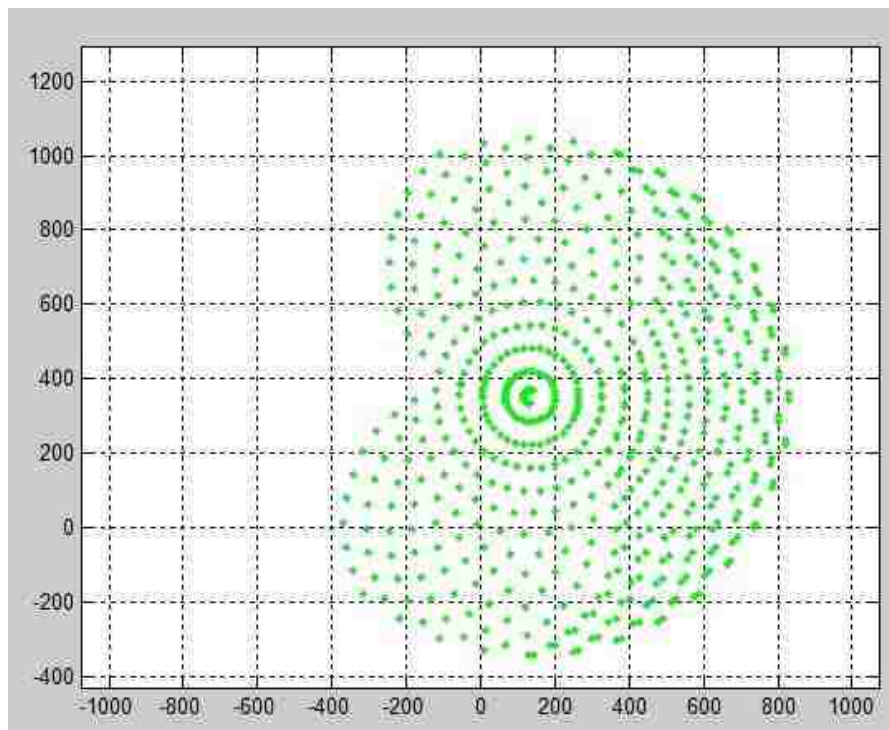
Figure 4-9 Analytical MATLAB functional workspace result for the 6R robot with the end effector at 90° (normal to the base). Note the robot origin is at 0,0 for this plot

The plot seen above is of all the points that passed the θ_5 condition and are within the limits. The robot base is positioned at (0, 0) on the grid. Each point in the graph represents the X and Z position of the end –effector. The plot represents all the points in

47

the X-Z plane that the robot can reach at 90° orientation. It has to be noted that, θ_6 is held constant and is actually an offset and the points generated are based on the θ_2, θ_3 and θ_5 values. It can be seen from the figure that several, 'C' shaped arcs are generated throughout. This is due to θ_3 being varied through it limits for every value of θ_2. It is observed that the points are generated, one after the other in the same manner as in the empirical approach when the robot is moved through each joint limit.

The graph is extended to -400 on the Y plane due to θ_2 and θ_3 minimum limits of -90 and -230 respectively. In the empirical methodology, the inner and outer boundaries are generated when θ_2, θ_3 or θ_5 is at its maximum limits and does not consider the effects of θ_4 and θ_6. The inner boundary is solely generated when θ_3 is at its maximum. A comparative figure with the results obtained in the empirical investigation and the analytical approach is detailed below. It is evident that, the analytical functional workspace (Fig. 4-10) curve is larger than the one obtained through the empirical investigation.

While constructing the functional workspace curve using the empirical method, θ_1, θ_4 and θ_6 are constrained and are always kept constant. θ_2, θ_3 and θ_5 are moved independently without changing θ_1, θ_4 and θ_6 values. This captures the majority of the points that are reachable at a said orientation with the empirical method but does not present the points that are reachable with a particular orientation when θ_1, θ_4 and θ_6 are varied. However, no change is observed in θ_1 since the curve generated is 2D and as mentioned rotation about θ_1 will help generate a three dimensional curve and is not a part of this research.

These constraints are not applied in the analytical approach; the forward kinematic equations that are computed include variations in θ_1, θ_4 and θ_6. X and Z positions for the tool when there is a change in θ_1, θ_4 and θ_6 are also included. Fig. 4-11 shows the position of the robot when θ_1, θ_4 and θ_6 are varied in the empirical method to reach a point in curve obtained from the analytical approach.

a) Functional workspace projection using empirical investigation

b) Functional workspace projection using analytical approach
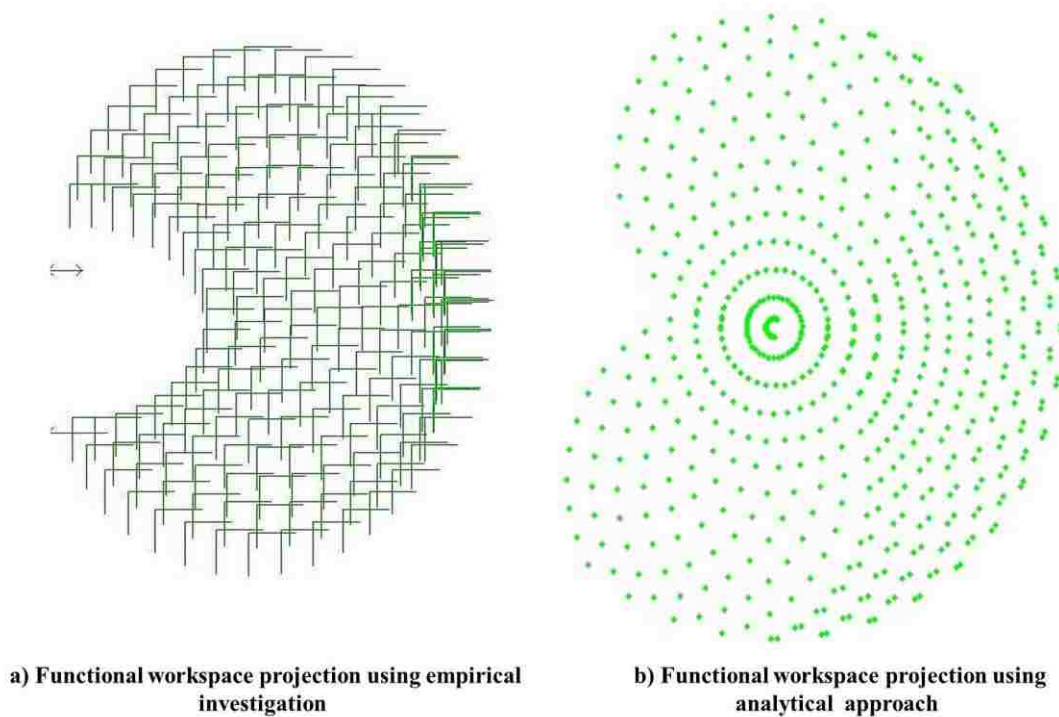
Figure 4-10 Comparison of functional workspace between empirical investigation and analytical approach

a) **Unconstrained**

$\theta_1 = 0$
$\theta_2 = -25.43$
$\theta_3 = -228.321$
$\theta_4 = 180$
$\theta_5 = 17.390$
$\theta_6 = 360$
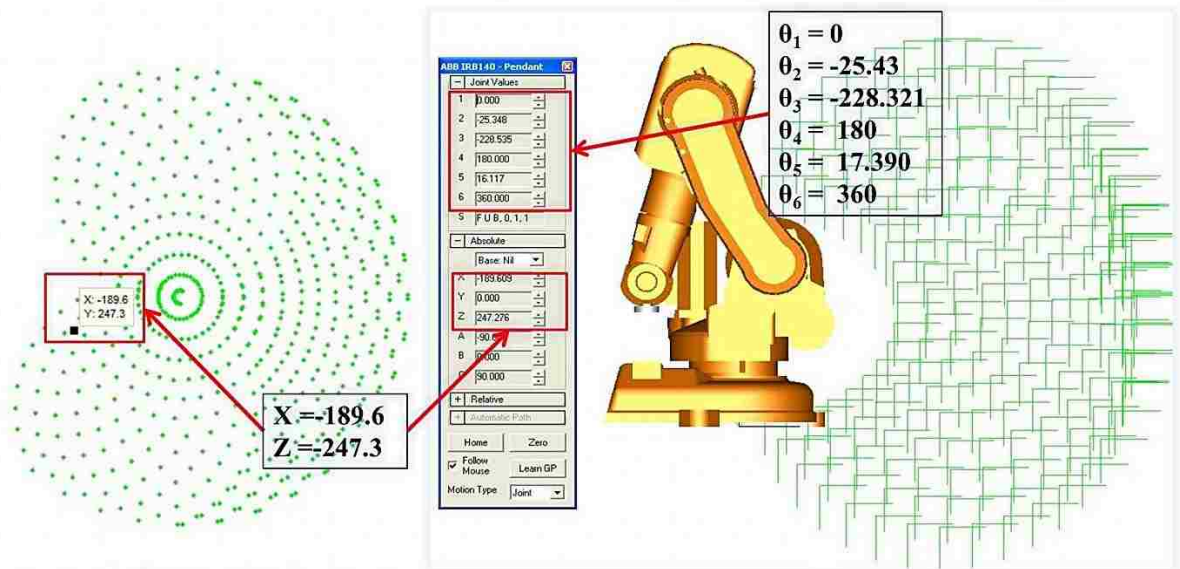
b) **constrained**

Point on analytical approach is reachable in empirical method when θ_1, θ_4 and θ_6 are varied

Figure 4-11 θ_1, θ_4 and θ_6 angles in the empirical method are varied to reach a point outside of the functional workspace curve
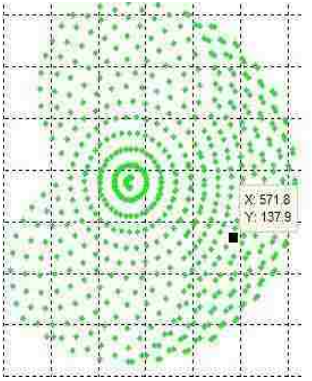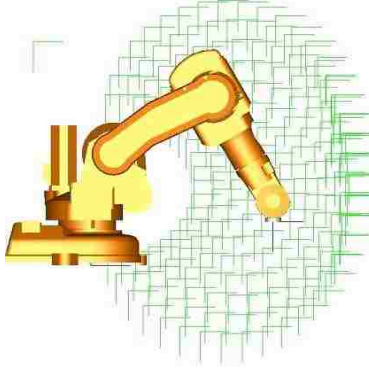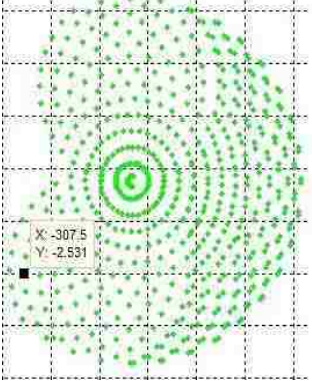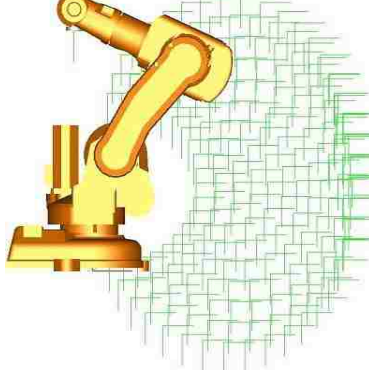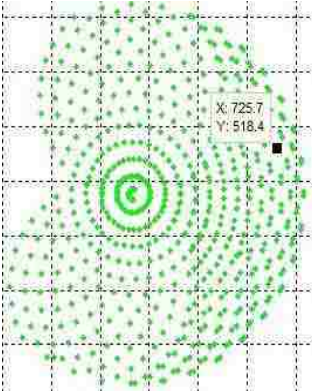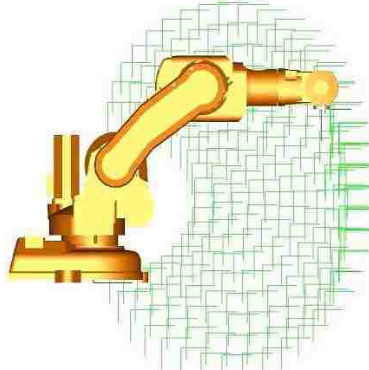
Due to constrained joint angles, the curve generated by empirical method looks to be a subset of the functional work space curve that is generated analytically as the analytical method captures the variation in θ_4 and θ_6 values as well. Fig. 4-12 shows the boundary of the curve generated by the empirical method within the analytical approach functional work space curve.
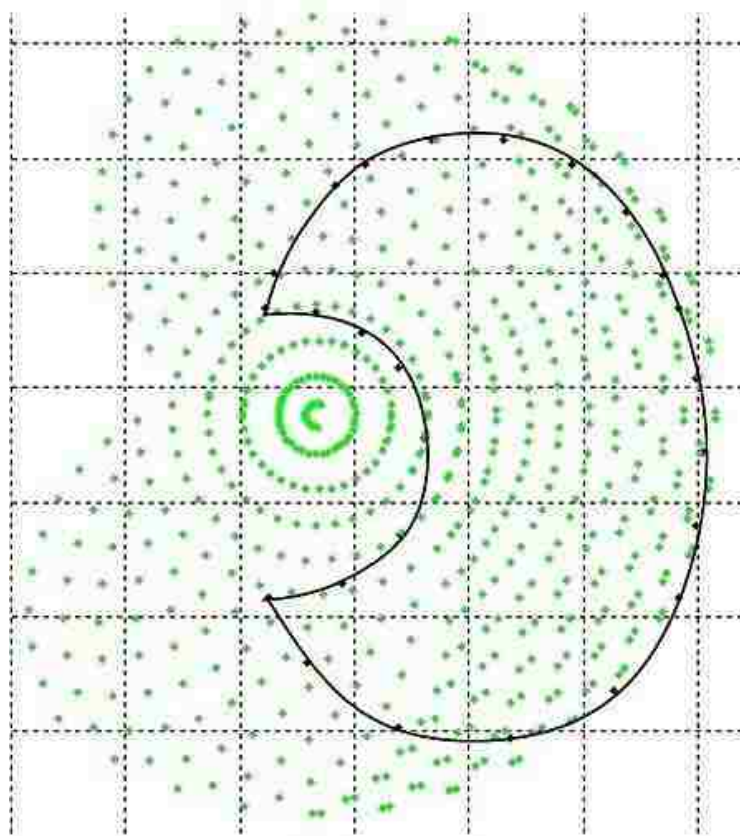
Figure 4-12 Functional workspace points generated by empirical method with constrained θ_4 and θ_6 overlaid on analytical approach functional workspace curve

The curve terminates at the same points on the right side of the curve. This is obvious since the robot reaches its geometric limits at that point and cannot travel beyond that point. The points that are present beyond the empirical method functional workspace curve are reachable when θ_4 and θ_6 are varied. The position of the robot and the theta angles for a set of random points in and out of the functional workspace is given in Table 4-2 below.

Table 4-2 Robot position for a set of X-Z points in and out of the functional work space generated by empirical method

Position		Joint angles ($\theta°_i$)	X-Z position on analytical approach curve	Robot position for the X-Z position
X	Z			
636.8	202.9	$\theta_1= 0°$ $\theta_2= 60°$ $\theta_3= 0°$ $\theta_4= 0°$ $\theta_5= 30°$ $\theta_6= 0°$		
-307.5	-2.531	$\theta_1= 0°$ $\theta_2= -78.8°$ $\theta_3= -181.1°$ $\theta_4= 180°$ $\theta_5= 10.0°$ $\theta_6= -180°$		
725.7	518.5	$\theta_1= 0°$ $\theta_2= 50°$ $\theta_3= -50°$ $\theta_4= 0°$ $\theta_5= 90°$ $\theta_6=0°$		

-59.23	729.8	$\theta_1 = 0°$		
		$\theta_2 = -37.1°$		
		$\theta_3 = -192.9°$		
		$\theta_4 = 180°$		
		$\theta_5 = 114.2°$		
		$\theta_6 = 180°$		

From the values of joint angles ($\theta°_i$) it is clear that the points that are inside the functional workspace curve generated by the empirical method when θ_4 and θ_6 are zero. The points are outside the functional workspace curve generated by the empirical method when θ_4 and θ_6 values are varied.

4.3.1 Error analysis of empirical and analytical functional workspace curves

The error between the functional workspace curves generated by empirical method and analytical approach is found to be minimal. It is to be noted that the accuracy of points plotted through analytical approach can be increased by decreasing the increment, Δ. This will result in a curve that is consists of more points thus resulting in a more accurate representation. Fig. 4-13 shows the analytical functional workspace plot with $\Delta = 5°$ i.e θ_2 and θ_3 are incremented by $5°$ between their limits instead of the previous increment of $10°$. The analytical plot is overlaid by the boundary X and Z positions (represented by '+' on the plot) obtained through the empirical method.

X-Z boundary positions obtained from empirical method overlaid on
analytically obtained points showing minimum error between points
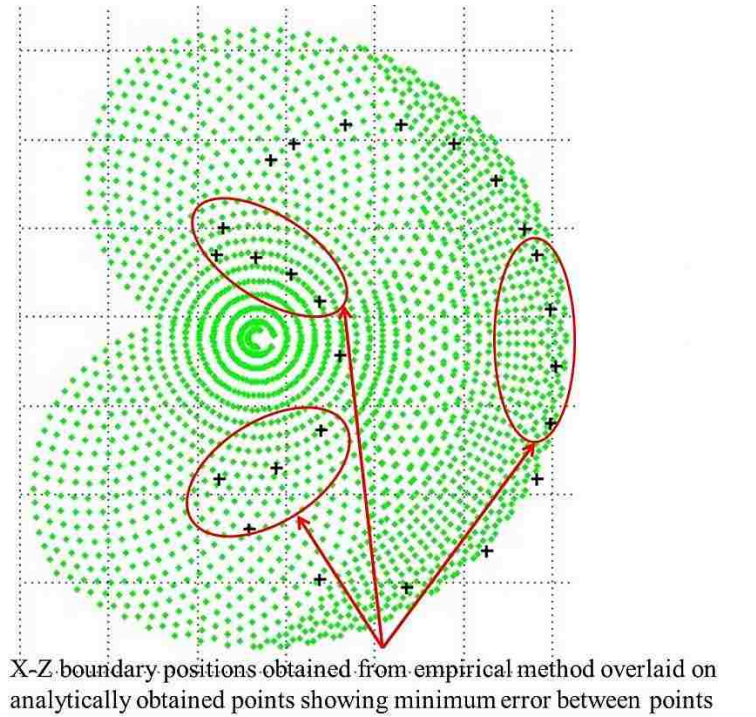
Figure 4-13 Overlaid empirical functional workspace boundary points on analytical result showing minimal error between methods with Δ = 5°

It can be seen that the majority of the '+' points close or above the dots '.'. This shows minimal distance between the points that are obtained. The user can further increase the accuracy of the analytical plot by decreasing the Δ. A thicker cloud of points can be obtained, which would reduce the error to $10^{-2\text{to-}3}$ decimal places.

However, to quantify the error for a sample of 25 points, the distance formula is used and the distance between X and Z positions of the points are obtained for the analytical and the empirical functional workspace curves that are generated with a Δ of 10°. The sample points used are the boundary points of the empirical method shown by '+' in Fig.4-13. The distance formula is used in analytical geometry to describe how far two points are from each other. In this case, the distance formula is employed to find the distance between the boundary point obtained through the empirical method and the

54

closest point to that boundary point in the analytical approach. The distance formula is given by:

$$d = \sqrt{(x_1 - x_2)^2 + (y_1 - y_2)^2} \qquad (4.3)$$

Where,

d = distance between two points

x_1, y_1 = x,z coordinates for one point (Empirical method)

x_2, y_2 = x,z coordinates for one point (Analytical approach)

Table 4-3 shows the average error computed for a sample of 25 points. It can be seen that, at a Δ of 10° the error is approximately 6mm. This error is representative and not comprehensive. As stated, this can error can be further reduced by decreasing Δ.

Table 4-3 Distance between X-Z positions in functional workspace curves obtained thourgh empirical and analytical methods

	Empirical method		Analytical approach		Distance between two
S.No	x_1	z_1	x_2	z_2	points (mm)
1	44.559	539.513	42.5	538.4	2.3406
2	60.8	600.127	68.54	598	8.0269
3	167.686	752.776	162.7	748.3	6.7004
4	219.09	788.769	221	791.2	3.0916
5	336.576	831.531	343.3	832.2	6.7572
6	461.603	831.531	459.1	832	2.5466
7	579.09	788.769	575.7	792.5	5.0411
8	674.866	708.404	681.2	709.8	6.4860
9	738.852	596.968	746.4	602.8	9.5386
10	765.373	540.095	768.6	533.7	7.1631
11	798.758	415	802.4	418.9	5.3361
12	810	287	803.9	290	6.7978
13	798.758	158.5	793.6	160.3	5.4631
14	765.373	33.905	763.6	27.24	6.8968
15	652.549	-127.224	655.3	-122.2	5.7279

16	474.276	-210.354	475.1	-206	4.4313
17	278.322	-193.21	278.8	-191.1	2.1635
18	117.192	-80.387	121.7	-76.26	6.1118
19	51.206	33.905	49.55	37.61	4.0582
20	180.271	58.416	183.4	54.23	5.2262
21	279.79	144.177	283.3	146	3.9552
22	322.513	312.441	325	321.1	9.0091
23	275.962	435.289	269.4	440.5	8.3794
24	212.823	496.79	219	493	7.2470
25	132.458	532.986	132.4	544.4	11.4141
				AVERAGE =	5.9964

The error between the functional workspace curve obtained analytically and the one developed through empirical method is minimal. The depiction of points is close and the empirical results match with the functional workspace obtained analytically. This validates the joint dependencies and the effect of the joint angles on the functional workspace. The confirmation of the same results obtained through analytical approach and the empirical method eliminates the need to have a visual simulator to sketch the functional workspace curve. Furthermore, the analytical approach can be used to include more kinematic structures involving translational joints and wrist manipulators.

4.3.2 Functional workspace behaviour

θ_5, θ_2 and θ_3 are at their maximum joint limits for a fixed θ_1, θ_4 and θ_6 (Fig. 4-10) it can be seen that the three angles reach their maximum limits at three different places in the functional workspace. As seen in Section-4.2 the solution algorithm will further needed to be adapted to fit another robot.
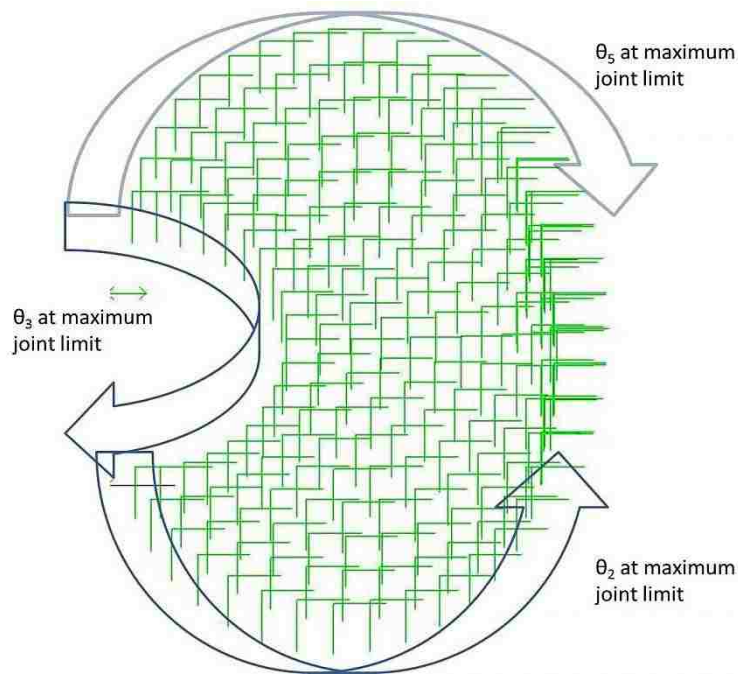
Figure 4-14 Maximum limits in functional workspace of ABB IRB 140 through empirical approach

Industrial robots are often operated with linked 'elbow' and 'shoulder' joints for applications such as pick and place, palletizing, material handling and packaging. In the case of the ABB IRB 140 joint 2 and 3 are linked. Linking the 'elbow' and 'shoulder' joints of the robot is not used by default at the design phase of the robot and in case of simulation. The 'joint frame' is used to design and study the properties of the robot. In joint frame each joint can move individually, independent of the preceding link and joint.

Most often, while using the Teach Pendant to jog the robot to a required point in space 'joint frame' is used. Once, the point is recorded the robot can be jogged to the point in various modes such as 'tool frame', 'world frame' or 'user frame'. In these frames, the robot moves as a linked joint. Studying the linked aspect of the robot is beneficial since it gives a projection of the work envelope in two dimensional space when θ_1 is kept

constant and provides a slice of work. An analytical program is created to depict this linked work envelope with an overlay of the functional workspace. A 2-3 joint envelope was depicted by Djuric, ElMaraghy, 2008 and the idea has been extended to the IRB 140 and programmed in this research.

The blue points ('.'s) represent the work envelope points generated when the joints 2 and 3 are linked. The 'X's are the functional workspace projection points. It is observed that, the work envelope and the functional workspace are relatively placed the same way as seen in the empirical approach. The functional workspace points extend beyond the work envelope in 2D since the whole kinematic structure is assessed. This does not however, signify that the functional workspace points are outside of the work envelope. The functional workspace points are inside the 3D work envelope of the manipulator. The density of points is high near the origin as observed previously. The work envelope obtained is also identical to the manufacturer defined work envelope given in Fig. 3-3. The comparison below shows the 90° orientation functional workspace with respect to the linked work envelope.
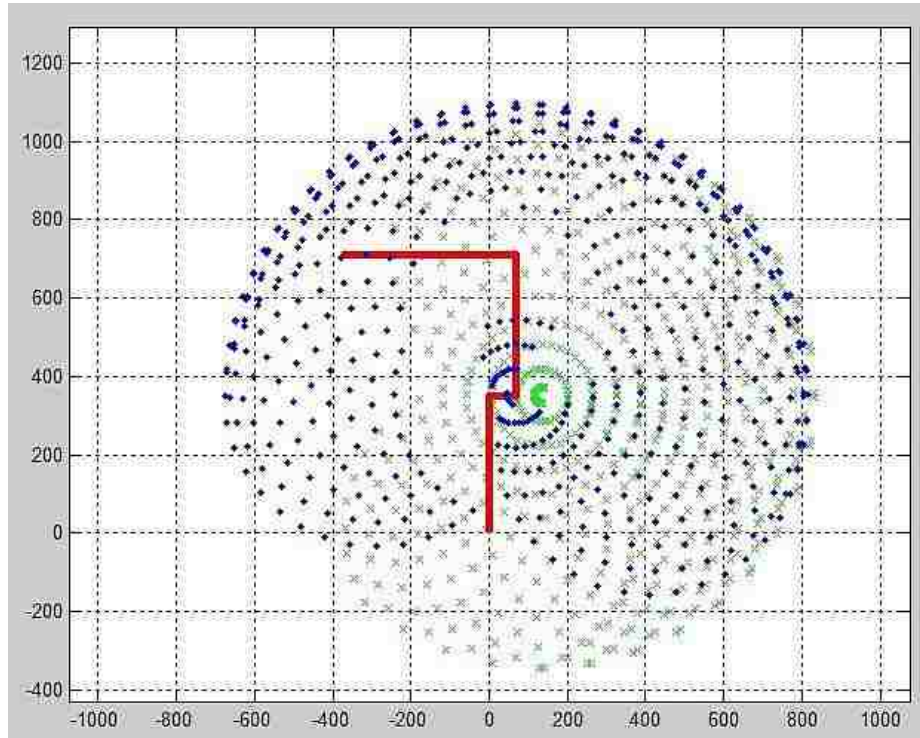
Figure 4-15 Comparison of shoulder and linked (constrained) joint space to the analytical functional workspace

The code used to obtain the linked work envelope is given in Appendix B. The D-H parameters are declared for the IRB 140. The increment $\Delta = 10°$ as with the functional workspace. θ_2 and θ_3 are varied between their limits. If the sum of θ_2 and θ_3 is between the least possible value and the maximum possible value of θ_2 and θ_3, then the homogenous transformations to obtain the end-effector value are calculated after the new θ_2 and θ_3 values calculated. For each end-effector value obtained the X and Z position vectors are plotted in an X-Z plane.

The analytical solutions provided help to create a visual representation using just D-H parameters and joint limits. Plotting the solutions in an X- Z plane gives a clear representation of a particular point in space. This representation also makes it easier to

understand the movement of the robot through the plotting pattern. All the constraints and conditions are mathematically represented, leaving room for manipulation if need arises. Automating the solution also eliminates the need to calculate the end-effector position for every increment of joints-2, 3and 5.

The constraints and conditions for the analytical approach need to be changed for a different robot and this will need referring to the empirical approach to change the formula for the functional workspace. The purpose of obtaining a solution from a minimum set of parameters is hence defeated.

A much simpler solution that can be deduced from the kinematic structure will eliminate the need to cross-reference empirical or visual approaches. The functional workspace needs to be looked at from a geometric standpoint that considers the kinematic structure of the robot. The information obtained through analytical and the empirical approach can then be merged into the geometrical solution so as to retain the limitations of the robot.

4.4 Geometrical approach to project two dimensional functional workspace[2]

To obtain a geometrical solution, the robot's kinematic structure needs to be assessed. The reduction of the IRB 140 kinematic structure into only the required joints and links has been detailed in Section- 3.1 and Fig. 3.1. Through the geometry it can be observed that θ_2, θ_3 and θ_5 are the rotation angles that are analysed, which is also echoed through

[2] Section 4.4 incorporates the outcome of a joint research undertaken in collaboration with Jill Urbanic, University of Windsor, Windsor, ON, Canada.

the visual, empirical and analytical approaches. A similar analysis can alternately be performed by varying θ_4 and θ_6.

The primary outer boundary of the functional workspace can be obtained by rotating a_2 and d_4 with its centre on the joint 2 rotary axis. It can thus be defined as:

$$OB_r = a_2 + d_4 \qquad (4.3)$$
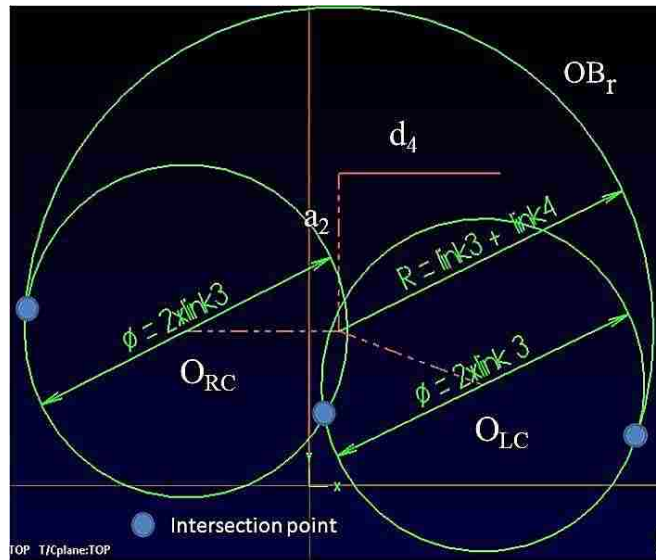
Figure 4-16 Outer boundary curve for 90 orientation Reference: Urbanic, J., Gudla, A (2012)

The boundary of the functional workspace can be trimmed using the joint limits of θ_2. The smaller right and the left circles O_{RC} and O_{LC} have their centres located at a_2 when rotated. O_{RC} is positioned at the θ_{2max} and O_{LC} is located at θ_{2min}. The radius for both these circles is d_4. At the points of intersection of these three circles, the curve is trimmed to obtain one continuous boundary curve. It can be seen from Fig. 4-10 that the inner boundary curve is generated when θ_3 is maximum. Geometrically, the inner circle radius

61

can be determined using the Cosine Law, as the two sides (a_2 and d_4) and θ_{3max} are known. The inner boundary curve thus obtained is given in Fig.-4-13.

$$I_{Br}{}^2 = a_2^2 + d_4^2 - 2a_2d_4 \cos(\min[90° + \theta_{3\max}, 90° - \theta_{3\min}]) \tag{4.4}$$

Figure 4-17 Inner boundary curve derived from θ_3 limits Reference: Urbanic, J., Gudla, A (2012)

A process flow to geometrically obtain the functional workspace is given in Fig. 4-14.
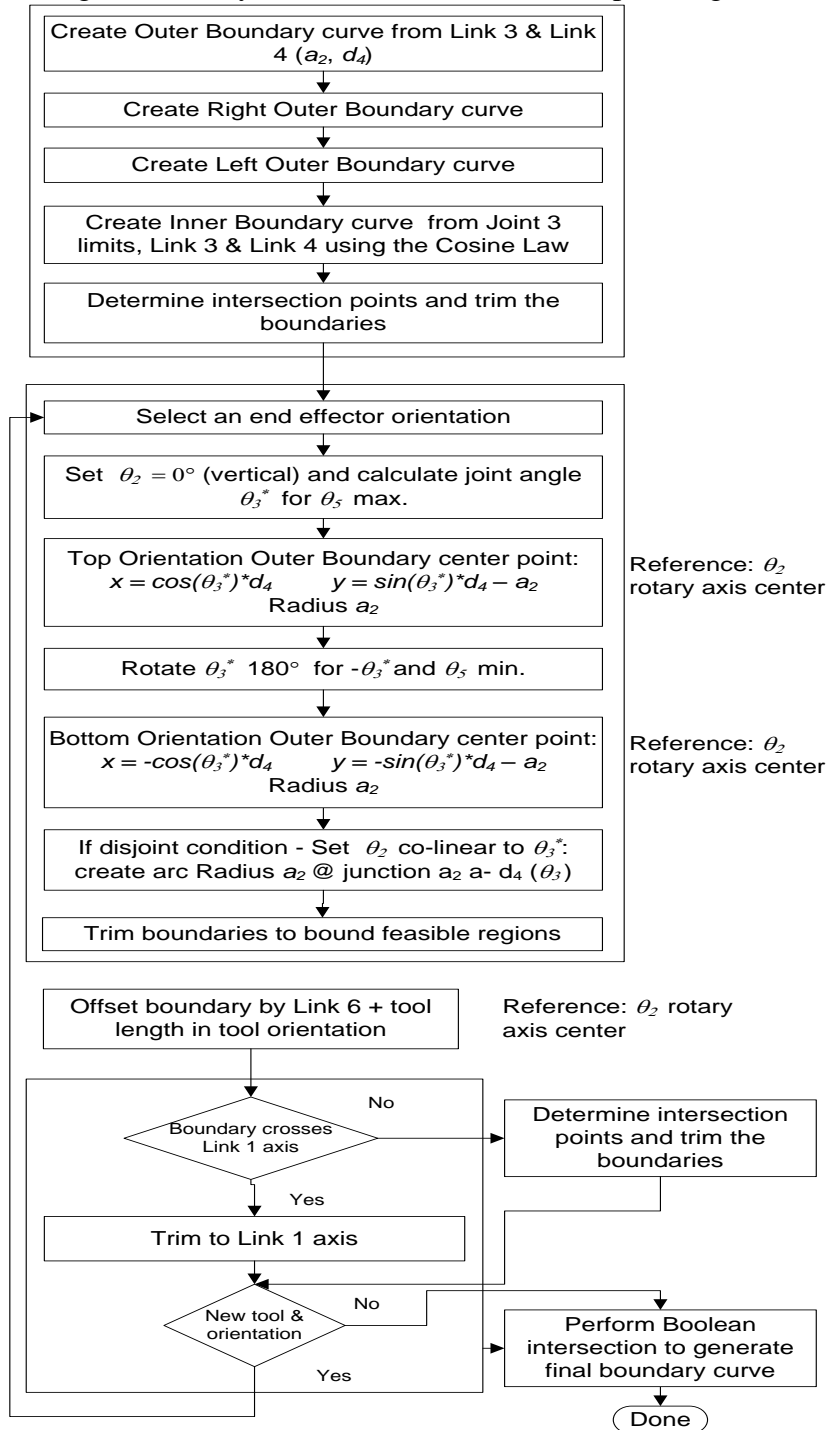
Figure 4-18 Flowchart to obtain the functional workspace for a given orientation Reference: Urbanic, J., Gudla, A (2012)

MATLAB is used to simulate this geometrical solution. As mentioned before, the manipulator still needs to obey the constraints and the limits. This is well imitated in the MATLAB simulation by imbibing the forward kinematic equations and extracting the position vectors for an increment between the joint limits. The code for the simulation is given below. For visual ease and understandable representation the length of the links is taken to be 1000. The code for the geometrical approach programming is given in Appendix B.

In the program the θ_2 and θ_3 are varied between their limits while θ_5 is fixed at $90°$. The position vectors for these varying angles are then extracted and are plotted in the X-Y plane. The result of this program is given in Fig. 4-15.
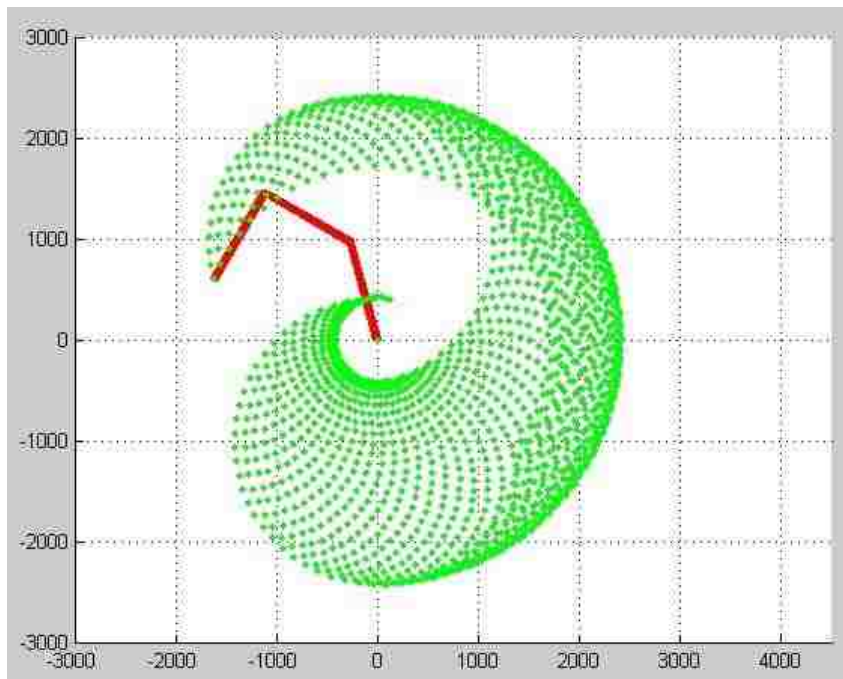
Figure 4-19 Functional workspace for 90° orientation using geometrical approach

The obtained result is a projection of the functional workspace region of the reduced kinematic structure. The plot of points represents all the reachable points by the manipulator at the 90° orientation. This representation of the boundary can impact the design and placement of a robotic manipulator in an environment. The functional workspace curve can be thus generated for different orientation angles. A common functional workspace region can be derived when the curve intersection points of two different orientations are overlaid. A Boolean intersection is then performed to determine the contour of the curve. In the Fig. 4-16, two orientations ϕ = -90° and ϕ = -45° are overlaid and the curves are shifted due to the end effector length and co-linear tool offsets along the end effector vector. Fig.4-16 shows a unique offset length for each orientation to illustrate this. If the curves intersect the vertical axis, θ3, they are trimmed to this line.
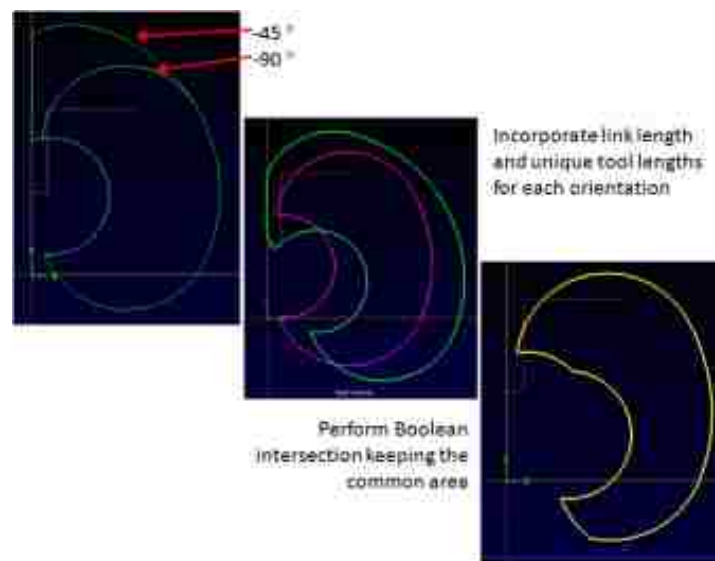
Figure 4-20 Trimming the functional workspace for common orientations Reference: Urbanic, J., Gudla, A (2012)

Automating this process would reduce the time and provide a solution to the reach problem. Fig-4-17 shows the overlay of $\phi = 90°$ and $\phi = 45°$. The '.'s are for the 45° end effector orientation and the 'X's are for 90° orientation. The common region of these points is very clearly visible, hence making it very easy to interpret the functional workspace region.
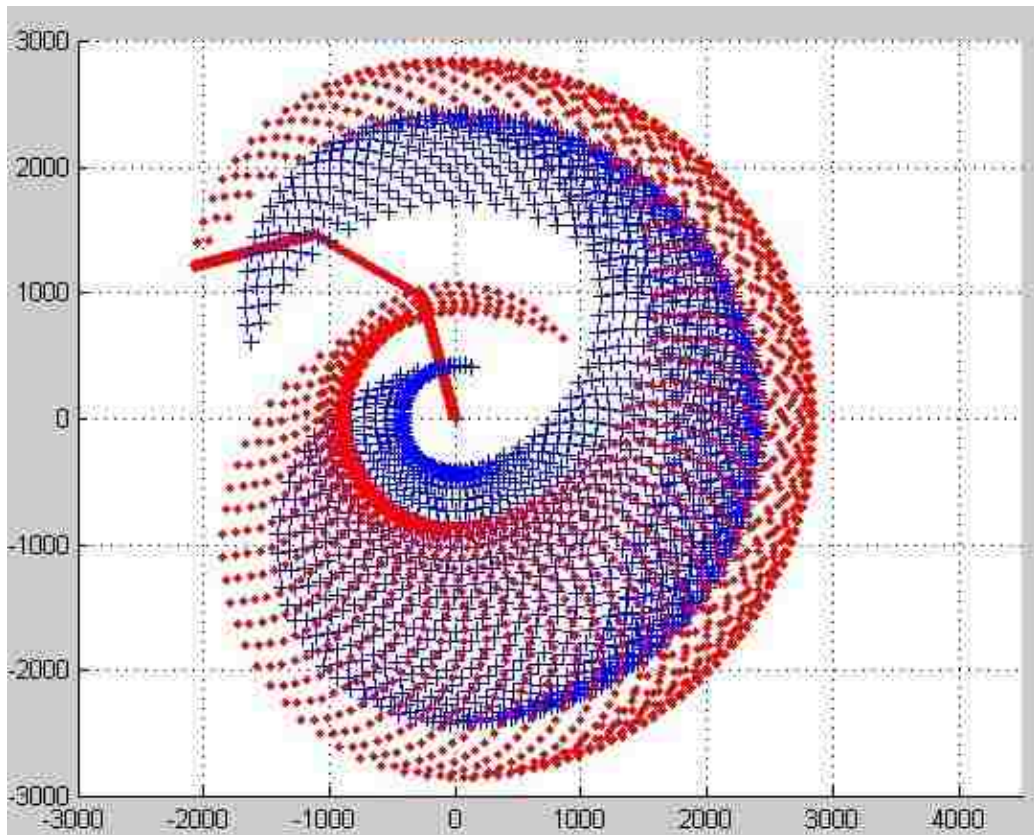
Figure 4-21 Functional workspace comparison of $\phi= 45°$ (red '.'s) and $\phi=90°$('X's)

The next comparison that can be made is to keep θ_2 at its maximum and vary θ_3 for a fixed orientation of θ_5. A much defined and a crisp functional workspace can be obtained.

A simple modification in the code will enable us to this result which is shown in Fig. 4-22.
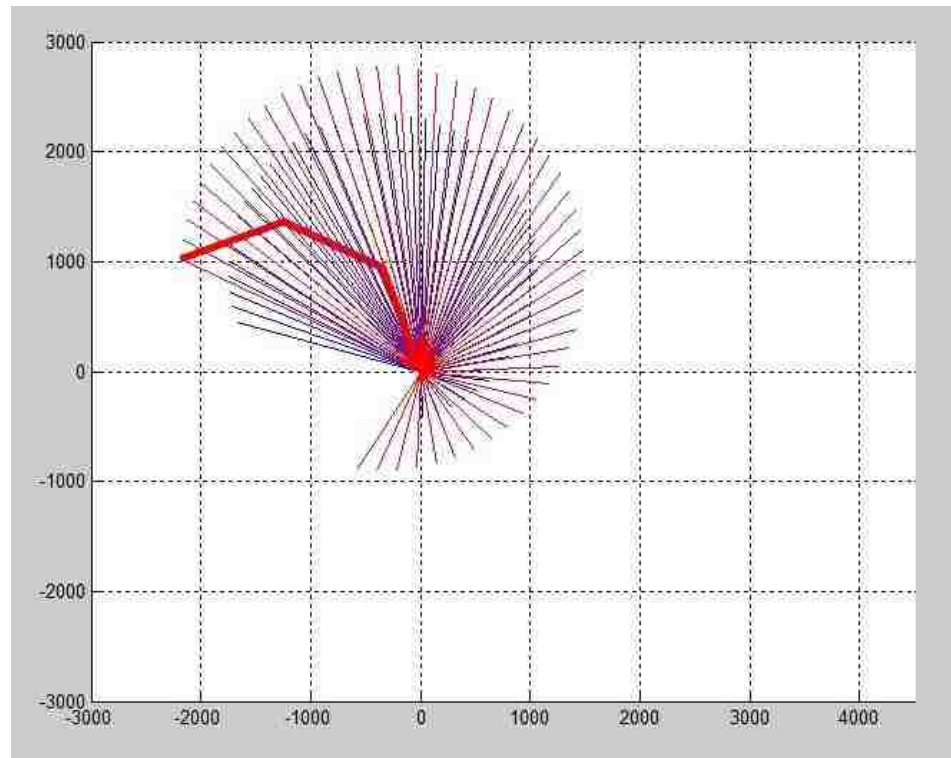
Figure 4-22 Functional workspace at θ_2 maximum $\phi= 45°$ (red) and $\phi=90°$(blue)

It is geometrically understandable due to the θ_5 orientation that the functional workspace for $\phi = 45°$ (red) is larger than $\phi = 90°$. This solution to obtain the functional workspace is simple and easy to arrive at. A good understanding of the kinematic structure and joint limits will enable to represent a filtered kinematic structure that can be used to project the functional work region for a set of desired orientations.

The solution is rapid and does not need any physical trial and error or complicated simulations. The solution presented here will work for any configuration that is similar. This solution is foundational to build upon different configurations and families of serial

manipulators. As mentioned before, the aim is to be able to come up with a simple solution that can aid in designing and not to optimise a reach issue.

The geometric solution simplifies the problem by taking into consideration the most necessary joints to construct the functional workspace. The kinematic structure is reduced into a four bar linkage indicating the valid functional space for a particular orientation. This does not imply breaking up the kinematic chain. It has been detailed in the sections above that the joint 2, 3 and 5 are the only joints that contribute to the 2D functional workspace shown in this research for a constant θ_4 and θ_6. Adding a different tool or a length to joint-6 will introduce an offset that can be incorporated in the valid space (Fig.4-20). Hence, the limitations and constraints of the robot are captured. This method is derived from and builds upon the kinematic analysis of the 6R manipulator.

4.4.2 Comparison of the analytical and geometric functional workspace

Analytically, to arrive at a solution the effect of θ_4 and θ_6 has to be considered since, the problem is computed on the basis of D-H parameters and homogenous matrices from the base to the end-effector. θ_4 and θ_6 are unconstrained resulting in a larger functional workspace region for the manipulator. These pose matrices increase the computational complexity that can be avoided by adopting the geometrical solution. The figure below highlights the results of the analytical and the geometrical approach.
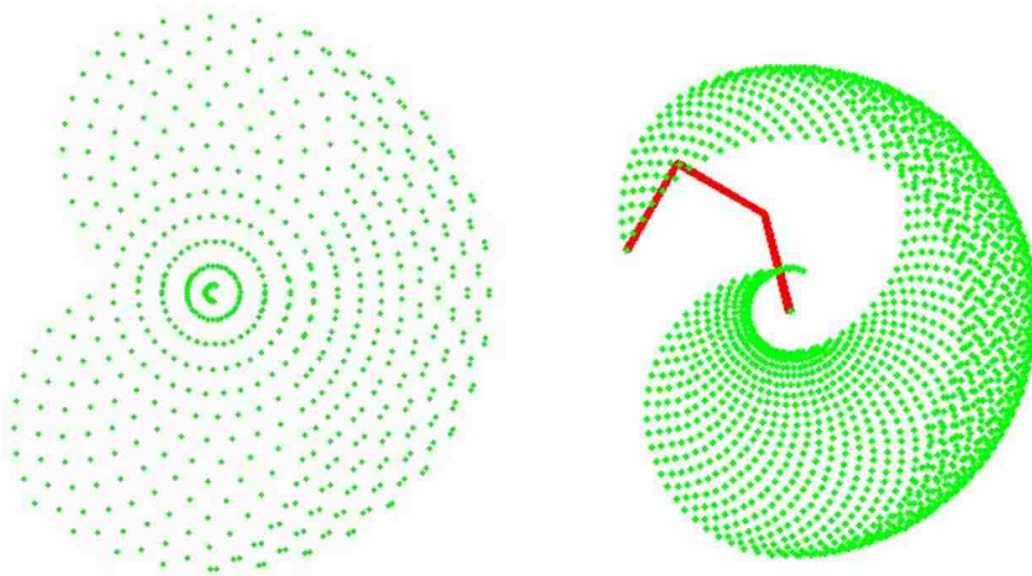
a) Analytical approach with unconstrained θ_4 and θ_6 are varied

b) Geometrical solution with θ_2, θ_3 and θ_5 for a fixed θ_4 and θ_6

Figure 4-23 Analytically unconstrained functional workspace in comparison with the geometrical functional workspace solution

The solution obtained in the geometrical solution is representative of the most valid functional workspace at a particular orientation. In the analytical solution, although the D-H parameters of θ_4 and θ_6 are considered the joint limits of these two joints are not taken into account. This results in a much larger functional workspace region. All the points in this solution while are reachable by the robot, the most valid functional workspace region is not highlighted. On the other hand, locking the joints-4 and 6 and considering only the joints that contribute to the 2D workspace details the ease of representing the functional workspace region in the geometrical solution. Also, the position matrices of joints 2, 3 and 5 are only considered resulting in a valid representation of the functional workspace.

4.4.2 Functional workspace in a robotic workcell

Consider a robotic work cell with three serial manipulators arranged parallel next to one another. There are several factors the need to be considered while designing such a work cell such as repeatability, accuracy, link length, range and payload capabilities. One of the most important parameters that need to be judged carefully is the functional workspace of the manipulators if they two are working together. Being able to design a non-interfering and well synced robotic work cell that can work in tandem can increase productivity.

The 2D functional workspace zones can be rotated around θ_1 to create a 3D representation. This will enable the user/designer to visualise the common work regions. A Boolean intersection will reveal the common regions where multiple kinematic chains can come in contact for the end effector orientations used in the 2D analysis ($\phi = -45°$ and $\phi = -90°$). Fig.4-23 shows the overlap regions for this case when θ_1 is rotated. This effectively shows the use of having a design tool that can find the functional work region of a manipulator in a work cell. As stated earlier, the developed design tool is not meant to optimise a reach issue but to indicate the valid functional space for multiple tool orientations.

Regions of overlap for 3 robots requiring end effector orientations
ϕ = -90° and for ϕ= -45°
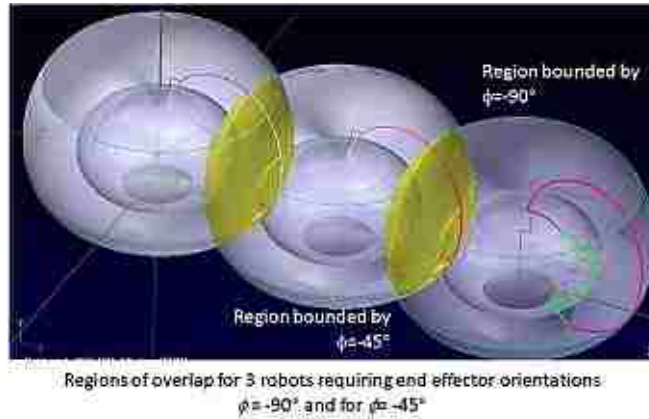
Figure 4-24 Overlap regions for robotic manipulators in a work cell Reference: Urbanic, J., Gudla, A (2012)

4.4.2 Errors in the geometrical projection methodology for the functional workspace

This research is foundational and a pre-cursor to the development of a 3D solution. In future, several additional parameters such as velocity of joints, manipulator configurations, acceleration, tools with offset, speed and acceleration, inverse kinematics, singularities etc. need to be considered. The error in the depiction of the functional workspace will be affected by some or all of these parameters. However, a short description how error in the curve of the functional workspace can be found is presented.

The points on the boundary of the functional workspace physically represent robot path. In this case the robot path is represented as a set of one closed polyline. The polyline is made up of many lines. In reality these lines can be lines or splines, arcs.
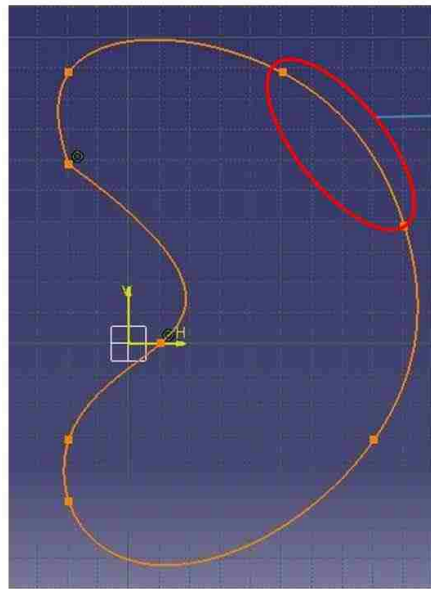
Replicated Functional workspace   Curve approximated to lines, arcs
                                         or splines
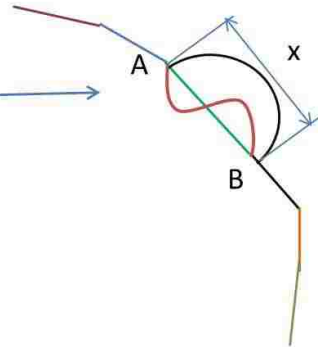
Figure 4-25 Error between two points on functional workspace

Fig. 4-24 shows a replicated shape of a functional workspace. On magnification of the

curve, it can be seen that it is made up of many lines. In reality, the distance between any

two points, '*x*' can be a line, arc or spline. The *error* in the shape of the real and projected

functional workspace will be the difference between the approximated line and the real

line or arc or spline.

It is also difficult to get an accurate functional workspace curve since the analytical

and geometrical points provide the whole functional workspace rather than just the

boundaries. That is to say, that the distribution of the points on the boundary is sparse.

However, the increment, Δ between the joint variations can be further decreased to

resulting in a much thicker curve. The boundary points thus obtained can then be

connected to generate a closed polyline. Since, the points will be much closer, the approximation between these points by a line, arc or spline will result in a smaller error and a more accurate functional workspace curve. The figure below shows the error between the empirical and the analytical functional workspace for different Δ's.

a) Error at Δ= 10°. Visible error. Range: 2-8 mm

b) Error at Δ= 5°. Error is reduced. Range: 0.5-2mm

c) Error at Δ= 1°. Range: 0.01-0.05 mm
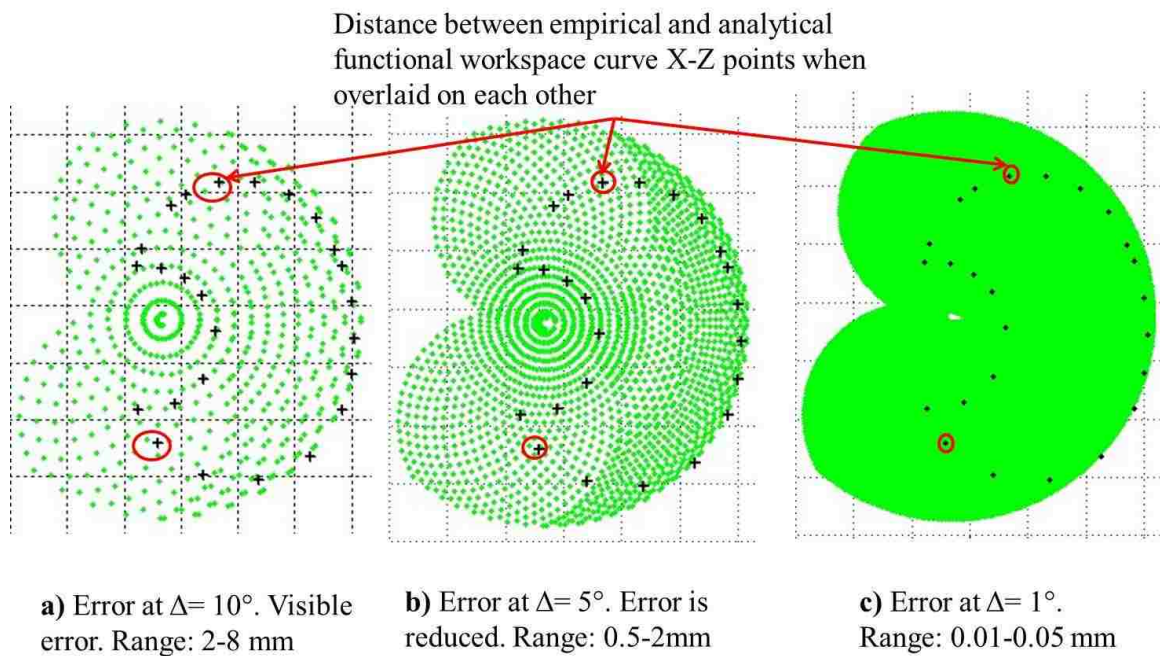
Figure 4-26 Reduction in error between the empirical and analytical functional workspace curves due to change in Δ

The '.'s represent the analytical X-Z points and the '+'s represent the empirical boundary points. It can be seen that the error between the empirical and the analytical points is visible at Δ=10°. This error is further reduced as the increment; Δ is reduced to 5°. The error is not visible to the naked eye when the Δ is further reduced to 1°. Hence, the increment can be changed depending on the level of accuracy needed between the two curves. However, as the Δ is reduced, the time to plot the points is increased.

CASE STUDY

The case study focuses on an application for a local manufacturing company, which performs non-destructive testing and residual measurements. The company also develops high speed X-Ray diffraction equipment that is used for residual stress measurements. The X-Ray tubes are mounted on a goniometer that is used for measuring angles between crystal faces.

The measuring system consists of two rotary and three translational axes. One rotational axis is used for positioning along with the translational axes and the other rotary axis is used measurement. A $\pm30°$ sweep is made from the surface normal. Data from this sweep is collected and the process is repeated for reliable results. The company is not only in need of an alternative system for an effective automated multi-measurement system but also requires a design tool that can facilitate measurements of curvilinear surfaces.

The company deals with complex geometrical surfaces such as those in turbine blades. The X-Ray goniometer needs to be at a normal to the surface orientation to achieve the required results (Fig-5-1). It is important to find a robotic manipulator that has high flexibility of θ_2 and θ_3 so as to reach curved and complex shaped work piece(s). The company can use the functional workspace solution to find an optimal solution for this problem. Fig. 5-2 highlights different lengths and orientations of links 2, 3 and 5. Accuracy for this application is ideal and having a constant θ_4 and θ_6 will provide a constrained functional workspace region. The link lengths are considered to be 1000 mm for easy representation and understanding in all cases.
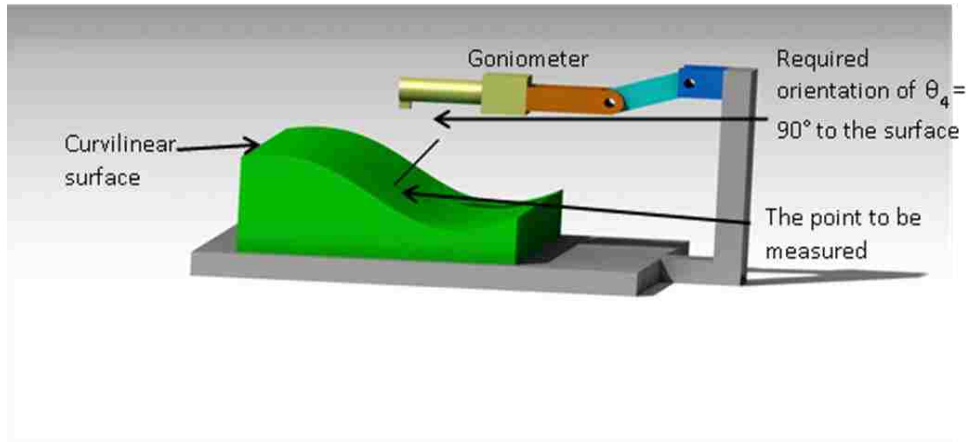
Figure 5-1 Goniometer attempting to measure a curvilinear surrface at a normal oreintation

$\theta_5 = 90°$
θ_2 limits:
-90 to 110
θ_3 limits:
-230 to 50

$\theta_5 = 45°$
θ_2 limits:
-50 to 120
θ_3 limits:
-130 to 150

$\theta_5 = 60°$
θ_2 limits:
-100 to 70
θ_3 limits:
-200 to 30

$\theta_5 = 135°$
θ_2 limits:
-70 to 150
θ_3 limits:
-120 to 120
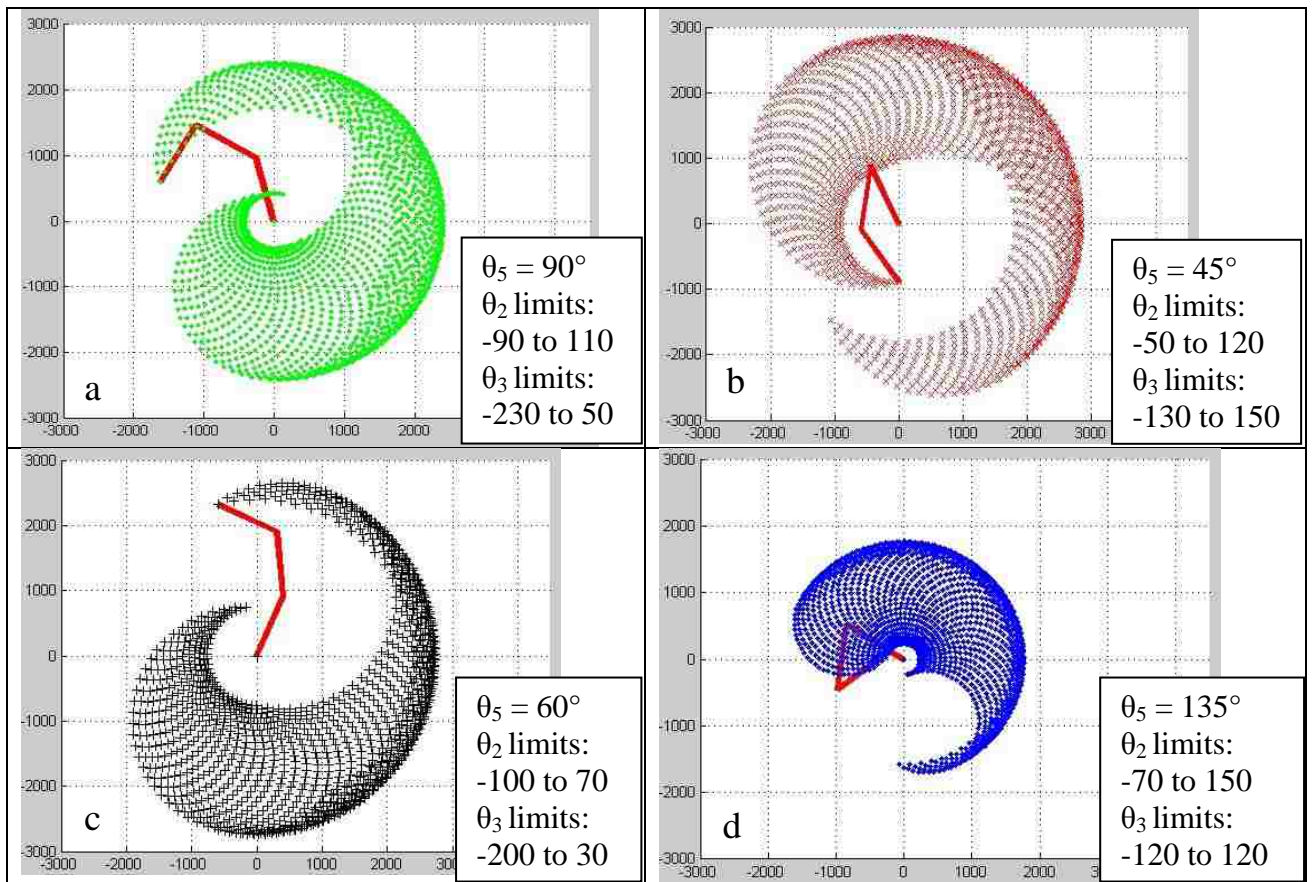
Figure 5-2 Different set of joint limits and link lengths of 1000 mm

The best joint limits and link lengths can now be selected based on the application. This information is available from any robotic manufacturer. There still will be the need to carry out tests pertaining to accuracy and repeatability but different trials to emulate reachability by simulation or visual inspection is eliminated. Even after selecting the most viable manipulator option, the company can use the functional workspace solution to setup different work pieces with complicated shapes and determine the best orientation and joint angles to reach a point on the work piece.

Furthermore, the solution can be used to overlay different orientations with respect to the end-effector for various tool designs. This will enable the designer to find out the most common or largest functional work space region. The work piece can then be placed appropriately near this region to ensure minimal or no reach issues. It is to be noted that a solution space is developed and further optimisation of the work piece placement is not a part of this research and the issue should be analysed separately in its entirety. Fig. 5-3 shows the overlay of three orientations, 90° ('.'), 120° ('X') and 60° ('+'). Placing the work piece in the recommended zone with the common functional workspace region (where all the three colors are present) will ensure maximum reach of the end-effector at these orientations. The error calculation and accuracy of the common region is not being studied.
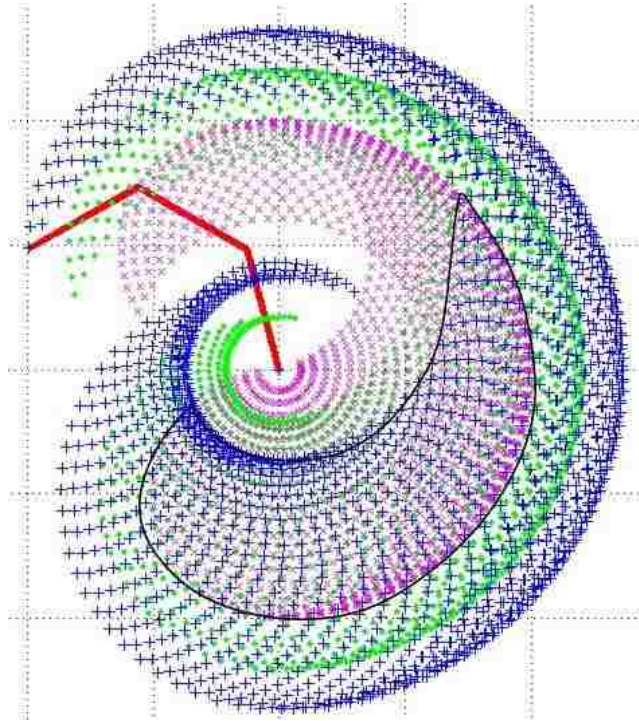
Figure 5-3 Overlay of reachable points for three orientations- 120°('X's), 90°('.'s)

and 60°('+'s)

This enables more tests and experiments to be conducted in a simulated environment which should lead to increase in productivity and also eliminate the error in visual judgement.

SUMMARY AND CONCLUSIONS

The work envelope of a serial 6 DOF robot does not convey information regarding the feasibility of a tool reaching at a desired orientation. The functional workspace plays an important role in the decision making of designing a robotic manipulator for a particular application and also work cell. An assessment methodology to capture the effect of orientation can enable downstream optimization for path planning and robot structures. This can further help process planners help select configuration/reconfiguration solution alternatives based on the task at hand. The functional workspace will vary based on kinematic structure, end-effector, tool characteristics, tool orientation and joint limits. A summary with the advantages and disadvantages of the manual, empirical and analytical methods used in this research to determine the functional workspace is presented below.

Table 6-1 Summary of advantages and disadvantages of using manual, empirical and analytical method to sketch functional workspace

Method/ Approach	Advantages	Disadvantages
Manual Point generation Method	• Size and shape of the functional workspace is demonstrated. • Parameters affecting the functional workspace are known. For e.g.: joint angles, orientation angles etc. • The functional workspace problem can be separated into – • Geometrical (causes of motion are not	• The manual approach is tedious and complex. • A number of points are required to obtain complete functional workspace. • Manual point generation lends itself to error.

	studied) • Mechanical (related to joints).	
Empirical method	• The empirical method is methodology based • The cloud of points required to construct functional workspace curve is reduced. • The joint dependencies are highlighted through the formula to obtain a 90° orientation, normal to the base.	• This method requires referring to visual approach to plot the functional workspace for a new robotic structure. • The formula depicted needs to be adapted for a new manipulator. • θ_4 and θ_6 are constrained and the effect of these joint angles is not evident. It has to be repeated for another set of joint values, which is time consuming and repetitive.
Analytical approach	• Only D-H parameters and joint limits are needed to create the functional workspace curve. • The representation is clear on a 2D grid with X-Z positions of the end-effector. • The solution is programmed in a software package, making it easy to modify variables and assess results.	• The solution provided is only for the 6R manipulator involved in this research.
Geometrical Solution	• The solution is easy to reproduce in a commercial simulation software package. • Different tool offsets and	• The effect of θ_4 and θ_6 is constrained in this case showing limited functional workspace. • The solution is in 2D.

	orientations can be programmed with minor modifications. • The solution is feasible for manipulators with similar kinematic structure. • The functional workspace for multiple tool orientations can be found.	• Alternate scenarios have to be explored to obtain a complete representation.

A 3D functional workspace of a 6R manipulator can be obtained by revolving a 2D functional workspace curve along the joint-1, Z axis as shown in the manual point generation approach. The reduction of the problem to 2D helps in concentrating on the necessary joints and links required to obtain the functional workspace for a given application.

The analytical solution presented is comprehensive. The effect of joints 4 and 6 are well captured by forward kinematic equations. The solution however, incorporates points that although are reachable, but should be avoided due to hard to reach positions of the manipulator and possible interference with the work piece or surroundings or additional rotary motions that may not be desired. It may be desirable to obtain a smaller and more representative valid functional workspace as you cannot predict the effect of θ_4 and θ_6.

The kinematic structure when studied in 2D enables visualisation of the required links to construct the functional workspace. Reduction of the problem to the first principles facilitates a geometric solution that can be used to represent the functional workspace for multiple orientations. This method is simple, easy to interpret, and can be readily implemented within a commercial software package unlike the analytical approach,

where, it is important to develop a visual and an empirical understanding first. The common region for multiple orientations has also been visualised using both the analytical and geometric solutions. This is a narrow region which would facilitate the reach of all the orientations. The region does not lend itself to any predictable geometric shape and is complicated. However, it is the optimal region for the placement of the work piece allowing the robot to reach at multiple orientations. For a complete representation the effect of θ_4 and θ_6 should be included.

The error between the points obtained from the empirical, geometrical and analytical approach is explored. The magnitude of the error varies between 2-8 mm for an increment, Δ of 10° which is minimal, validating the approach taken in this research.

A brief discussion on the impact of functional workspace in a work cell and the error in functional workspace curve has also been presented. The valid solution space for a particular orientation set will enable down-stream optimization for path planning, robot structures and tool orientations. Applications that require the tool to be at a certain orientation will benefit by being able to understand the functional work space limitations of the machine so as to plan and execute operations better, potentially saving both time and money. In conclusion, this solution should be implemented as a part of a design/analysis environment to evaluate initial configurations and reconfiguration options.

FUTURE WORK

The research presented here is not mature. The geometrical solution should be extended to include joint-1 providing a 3D solution. The areas of transitional functional workspace between different sets of orientations of a manipulator, that will help designers visualise the regions of common valid space for multiple orientations needs to be explored. The regions of high and low density of points in the functional workspace should be further examined. The effect of singularities in the robot will reveal zones of redundancies and methods to avoid these zones should be further developed.

Most 6 DOF industrial robots have last three joints intersecting at a point allowing the Jacobian (6X6) matrix to be decoupled into two determinants of (3X3). This can facilitate in generating a formula for internal boundary to find the reasons for singularity. Disjoint workspace will occur for specific end effector orientations and configurations with co-linear tools that are not straight and possess a normal or angular offset on axis-6. These regions of disjoint workspace needs to be investigated leading to a more ideal representation functional workspace.

Finding a solution for multiple kinematic chains and reconfigurable manipulator will enable an inclusive solution. Addition of inverse kinematics will lead to a more dynamic design tool that can assess the reach of the manipulator at a desired orientation. Motion and path planning can also be done using functional workspace solution, transforming the motion plan into the required joint actuator and orientation trajectories for the robot.

APPENDICES

APPENDIX A LITERATURE REVIEW MATRIX

LEGEND:	
5-Strongest reference to the key word	
4- Strong reference to the keyword	
3- Moderate reference to the keyword	
2- Weaker reference to the keyword	
1- Weakest reference to the keyword	
0- No reference to the keyword	
Most Important Reference-	

S. NO	Authors	Workspace	Dexterity	General open Kinematic chain	Optimal robot/machine Placement	Forward Kinematics	Specific Kinematic chain	Functional Workspace
1	Abdel-Malek, Yu (2004)	5	5	0	5	3	5	0
2	Abdel-Malek, Yeh (1997)	5	2	0	0	3	5	2
4	Borcea, Streinu(2011)	5	0	3	3	3	0	0
5	Cao *et.al* (2009)	5	3	4	2	4	3	0
6	Cao et.al (2011)	5	0	4	0	0	0	0
7	Badescu, Mavroidis,(2004)	5	3	0	4	3	5	0
8	Bi, Lang (2007)	5	0	0	3	4	5	2
9	Cebula, Murray (2006)	5	3	0	0	3	5	3
10	Ceccarelli (1995)	5	0	4	0	4	5	0
11	Ceccarelli, Vinciguerra (1995)	5	0	0	4	0	5	0
12	Djuric *et.al* (2010)	0	0	5	0	3	0	0

83

#	Reference							
13	Urbanic, Djuric (2009)	3	0	5	5	0	0	5
14	Feddema (1996)	5	3	0	5	3	5	2
15	Gilpin, Rus (2010)	0	0	5	0	0	0	0
16	Gupta (1984)	5	3	4	2	3	4	4
17	Gupta, Roth (1981)	5	1	4	2	4	5	2
18	Hideg, Juad (1987)	5	4	4	2	4	3	3
19	Lee *et.al* (2011)	5	2	0	0	3	5	0
20	Liu *et.al* (2011)	5	0	0	3	3	5	0
21	Mansuer, Doty (1995)	2	0	4	0	1	5	0
22	Moon, Kota (2002)	4	3	0	0	0	5	0
23	Pamanes, Zeghioul (1991)	3	0	4	5	3	0	0
24	Panda *et.al,* (2009)	5	0	0	3	4	5	3
25	Szep *et.al,* (2009)	5	0	0	0	4	5	0
26	VijayKumar *et.al,* (1986)	5	5	0	3	3	5	4
27	Yang *et.al,* (2008)	5	3	4	0	3	0	0
28	Zacharias *et.al* (2007)	5	4	0	0	0	5	0
	Total (Out of 140)	117	44	54	51	68	95	30

1. MATLAB code for analytical approach

```matlab
%%

clc
clear

% declaration of the dh parameters

a1 = 70;   d1 = 352;   alpha1 = -pi/2;   th1 = 0;
a2 = 360;  d2 = 0;     alpha2 = 0;       th2 = -pi/2;
a3 = 0;    d3 = 0;     alpha3 = pi/2;    th3 = pi;
a4 = 0;    d4 = 380;   alpha4 = -pi/2;   th4 = 0;
a5 = 0;    d5 = 0;     alpha5 = pi/2;    th5 = 0;
a6 = 0;    d6 = 65;    alpha6 = pi/2;    th6 = -pi/2;
k = cos(alpha2);
phi = pi/2;

%%%%%%%%%%%%%%%%%%%%%%%%%%%%%%%%%%%%%%%%%%%%%%%%%%%%%%%%%%%%
%Limits of th2, th3 and th5

th2_min = -pi/2;
th2_max = +110*pi/180;
th3_min = -230*pi/180;
th3_max = 50*pi/180;
th5_min = -120*pi/180;
th5_max = 120*pi/180;

%%%%%%%%%%%%%%%%%%%%%%%%%%%%%%%%%%%%%%%%%%%%%%%%%%%%%%%%%%%%%%
%Homogenous Transformation Matrices

A01  = @(th2,th3,th5) [cos(th1) -cos(alpha1)*sin(th1)
sin(alpha1)*sin(th1) a1*cos(th1);sin(th1) cos(alpha1)*cos(th1) -
sin(alpha1)*cos(th1) a1*sin(th1);0 sin(alpha1) cos(alpha1) d1;0 0 0 1];

A12  = @(th2,th3,th5) [cos(th2) -cos(alpha2)*sin(th2)
sin(alpha2)*sin(th2) a2*cos(th2);sin(th2) cos(alpha2)*cos(th2) -
sin(alpha2)*cos(th2) a2*sin(th2);0 sin(alpha2) cos(alpha2) d2;0 0 0 1];

A23  = @(th2,th3,th5) [cos(th3) -cos(alpha3)*sin(th3)
sin(alpha3)*sin(th3) a3*cos(th3);sin(th3) cos(alpha3)*cos(th3) -
sin(alpha3)*cos(th3) a3*sin(th3);0 sin(alpha3) cos(alpha3) d3;0 0 0 1];

A34  = @(th2,th3,th5) [cos(th4) -cos(alpha4)*sin(th4)
sin(alpha4)*sin(th4) a4*cos(th4);sin(th4) cos(alpha4)*cos(th4) -
sin(alpha4)*cos(th4) a4*sin(th4);0 sin(alpha4) cos(alpha4) d4;0 0 0 1];
```

```matlab
A45  = @(th2,th3,th5) [cos(th5) -cos(alpha5)*sin(th5)
sin(alpha5)*sin(th5) a5*cos(th5);sin(th5) cos(alpha5)*cos(th5) -
sin(alpha5)*cos(th5) a5*sin(th5);0 sin(alpha5) cos(alpha5) d5;0 0 0 1];

A56  = @(th2,th3,th5)  [cos(th6) -cos(alpha6)*sin(th6)
sin(alpha6)*sin(th6) a6*cos(th6);sin(th6) cos(alpha6)*cos(th6) -
sin(alpha6)*cos(th6) a6*sin(th6);0 sin(alpha6) cos(alpha6) d6;0 0 0 1];

%%%%%%%%%%%%%%%%%%%%%%%%%%%%%%%%%%%%%%%%%%%%%%%%%%%%%%%%%%%%%%%

%Iteration of th2,th3 and th5

A06=A01(th2,th3,th5)*A12(th2,th3,th5)*A23(th2,th3,th5)*A34(th2,th3,th5)
*A45(th2,th3,th5)*A56(th2,th3,th5)
X=[0 0 a1 a1 a1 a1-d4 a1-d4-d6];
Z=[0 d1 d1 d1+a2 d1+a2-a3 d1+a2-a3 d1+a2-a3];
Tool = plot(X,Z,'r','LineWidth',8,'XDataSource','X','YDataSource','Z');
axis([-2.5*(a1+a2) 2.5*(a1+a2) -(a1+a2) 3*(a1+a2)]);
set(gca, 'DataAspectRatio',[1 1 1])
grid on
hold('all')
disp ('Arun')

for k_1 = [th2_min:10*pi/180:th2_max]

    for k_2 = [th3_min:10*pi/180:th3_max]

        th5 = k*phi-((k_1)+(k*k_2))

        if (th5 >=th5_min)


A06=A01(k_1,k_2,th5)*A12(k_1,k_2,th5)*A23(k_1,k_2,th5)*A34(k_1,k_2,th5)
*A45(k_1,k_2,th5)*A56(k_1,k_2,th5)

            X=A06(1,4)

            Z=A06(3,4)

            hold 'all'

            Envelope_1 = plot(X, Z,'g.')
            refreshdata(Tool,'caller')
            drawnow
            disp ('plotted')
        end
    end
   end
```

2. Linked work envelope

```
%ABB Linked

clc
clear all

% D-H Parameters

a1 = 70;   d1 = 352;   alpha1 = -pi/2;    theta1 = 0;
a2 = 360;  d2 = 0;     alpha2 = 0;        theta2 = -pi/4;
a3 = 0;    d3 = 0;     alpha3 = pi/2;     theta3 = 3*pi/4;
a4 = 0;    d4 = 380;   alpha4 = -pi/2;    theta4 = 0;
a5 = 0;    d5 = 0;     alpha5 = pi/2;     theta5 = pi/2;
a6 = 0;    d6 = 65;    alpha6 = pi/2;     theta6 = 0;

% Axis Properties

X=[0 0 a1 a1 a1 a1-d4 a1-d4-d6];
Z=[0 d1 d1 d1+a2 d1+a2-a3 d1+a2-a3 d1+a2-a3];
Tool = plot(X,Z,'r','LineWidth',4,'XDataSource','X','YDataSource','Z');
axis([-2.5*(a1+a2) 2.5*(a1+a2) -(a1+a2) 3*(a1+a2)]);
set(gca, 'DataAspectRatio',[1 1 1])
grid on
hold('all')

% Iteration of th2,th3 within maximum and minimum limits

for theta2_0 = -90:10:110;
   for theta3_0 = -230:10:50;

      if (((theta2_0+theta3_0) >= -230) && ((theta2_0+theta3_0) <= 110))

theta2 = (-90+theta2_0)*pi/180;
theta3 = (180+theta3_0+theta2_0)*pi/180;

A01 = [cos(theta1), -cos(alpha1)*sin(theta1), sin(alpha1)*sin(theta1),
a1*cos(theta1); sin(theta1), cos(alpha1)*cos(theta1), -
sin(alpha1)*cos(theta1), a1*sin(theta1); 0, sin(alpha1), cos(alpha1),
d1; 0, 0, 0, 1 ];

A12 = [cos(theta2), -cos(alpha2)*sin(theta2), sin(alpha2)*sin(theta2),
a2*cos(theta2); sin(theta2), cos(alpha2)*cos(theta2), -
sin(alpha2)*cos(theta2), a2*sin(theta2); 0, sin(alpha2), cos(alpha2),
d2; 0, 0, 0, 1 ];

A23 = [cos(theta3), -cos(alpha3)*sin(theta3), sin(alpha3)*sin(theta3),
a3*cos(theta3); sin(theta3), cos(alpha3)*cos(theta3), -
sin(alpha3)*cos(theta3), a3*sin(theta3); 0, sin(alpha3), cos(alpha3),
d3; 0, 0, 0, 1 ];

A34 = [cos(theta4), -cos(alpha4)*sin(theta4), sin(alpha4)*sin(theta4),
a4*cos(theta4); sin(theta4), cos(alpha4)*cos(theta4), -
```

87

```matlab
sin(alpha4)*cos(theta4), a4*sin(theta4); 0, sin(alpha4), cos(alpha4),
d4; 0, 0, 0, 1 ];

A45 = [cos(theta5), -cos(alpha5)*sin(theta5), sin(alpha5)*sin(alpha5),
a5*cos(alpha5); sin(theta5), cos(alpha5)*cos(theta5), -
sin(alpha5)*cos(theta5), a5*sin(theta5); 0, sin(alpha5), cos(alpha5),
d5; 0, 0, 0, 1 ];
A56 = [cos(theta6), -cos(alpha6)*sin(theta6), sin(alpha6)*sin(theta6),
a6*cos(theta6); sin(theta6), cos(alpha6)*cos(theta6), -
sin(alpha6)*cos(theta6), a6*sin(theta6); 0, sin(alpha6), cos(alpha6),
d6; 0, 0, 0, 1 ];

A06 = A01*A12*A23*A34*A45*A56;

Envelope_1 = plot(A06(1,4), A06(3,4),'g.')
refreshdata(Tool,'caller')
drawnow

pause(.1)

else

fail = 1;

        end
    end
end
```

3. Functional workspace matlab code for geometrical solution

```matlab
%%
clc
clear all
close all

% Link length- can be changed

a2 = 1000; % length of first arm
a3 = 1000; % length of second arm
a5 = 1000; % length of third  arm
hold('on')

% Axis Properties

X=[0 a2 a2+a3 a2+a3+a5];
Y=[0 0 0 0];
Tool = plot(X,Y,'r','LineWidth',4,'XDataSource','X','YDataSource','Y');
axis([-(a2+a3+a5) 1.5*(a2+a3+a5) -(a2+a3+a5) (a2+a3+a5)]);
set(gca,'DataAspectRatio',[1 1 1])
grid on
hold('on')

% Movement of links between maximum and minimum limits- Limits can be
changed to suit the manipulator

for theta1 = -90*pi/180:0.1:110*pi/180
    for theta2 = -230*pi/180:0.1:50*pi/180
        for theta3 = 90*pi/18

X= [0 a2 * cos(theta1) a2 * cos(theta1) + a3 * cos(theta1 + theta2)
a2*cos(theta1) + a3*cos(theta1+theta2)+a5*cos(theta1+theta2+theta3)];

Y=[0 a2 * sin(theta1) a2 * sin(theta1) + a3 * sin(theta1 + theta2)
a2*sin(theta1) + a3*sin(theta1+theta2)+a5*sin(theta1+theta2+theta3)];

X1= [0 a2 * cos(theta1) + a3 * cos(theta1 + theta2)+ a5 * cos(theta1 +
theta2 + theta3)];

Y1= [0 a2 * sin(theta1) + a3 * sin(theta1 + theta2)+ a5 * sin(theta1 +
theta2 + theta3)];

plot (X1, Y1, 'g.')
refreshdata(Tool,'caller')
drawnow

        end
    end
end
```

1. MATLAB Trial #1:

A plotter function is introduced in this trial with the D-H parameters and homogenous transformations. The TRIAL#1 program calls the result of this program at every increment Δ of θ_2, θ_3 or θ_5. In TRIAL#1 the minimum and maximum limits of each joint are defined. The value of θ_5 using the formula, $\theta_5 = k\phi - (\theta_2 + k\theta_3)$ (Eq. 4.1) is first checked. If the result is within the limits it is then plotted. If not, θ_2 is decremented by Δ and the loop is run again. Once the loop reaches the minimum value of θ_3 or θ_2 reaches minimum the values of the homogenous transformation matrices are plotted. If not, the loop is run again while a decrement of Δ is applied to θ_2 and θ_3. The result of the program is presented in the Appendix Fig.-1.

PLOTTER

```
function [X,Y ] = trial5( a,b,c,n)
% this function contains the homogeneous transformations and a plotter

a1 = 70;    d1 = 352;    alpha1 = -pi/2;    th1 = 0;
a2 = 360;   d2 = 0;      alpha2 = 0;        th2=a;
a3 = 0;     d3 = 0;      alpha3 = pi/2;     th3=b;
a4 = 0;     d4 = 380;    alpha4 = -pi/2;    th4 = 0;
a5 = 0;     d5 = 0;      alpha5 = pi/2;     th5=c;
a6 = 0;     d6 = 65;     alpha6 = pi/2;     th6 = -pi/2;

A01  = @(th2,th3,th5) [cos(th1) -cos(alpha1)*sin(th1)
sin(alpha1)*sin(th1) a1*cos(th1);sin(th1) cos(alpha1)*cos(th1) -
sin(alpha1)*cos(th1) a1*sin(th1);0 sin(alpha1) cos(alpha1) d1;0 0 0 1];

A12  = @(th2,th3,th5) [cos(th2) -cos(alpha2)*sin(th2)
sin(alpha2)*sin(th2) a2*cos(th2);sin(th2) cos(alpha2)*cos(th2) -
sin(alpha2)*cos(th2) a2*sin(th2);0 sin(alpha2) cos(alpha2) d2;0 0 0 1];

A23  = @(th2,th3,th5) [cos(th3) -cos(alpha3)*sin(th3)
sin(alpha3)*sin(th3) a3*cos(th3);sin(th3) cos(alpha3)*cos(th3) -
sin(alpha3)*cos(th3) a3*sin(th3);0 sin(alpha3) cos(alpha3) d3;0 0 0 1];
```

90

```matlab
A34  = @(th2,th3,th5) [cos(th4) -cos(alpha4)*sin(th4)
sin(alpha4)*sin(th4) a4*cos(th4);sin(th4) cos(alpha4)*cos(th4) -
sin(alpha4)*cos(th4) a4*sin(th4);0 sin(alpha4) cos(alpha4) d4;0 0 0 1];

A45  = @(th2,th3,th5) [cos(th5) -cos(alpha5)*sin(th5)
sin(alpha5)*sin(th5) a5*cos(th5);sin(th5) cos(alpha5)*cos(th5) -
sin(alpha5)*cos(th5) a5*sin(th5);0 sin(alpha5) cos(alpha5) d5;0 0 0 1];

A56  = @(th2,th3,th5)  [cos(th6) -cos(alpha6)*sin(th6)
sin(alpha6)*sin(th6) a6*cos(th6);sin(th6) cos(alpha6)*cos(th6) -
sin(alpha6)*cos(th6) a6*sin(th6);0 sin(alpha6) cos(alpha6) d6;0 0 0 1];

A06=A01(th2,th3,th5)*A12(th2,th3,th5)*A23(th2,th3,th5)*A34(th2,th3,th5)
*A45(th2,th3,th5)*A56(th2,th3,th5);


        X=A06(1,4)

        Y=A06(3,4);


        hold 'all'

        plot(X,Y, 'rx')


end
```

TRIAL#1

```matlab
%%
clear
clc
k= 1
phi = pi/2
th2_min = -pi/2;
th2_max = +110*pi/180;
th3_min = -230*pi/180;
th3_max = 50*pi/180;
th5_min = -120*pi/180;
th5_max = 120*pi/180;
th2 = th2_max;
th3=th3_max;
dec = 10*pi/180;
while (1)
 disp('onto function')
 th5=k*phi-(th2+k*th3);
 fprintf(' theta 5 in %f degrees  calculated at the head \n',th5*180/pi)
 if ( (th5>=th5_min && th5<=th5_max)==1)
   mint=th5>=th5_min
```
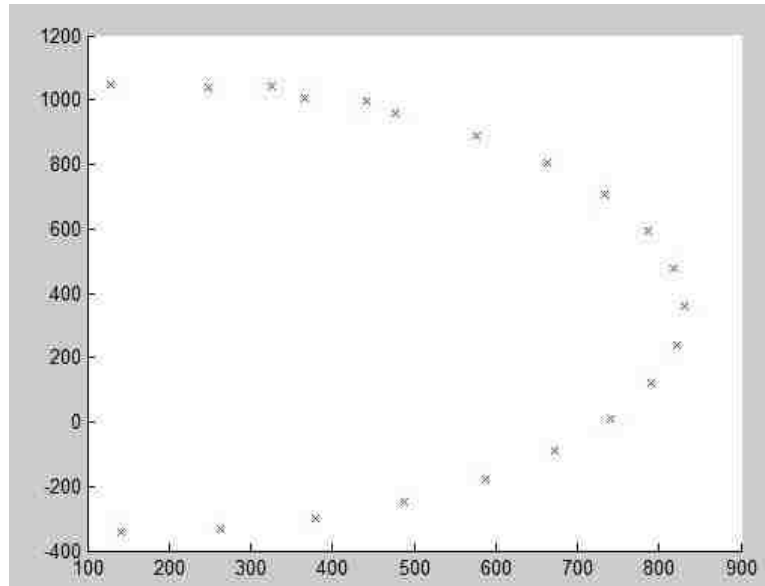
```
maxt=th5<=th5_max
pause(0.01)
trial5(th2,th3,th5)
    if th2<=th2_min
     break
        else
            th2=th2-dec;
             fprintf(' theta 2 in %f degrees \n',th2*180/pi)
        end
else
    if th3<=th3_min
        trial5(th2,th3,th5)
        if th2<=th2_min;
            fprintf(' theta 2 in %f degrees \n',th2*180/pi)
           break
        else
            th2=th2-dec;
            fprintf(' theta 2 in %f degrees \n',th2*180/pi)
        end
    else
        th3=th3-dec;
        fprintf(' theta 3 in %f degrees \n',th3*180/pi)
        pause(0.1)
    end


    end
end
```


Figure A-11-1 Plot result for MATLAB Trial#1

2. MATLAB Trial #2

In this trial, an attempt was made to find the two dimensional work envelope of the robot.

Every point between the limits of θ_2 and θ_3 is plotted. The result is given in Appendix

Fig.-2.

```
clc
clear

% declaration of the dh parameters

a1 = 70;   d1 = 352;   alpha1 = -pi/2;   th1 = 0;
a2 = 360;  d2 = 0;     alpha2 = 0;       th2 = -pi/4;
a3 = 0;    d3 = 0;     alpha3 = pi/2;    th3 = 3*pi/4;
a4 = 0;    d4 = 380;   alpha4 = -pi/2;   th4 = 0;
a5 = 0;    d5 = 0;     alpha5 = pi/2;    th5 = 0;
a6 = 0;    d6 = 65;    alpha6 = pi/2;    th6 = 0;
k = cos(alpha2);
phi = pi/2;


%%%%%%%%%%%%%%%%%%%%%%%%%%%%%%%%%%%%%%%%%%%%%%%%%%%%%%%%%%%
%Limits of th2, th3 & th5

th2_min = -pi/2;
th2_max = +110*pi/180;
th3_min = -230*pi/180;
th3_max = 50*pi/180;


%%%%%%%%%%%%%%%%%%%%%%%%%%%%%%%%%%%%%%%%%%%%%%%%%%%%%%%%%%%%%%%
%Homogenous Transformation Matrix
for th2 = [th2_min:10*pi/180:th2_max]

    for th3 = [th3_min:10*pi/180:th3_max]

A01  =  [cos(th1) -cos(alpha1)*sin(th1) sin(alpha1)*sin(th1)
a1*cos(th1);sin(th1) cos(alpha1)*cos(th1) -sin(alpha1)*cos(th1)
a1*sin(th1);0 sin(alpha1) cos(alpha1) d1;0 0 0 1];

A12  =  [cos(th2) -cos(alpha2)*sin(th2) sin(alpha2)*sin(th2)
a2*cos(th2);sin(th2) cos(alpha2)*cos(th2) -sin(alpha2)*cos(th2)
a2*sin(th2);0 sin(alpha2) cos(alpha2) d2;0 0 0 1];

A23  =  [cos(th3) -cos(alpha3)*sin(th3) sin(alpha3)*sin(th3)
a3*cos(th3);sin(th3) cos(alpha3)*cos(th3) -sin(alpha3)*cos(th3)
a3*sin(th3);0 sin(alpha3) cos(alpha3) d3;0 0 0 1];

A34  =  [cos(th4) -cos(alpha4)*sin(th4) sin(alpha4)*sin(th4)
a4*cos(th4);sin(th4) cos(alpha4)*cos(th4) -sin(alpha4)*cos(th4)
a4*sin(th4);0 sin(alpha4) cos(alpha4) d4;0 0 0 1];
```

```
A45 = [cos(th5) -cos(alpha5)*sin(th5) sin(alpha5)*sin(th5)
a5*cos(th5);sin(th5) cos(alpha5)*cos(th5) -sin(alpha5)*cos(th5)
a5*sin(th5);0 sin(alpha5) cos(alpha5) d5;0 0 0 1];

A56 = [cos(th6) -cos(alpha6)*sin(th6) sin(alpha6)*sin(th6)
a6*cos(th6);sin(th6) cos(alpha6)*cos(th6) -sin(alpha6)*cos(th6)
a6*sin(th6);0 sin(alpha6) cos(alpha6) d6;0 0 0 1];

A06=A01*A12*A23*A34*A45*A56;

X=A06(1,4)
Y=A06(3,4);
hold 'all'
plot(X,Y, 'xr')

    end
end

%th2 = between limits
%th3 = between limits
%all else constant
%vary th2 and th3 between limits
```
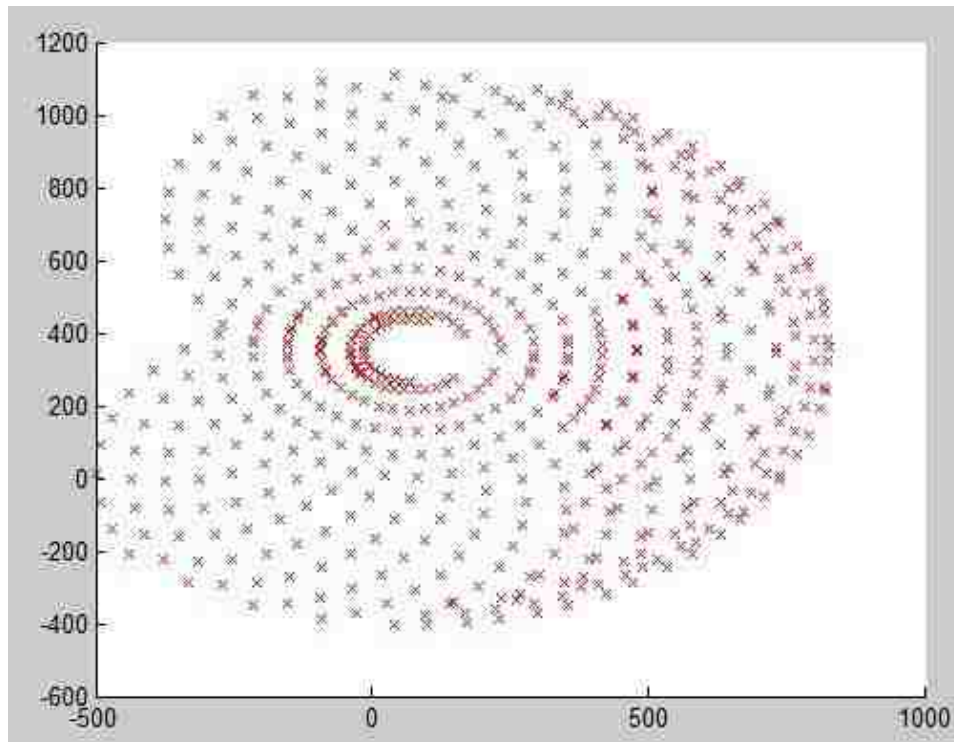

Figure A-11-2 Plot result for MATLAB Trial#2

3. MATLAB Trial#3

In Trial#3, for every increment Δ of θ_2 and θ_3 the Eq. 4-1 is checked and the matrix obtained with the new Δ value of θ_2 and θ_3 is plotted.

```
dec = 10*pi/180;
th2_min = -pi/2;
th2_max = +110*pi/180;
th3_min = -230*pi/180;
th3_max = 50*pi/180;
th5_min = -120*pi/180;
th5_max = 120*pi/180;
th2 = th2_max
th3=th3_max;
dec = 10*pi/180;
k = 1;
phi = pi/2;
for l= (th3_min: dec: th3_max)
      th5=k*phi-(th2+k*th3);
      plotter(th2,l,th5)
end
th3= th3_min;
for l= (th2_min: dec: th2_max-2*dec)
      th5=k*phi-(th2+k*th3);
      plotter(l,th3,th5)
end
```
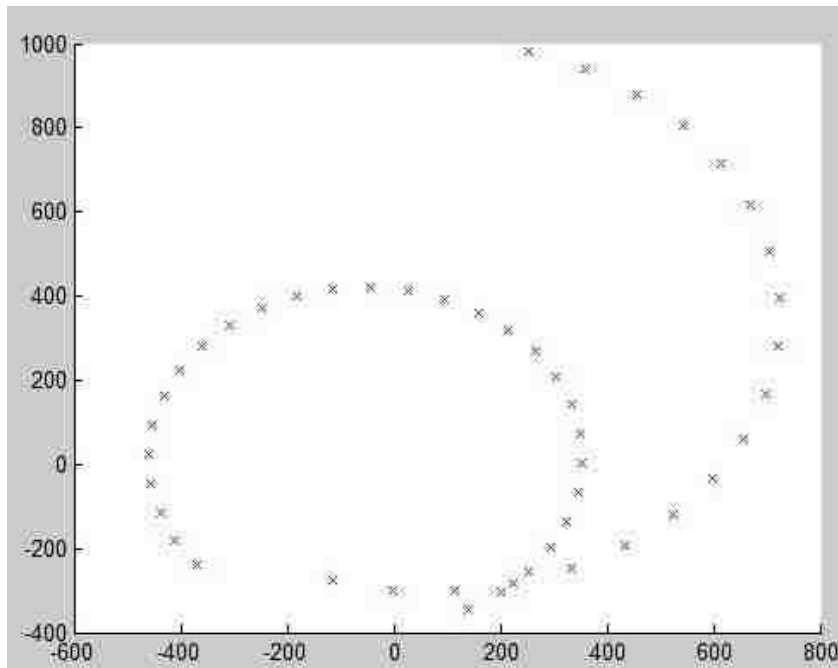

Figure A-11-3 : Plot result for MATLAB Trial#3

95

Many additional approaches were tried before the geometrical solution presented in the research. It is essential to discuss some of the important approaches so as to aid the future development of this research.

Approach #1: Minimum and Maximum X, Y Points

An alternative geometrical approach was to find out the functional workspace curve through the minimum and maximum X, Y positions. These X, Y positions can be derived from the homogenous transformation matrices applied for every increment, Δ of θ_2 and θ_3. The Appendix Fig.- 4 shows these points on a X-Y plane.
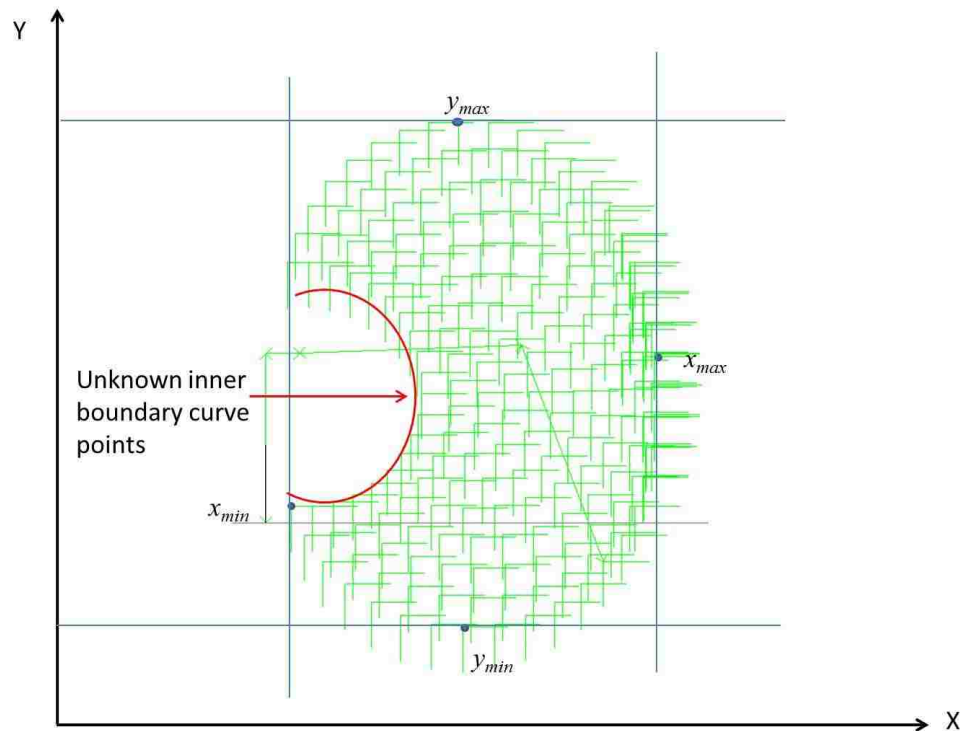

**Figure A-11-4 X and Y minimum and maximum points**

It was assumed that the shape between these minimum and maximum points could be interpolated as arcs. Although, the minimum and the maximum X and Y positions could be found, there is no way to find the inner boundary curve. Also, not every functional workspace curve has a unique X_{min} value on the top and bottom part of the curve (Refer Fig. 4-7). This means only one X_{min} is not enough to depict the whole curve. It is not possible to find all the ends of the functional workspace curve with this approach. Also, interpolating between the curves is always not feasible. It is not guaranteed that the shape between two points will always be a perfect arc. This can lead to confusion on deciding which arc to consider and also present an inaccurate curve.

Approach #2: Dividing the plane

The plane was next divided into two parts. The division was made based on the 90° position of the joints- 2 and 5 and -90° for joint-3. At this position, the robot is parallel to the X-axis. The line parallel to the Y-axis is made through the joint-3 axis. Appendix Fig.- 5 details this type of demarcation.

Consider the plane divided into four zones numbered clockwise. Homogenous matrices are calculated in batches based on the joint angles. For example, the joint limits are restricted to increment between -90° and 0° of joint-3. These points can then be joined through arcs. Although, this does break up the curve into smaller zones, there exists more than one minimum X and Y point in one quadrant which makes it difficult to decipher the right point to consider. The example of this can be seen in quadrant-4 and 1 where the inner boundary produces conflict in deciding the minimum X position.
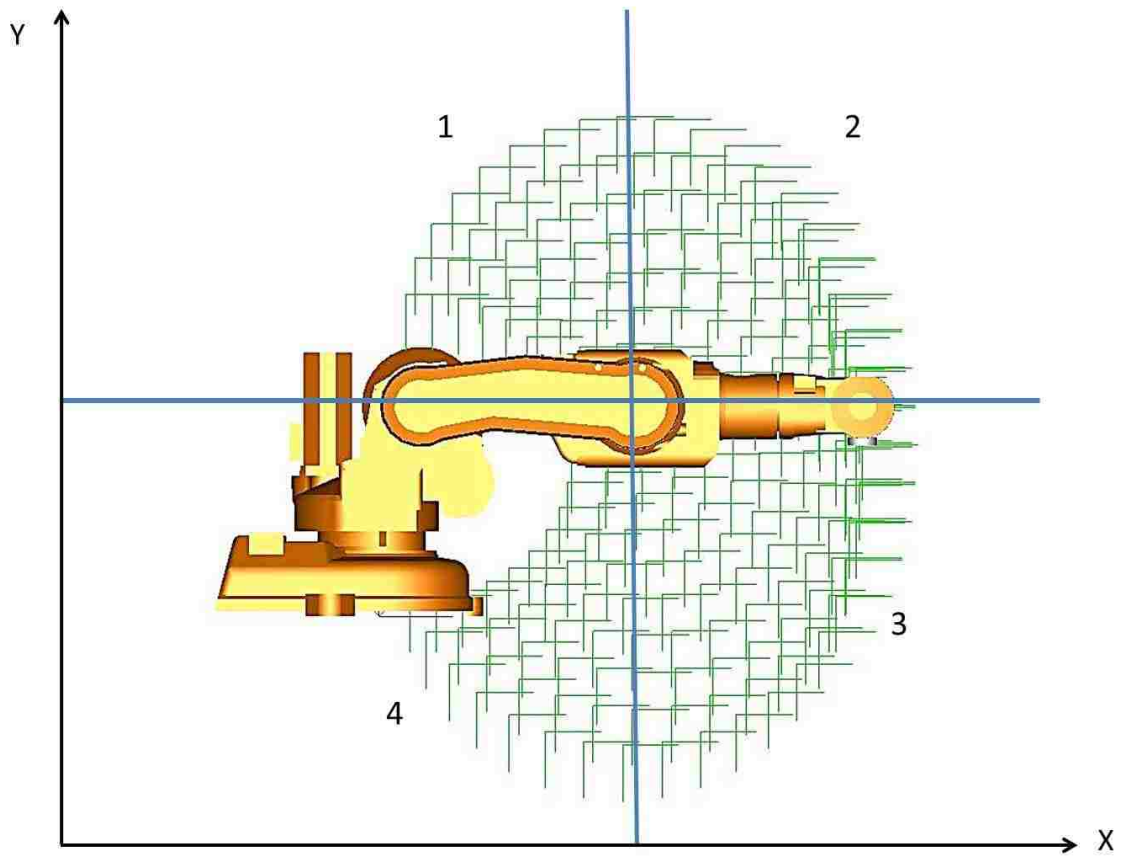
Figure A-11-5 Divison of functional workspace

REFERENCES

Abdel-Malek, K., Yu, W., Yang, J.,. "Placement of Robot Manipulatore to Maximize Dexterity." *International Journal of Robotics and Automation*, 2004: 19(1), 6-14.

Abdel-Malik, K., Yeh, H.J. "Analytical Boundary of the Workspace for General 3 DOF Mechanism." *The International Journal of Robotics Research*, 1997: Vol.16, No.2, pp.198-213.

Alciatore, David G., Ng, Chung-Ching, D. "Determining Workspace boundaries using the Monte Carlo Method and Least Squares." *American Society of Mechanical Engineers, Design Engineering Divison.* DE: Design Engineering Divison, 1994. 141-146.

Alfonso Pamanes, G., Zeghioul, S.,. "Optimal Placement of Robotic Manipulators Using Multiple Kinematic Criteria." *International Conference of Robotics and Automation.* 1991. Vol.1, pp. 933-938.

Badescu, M., Mayroidis, C. "Workspace Optimisation of 3-legged UPU and UPS Parallel Platforms with Joint Constraints." *ASME Journal of Mechanical Design*, 2004: Vol. 126 (2), pp.291-300.

Bergamaschi, P.R., Nogueira, Fatima Pereira, S., Saramago. "Design and Optimization of 3R Manipulators using the Workspace Features." *Applied Mathematics and Computation*, 2006: Vol.172, No.1, pp. 439-463.

Bi, Z.M., Lang Z.M. "Joint Workspace of Parallel Kinematic Machines." *Robotics and Computer-Integrated Manufacturing*, 2009: Vol.25., Issue 1, pp.57-63.

Canuto. "internal personal correspondence." 2012.

Cao, Y., Lu, K., Li,X., Zang, Y. "Accurate Numerical Methods For Computing 2D and 3D." *International Journal of Advanced Robotic Systems*, 2011: 1-13.

Cao, Y., Qi, S., Lu, K., Zhang, Y., Yang, G. "An Integrated Method for Workspace Computation of Robot Manipulator." *International Joint Conference on Computational Sciences and Optimisation.* 2009. Vol. 1, pp. 309-312.

Cao, Y., Zang, H., Wu, L., Lu, T. "An Engineering-Oriented Method for the Three Dimensional Workspace Generation of Robot Manipulator." *Journal of Information and Computational Science*, 2011: 8:1, pp.51-61.

Carbone, G., Nakadate, R., Solis, J., Ceccarelli, M., Takanishi, A., Minagawa, E., Sugawara, M., Niki, K. "Workspace Analysis and Design Improvement of Cartoid Flow Measurement System." *Proceedings of the Institute of Mechanical Engineers.* 2010. Vol.224, Part-H: Engineering in Medicine.,1311-23.

Cebula, A.J., Zsombor-Murray, P. "Formulaiton of Workspace for Wrist-partitioned Spatial Manipulators." *Mechanism and Machine Theory.* 2006. Vol.41, Issue-7, pp. 778-789.

Ceccarelli, M. "A Formulation for the Workspace Boundary of General n-Revolute Manipulators." *Mechanism and Machine Theory*, 1996: Vol.31, No.5, pp. 637-646.

Ceccarelli, M., Vinciguerra, A. "On the Workspace of 4R manipulators." *The International Journal of Robotics Research*, 1995: Vol. 14, No.2, pp. 152-160.

Cimino, W.W., Pennock, G.R. "Workspace of a six-revolute Decoupled Robot Manipulator." *Processidngs of the IEEE International Conference on Robotics and Automation.* San Francisco, California: IEEE, 1986. Vol.3, pp.1818-1852.

Corke, P. "A Computer Tool for Simulation and Analysis: The Robotics Toolbox for MATLAB." *National Conference of the Australian Robot Association.* Melbourne, Australia, 1995. pp.319-330.

—. "MATLAB Toolboxes: Robotics and Vision for students and Teachers." *IEEE Robotics and Automation Magazine*, 2007: Vol.14 (4), pp.16-17.

Denavit, J., Hartenberg R.S.,. "A Kinematic Notation for Lower-pair Mechanisms Based on Matrices." *Journal of Applied Mechanics*, 1955: Vol,77, 215-221.

Djuric, A., Urbanic, R.J.,. "Utilizing the Functional Work Space Evaluation Tool for Assessing a System Design and Reconfiguration Alternatives." In *Robotic Systems - Applications, Control and Programming (Ed.), ISBN: 978-953-307-941-7*, by Ashish Dutta. InTech, 2012.

Djuric, A.M., Al Saidi, R., ElMaraghy, W.,. "Global Kinematic Model generation for n-DOF Reconfigurable Machinery Structure." *6th Annual IEEE conference on Automation, Science & Engineering.* 2010. pp. 804-809.

Djuric, A.M., Urbanic, R.J. "Definition of the Functional Space (Work window) for a Material Deposition Machine Configuration." *3rd International Conference on Changeable, Agile, Reconfigurable and Virtual Production, CD-ROM.* Munich, 2009.

Feddema, J.T. "Kinematically Optimal Placement for Minimum Time Coordinated Motion." *Robotics and Automation, IEEE International Conference.* 1996. Vol.4, pp.3395-3400.

Ghoshray, S. "Optimal path determination for a robot in a 2D workspace using quadtree." *IEEE International Conference on Intelligent Engineering Systems, Proceedings.* INES: IEEE, 1997. 175-181.

Hackose, J.T., Redish, J.C. "User and Task Analysis for Interface Design." *Special Interest Group on Computer-Human Interaction (SIGCHI)*, 1997: Vol. 31, No.3 .

K.C., Gupta. "On the Nature of Robot Workspace." *The International Journal of Robotics Research*, 1986: Vol 5., No.2, pp.112-121.

Khan, W.A., Caro, S., Angeles, J., Pasini, D. "A Formulation of Complexity Based Rules for the Preliminary Design Stage of Robotic Architectures." *International Conference on Engineering Design, ICED' 07, 28-31 August, 2007, Citedes Sciences, et DE L'Industrie, Paris, France.* Paris, 2007.

Kohli, D., Spanos, J. "Workspace Analysis of Mechanical Manipulators Using Polynomial Discrimants." *ASME Journal of Mechanisms, Transmissions, and Automation in Design*, 1985: Vol.107, pp. 216-222.

Lee, D., Seo, T.W., Kim, J. "Optimal Design and Workspace Analysis of a Mobile Welding Robot with a 3P3R Serial Manipulator." *Robotics and Autonomous Systems* , 2011: 59 (10): 813-826.

Lee, T.W., Yang, D.C.H. "On the Evaluation of Manipulator Workspace." *ASME Journal of Mechanisms, Transmissions, and Automation in Design*, 1983: Vol.105, pp.70-77.

Litvin, F.L. "Application of Theorem of Implicit Function Systems Existence for Analysis and Synthesis of Linkages." *Mechanism and Machine Theory*, 1980: Vol.15, No.2, pp. 115-125.

Liu, C., Chen, Q., Wang, D. "CPG- Inspired Workspace Trajectory Generation and Adaptive Locomotion Control for Quadruped Robots." *IEEE Transactions on Systems, Manufacturing and Cybernetics*, 2011: Vol.41, No.3, pp.867-880.

Manseur, R., Doty, K.L. "Structural Kinematics of 6-Revolute-Axis Robot Manipulators." *Mechanism and Machine Theory*, 1996: 31(5), 647-657.

Manseur, R., Doty, K.L. "Sturctural Kienmatics of 6R Axis Robot Manipulators." *Mechanism and Machine Theory*, 1996: Vol.31, No.5, pp. 647-657.

Mansuer, R. *Robot Modeling and Kinematics, 1st Edition* . Da Vinci Engineering Press, 2006.

Moon, Y., Kota, S.,. "Design of Complaint Parallel Kinematic Machines." *ASME conference Proceedings. 2002,35(2002).* 2002. pp.35-41.

Panda, S., Mishra, D., Biswal, B.B. "An Appropriate Tool for Optimizing the Workspace of 3R Robot Manipulator." *World Congress on Nature and Biologically Inspired Computing.* 2009. Articale Number 5393780, pp. 1156-1161.

Selfridge, R.G. "The Reachable Workarea of a Manipulator." *Mechanism and Machine Theory*, 1983: Vol.18,no.2, pp.131-137.

Szep, C., Stan S.D.,. "Kinematics, Workspace, Design and Accuracy Analysis of RPRPR Medical Parallel Robot." *2nd Conference on Human System Interactions.* IEEE, 2009.

Urbanic, J., Gudla, A.,. "Functional Work space Estimation of a Robot Using Forward Kinematics, D-H Parameters and Shape Analyses." *The ASME 2012 11th Biennial Conference on Engineering Systems Design and Analysis (ESDA2012).* Nantes: ASME ESDA 2012, 2012.

Vijaykumar, R., Waldron, K., Tsai, M.,. "Geometric Optimization of Serial Chain Manipulator Structures for Working Volume and Dexterity." *International Journal of Robotics Research*, 1986: Vol.5, No.2, pp.91-103.

Yang, J., Yu, W., Kim, J., Abdul-Malek, K.,. "On the Placement of open-loop Robotic Manipulators for Reachability." *Mechanism and Machine Theory*, 2009: Vol.44,No.4, pp.671-684.

Zacharias, F., Borst, C., Hirzinger, G.,. "Capturing Robot Workspace Structure: Representing Robot Capabilities." *Intelligent Robots and Systems* . IROS 2007, IEEE/RSJ, 2007. pp.3229-3236.

VITA AUCTORIS

NAME	Arun Gowtham Gudla
PLACE OF BIRTH	India
YEAR OF BIRTH	1985
EDUCATION	B.Tech (Mechanical Engineering), JNTU, Hyderabad, India
	2005-2009
	M.Eng, University of Windsor, Windsor, ON, Canada
	2009-2010 .